

A HIGH-THROUGHPUT SCREEN TO DISCOVER NOVEL GFAT INHIBITORS

A HIGH-THROUGHPUT SCREENING CAMPAIGN TO DISCOVER NOVEL INHIBITORS OF
HUMAN L-GLUTAMINE: D-FRUCTOSE-6-PHOSPHATE AMIDOTRANSFERASE 1

BY: LISA ANNE WALTER, B.Sc. (Honours)

A Thesis Submitted to the School of Graduate Studies in Partial Fulfillment of the
Requirements for the Degree Doctorate of Philosophy

McMaster University © Copyright by Lisa A. Walter, July 2013

DOCTORATE OF PHILOSOPHY (2013)
(Chemical Biology)

McMaster University
Hamilton, Ontario

TITLE: A High-throughput Screening Campaign to Discover Novel Inhibitors of Human L-glutamine:D-fructose-6-phosphate amidotransferase 1

AUTHOR: Lisa A. Walter, B.Sc. (Honours) (McMaster University)

SUPERVISORS: Professor A. Capretta & Professor G.H. Werstuck

NUMBER OF PAGES: xxiv, 176

Abstract

Human L-glutamine:D-fructose-6-phosphate amidotransferase 1 (hGFAT1) is the first and rate-limiting enzyme of the hexosamine biosynthesis pathway (HBP) and is a potential target to help prevent secondary complications of type II diabetes. GFAT catalyzes the irreversible reaction between L-glutamine and D-fructose-6-phosphate to produce L-glutamate and D-glucosamine-6-phosphate. hGFAT1 is not commercially available and is difficult to obtain from natural sources. Thus, a recombinant method to generate and purify the enzyme was developed and is discussed herein.

There are only a handful of known inhibitors available to study the enzyme and the majority of these are toxic, non-specific, or substrate analogs. A high-throughput screening campaign was undertaken in pursuit of novel hGFAT1 inhibitors. The bioactive subset of the Canadian Compound Collection was assayed in duplicate for GFAT inhibitory activity using a modified version of the Morgan-Elson assay. Out of the 3950 bioactives, 9 were identified as lead compounds. All of the compounds identified from the bioactive collection are novel GFAT inhibitors.

A structure-activity relationship (SAR) analysis was performed on the lead compounds. Derivatives of the leads were also purchased or synthesized for inhibitory testing. Four distinct classes of compounds were identified as GFAT inhibitors: isoquinolines, aminothiazoles, pyridinones and quinones. The most potent lead compound elucidated from the SAR was dehydroiso- β -lapachone (IC_{50} 1.5 ± 0.5 μ M). The mode of inhibition of dehydroiso- β -lapachone was determined to be non-competitive for both binding domains of recombinant hGFAT1.

To validate the lead compounds as inhibitors of native hGFAT1 and to determine their cell permeability, a cell based assay was developed. HepG2 cell cultures were treated with an inhibitor and HBP metabolism was determined by measuring the levels of the end-product uridine diphosphate *N*-acetylglucosamine (UDP-GlcNAc). UDP-GlcNAc was separated and detected by UPLC-ESI-TOF-MS and metabolite levels were normalized to cell concentration. The leads, alloxan, lapachol and amrinone all displayed hGFAT1 inhibition in cell culture.

Acknowledgements

There are countless people I need to thank for their support as I pursued this academic endeavour. First and foremost I owe my endless gratitude towards my supervisors, Prof. Fred Capretta and Prof. Geoff Werstuck. To Fred, thank you for taking a chance on a biochemist with no experience, and to Geoff, thank you for making me feel at home in your lab.

I would like to acknowledge my committee member, Dr. John Brennan. Thank you for always being available to discuss any challenges along the way. Your input was always well received.

I would also like to thank Dr. Paul Berti for allowing me into his lab to spend countless hours performing the cloning, expression and protein purification experiments.

I'd like to thank Jan Blanchard, Jenny Wang and Susan McCusker at the CMCB. Your input and help with the screening and scale-up of GFAT production was invaluable. Everyone went above and beyond for my project.

I would like to thank Tammy Feher for all of her administrative assistance over the years and helping to sort out any issues I had.

I'd like to thank members of the Capretta research group, past and present. Dave Gerritsma for getting me started with my first synthesis, Emelia Awuah for providing me with inhibitors, Meaghan O'Brien for her work with the magnetic-bead assay, Bilal Bagha, Thomas Floyd and Sam Dalton for providing me with plenty of

compounds for an SAR, Silvia Albu and Salma Al-Karmi for being a constant source of support and strength.

Many thanks go out to members of the Werstuck research group. In particular, Christina Petlura, who provided me an extra set of hands as I neared completion of my project, Dan Beriault, for help with cell cultures, and Peter Shi, for all your help in the lab.

To the members of the Berti research group, Naresh Balachandran, Vincent Azhikannickal, Shan Jiang and Vladimir Popovic, I enjoyed every day we worked together.

To members of the Brennan research group, thank you for adopting me as a member, Erica Forsberg and Meghan McFadden, your expertise and patience were greatly appreciated.

I would also like to acknowledge the late Prof. Brian McCarry and his research group. I thoroughly enjoyed our collaboration together; Ken Chalcraft and Vi Dang, your input and assistance were tremendously appreciated.

I cannot thank my friends and family enough for being there every step of the way. To my chemist friends, you made these past six years unforgettable. To my non-chemist friends, thanks for being non-chemists. To MC, thanks for making me smile. To my grandma, thanks for the phone calls. To my parents, I've reached the end, but not without your encouragement and support.

Table of Contents	Page
	#
<u>Chapter 1: L-glutamine:D-fructose-6-phosphate amidotransferase (GFAT) and its role in the secondary complications of diabetes</u>	1
<hr/>	
The socio-economic impact of Type 2 diabetes mellitus	2
Current and future pharmaceutical treatments for Type II diabetes mellitus	4
Introduction to the Hexosamine Biosynthesis Pathway, ER Stress and their role in diabetes and diabetic complications	5
Background to GFAT	8
Enzyme mechanism of action and structural characteristics	9
<i>In vitro</i> GFAT stability	12
Measurement of GFAT activity with the Morgan-Elson assay	12
Known GFAT inhibitors	15
Rationale and Thesis Goals	17
Objectives	17
References	19
<u>Chapter 2: Cloning, Expression and Large-Scale Purification of rhGFAT1-His₆²⁹⁸</u>	26
<hr/>	
Preface	27
Abstract	28
Introduction	29
Results & Discussion	32
Generation of a recombinant human GFAT1 protein expression vector utilizing Multi-Site Gateway® cloning technology	32

Insertion of an internal hexa-histidine tag into hgf _{at} 1-cDNA genetic position 894	35
Protein expression and purification of rhGFAT1-His ₆ ²⁹⁸	37
Large-Scale GFAT Expression	41
Characterization of rhGFAT1-His ₆ ²⁹⁸	41
Conclusion	45
Materials & Methods	46
GFAT Cloning: Multi-Site Gateway® Cloning Technology	46
i) PCR amplification of hgf _{at} 1-cDNA	46
ii) Creation of the hgf _{at} 1-cDNA entry clone	47
iii) Creation of the hgf _{at} 1-cDNA expression clone	48
Induced protein expression with Rosetta 2™ E.coli transformed with the hgf _{at} 1-cDNA expression clone	49
SDS-PAGE of E.coli cell lysates following protein expression of rhGFAT-1	49
Entry clone hexa-histidine tag insertion by site-directed mutagenesis <i>via</i> PCR	50
Optimizing protein expression of recombinant human GFAT1-His ₆ ²⁹⁸	51
Purification of rhGFAT1-His ₆ ²⁹⁸ by Immobilized Metal Affinity Chromatography (IMAC) <i>via</i> FPLC	52
Large-scale expression of rhGFAT1-His ₆ ²⁹⁸ with industrial fermentor & tandem centrifuge	53
Standard Morgan-Elson Assay for Detection of GFAT Activity	54
Measurement of rhGFAT1-His ₆ ²⁹⁸ activity in E.coli cell lysates	55
Determination of Michaelis-Menten Kinetics of rhGFAT1-His ₆ ²⁹⁸	56
Determination of the Inhibitory Effect of DON on rhGFAT1-His ₆ ²⁹⁸	57

References	58
<u>Chapter 3: Identification of GFAT Inhibitors: Assay</u>	59
Development and High-Throughput Screening Campaign	
<hr/>	
Preface	60
Abstract	61
Introduction	62
Results & Discussion	64
Modification and Optimization of the Morgan-Elson Assay for a High-Throughput Screening Platform	64
Controls and reference inhibitors for the HTS Screen	68
HTS Pilot Screen with the Modified Morgan-Elson Assay	72
GFAT hits identified from the HTS	75
Validation of hits via secondary dose-response screening	78
Conclusion	96
Materials & Methods	97
Protocol for the modified Morgan-Elson Assay in 384-well plate format for HTS	97
Optimization of protein concentration	99
Optimization of enzyme incubation time	99
Solvent optimization for acetylation	100
Ehrlich's Reagent incubation optimization	100
Measurement of GlcN standards with the standard and modified Morgan-Elson assay	100
Z-factor determination for the standard Morgan-Elson assay	100
Z-factor determination for the HTS-modified Morgan-Elson assay	101

Five-step synthesis of N^3 -(4-methoxyfumaryl)-L-2,3-diaminopropanoic acid (FMDP)	101
i) Formation of monomethyl fumarate from dimethyl fumarate	101
ii) Synthesis of N^2 - tert-butoxycarbonyl-L-2,3-diaminopropanoic acid	102
iii) Synthesis of <i>N</i> -succinimidoyl ester of monomethyl fumarate	102
iv) Preparation of N^3 -tert-butoxycarbonyl-(4-methoxyfumaramoyl)-L-2,3-diaminopropanoic acid	103
v) Removal of the tert-butoxycarbonyl protecting group	103
Pilot screen	104
Primary screen	104
Dose-Response Assays	105
References	107
<u>Chapter 4: Characterization of GFAT Inhibitors: Cell Toxicity, Efficacy, Structure-Activity Relationship Analysis and Determination of Mode of Inhibition</u>	110
<hr/>	
Preface	111
Abstract	112
Introduction	113
Results and Discussion	114
Cell toxicity of inhibitors with HepG2 cells	114
Development of a UPLC-TOF-MS Assay for UDP-GlcNAc Detection and Assessment of Downstream HBP Activity	116
Structure-Activity Relationship Analysis of GFAT Inhibitors	123

i) 6,7-dimethoxyisoquinolines	124
ii) Aminothiazoles	127
iii) Pyridinones	129
iv) Quinones	131
Mode of inhibition of dehydroiso- β -lapachone at the isomerase and glutaminase binding domains	139
Conclusion	143
Materials & Methods	144
Measurement of inhibitor cell toxicity in HepG2 cells	144
UPLC-TOF-MS assay for detection of UDP-GlcNAc, Sample Preparation and Analysis	144
Dose-response of dehydroiso- β -lapachone	147
HepG2 cell viability with dehydroiso- β -lapachone measured with the Countess [®] cell counter	147
Dose-response of dehydroiso- β -lapachone with varied F6P	148
Dose-response of dehydroiso- β -lapachone with varied L-gln	148
References	149
<u>Chapter 5: Development of Alternate Screening Strategies</u>	152
for GFAT Inhibitors and Future Research Directions	
<hr/>	
Preface	153
Introduction	154
Initial development of a mass spectrometry based assay for measuring GFAT activity	154
Development of a magnetic-bead pull-down assay for mixture screening of GFAT inhibitors	158

Enhanced characterization of dehydroiso- β -lapachone	164
Secondary SAR analysis with dehydroiso- β -lapachone derivatives	166
<i>In vivo</i> inhibition of GFAT to probe for modulation of downstream effects	168
Alternative therapeutic uses for GFAT inhibitors	169
Conclusion	171
Materials & Methods	172
Sample preparation of L-gln, L-glu, F6P and GlcN6P for MS-detection	172
Sample preparation of L-gln and F6P for MS-detection	172
Protocol for Magnetic Bead (MB) Pull-Down Assay with rhGFAT1-His ₆ ²⁹⁸	172
References	175

List of Figures	Page
	#
Figure 1-1. Overview of diabetes.	3
Figure 1-2. The reaction catalyzed by L-glutamine:D-fructose-6-phosphate amidotransferase (GFAT).	5
Figure 1-3. An adaptation of the Hexosamine Biosynthesis Pathway (HBP).	6
Figure 1-4. The unfolded protein response.	8
Figure 1-5. Proposed mechanism of F6P catalysis in <i>E.coli</i> GlmS.	10
Figure 1-6. Proposed mechanism of L-gln hydrolysis in <i>E.coli</i> GlmS.	11
Figure 1-7. Morgan-Elson assay mechanism for detection of GlcN6P produced by GFAT.	14
<hr/>	
Figure 2-1. A representation of the rhGFAT-1 monomer identifying the glutaminase and isomerase binding domains along with the affinity tag insertion site.	30
Figure 2-2. Schematic of Gateway® Cloning procedure.	32
Figure 2-3. Photograph of agarose gel with purified <i>hgfat1</i> -cDNA PCR amplified samples.	33
Figure 2-4. Photograph of SDS-PAGE stained with Coomassie Blue.	36
Figure 2-5. <i>hgfat1</i> -cDNA genetic sequence with hexa-histidine insertion at position 894.	38
Figure 2-6. Sequencing of the His-tag insert at position 894 with upstream primer LW5HISUP.	39
Figure 2-7. Photograph of SDS-PAGE gel (4% stacking, 10% resolving) with pET-301/CT-DEST <i>rhgfat1</i> -His ₆ ⁸⁹⁴ transformed Rosetta 2™ <i>E.coli</i> cell cultures.	39
Figure 2-8. SDS-PAGE gel (8% stacking, 16% resolving) of FPLC purified rhGFAT-His ₆ ²⁹⁸ , purified with a 5 mL HisTrap FF Ni (II) column (GE Healthcare) on an ÄKTA 100 Purifier FPLC™ system (GE Healthcare).	40

Figure 2-9. Comparison of GFAT activity measured in Rosetta 2™ <i>E.coli</i> cell lysates with the pET-301/CT-DEST hGFAT1-His ₆ ⁸⁹⁴ protein expression clone.	42
Figure 2-10. Determining the activity of rhGFAT-His ₆ ²⁹⁸ following protein purification and buffer exchange assessed by the Morgan-Elson assay.	43
Figure 2-11. Michaelis-Menten kinetics for the glutaminase and isomerase domains of rhGFAT-His ₆ ²⁹⁸ .	43
Figure 2-12. Dose-Response curves for GFAT inhibitor 6-diazo-5-oxo-L-norleucine (DON).	44
<hr/>	
Figure 3-1. Optimal enzyme incubation time for the Morgan-Elson assay.	65
Figure 3-2. Use of acetone and acetonitrile solvents in the Morgan-Elson assay.	66
Figure 3-3. Standard curve with the Morgan-Elson assay, comparison of the “standard” versus the modified method.	68
Figure 3-4. Z-factor determination for the standard Morgan-Elson assay.	69
Figure 3-5. Z-factor determination for HTS-modified Morgan-Elson assay.	69
Figure 3-6. Synthesis of GFAT inhibitor FMDP.	71
Figure 3-7. Dose-response of FMDP.	71
Figure 3-8. Microwave-assisted Bischler-Napieralski reaction scheme to synthesize 6,7-dimethoxy-1-(naphthalen-2-yl)-isoquinoline or EME 384.	72
Figure 3-9. GFAT inhibitor EME 384 dose-response.	72
Figure 3-10. Control data from the pilot screen.	73
Figure 3-11. Duplicate plot of the compounds tested for GFAT inhibitory activity in the pilot screen.	74
Figure 3-12. Structure, name, molecular formula and molecular weight of lead compound identified from pilot screen.	74
Figure 3-13. Dose-response for the aminothiazole hit identified from the pilot screen.	75

Figure 3-14. Controls for the complete HTS of 3950 compounds.	77
Figure 3-15. Duplicate plot of compounds from the primary screen.	77
Figure 3-16a. Dose-response curves for hit compounds 1-16 out of 58.	79
Figure 3-16b. Structure, name, molecular formula, molecular weight, half-maximal inhibitory concentration and supplier ID# for hit compounds 1-16 out of 58.	80
Figure 3-16c. Dose-response curves for hit compounds 17-32 out of 58.	81
Figure 3-16d. Structure, name, molecular formula, molecular weight, half-maximal inhibitory concentration and supplier ID# for hit compounds 17-32 out of 58.	82
Figure 3-16e. Dose-response curves for hit compounds 33-48 out of 58	83
Figure 3-16f. Structure, name, molecular formula, molecular weight, half-maximal inhibitory concentration and supplier ID# for hit compounds 33-48 out of 58.	84
Figure 3-16g. Dose-response curves for hit compounds 49-58 out of 58.	85
Figure 3-16h. Structure, name, molecular formula, molecular weight, half-maximal inhibitory concentration and supplier ID# for hit compounds 49-58 out of 58.	86
Figure 3-17. Structural comparison of UDP- <i>N</i> -acetyl-glucosamine and GFAT hit alloxan.	90
Figure 3-18a. Secondary dose-response curves 1-9 of 13 selected validated hits.	93
Figure 3-18b. Secondary dose-response curves 10-13 of 13 selected validated hits and control EME 384.	94
Figure 3-19. Assay plate layout for the primary screen.	106
<hr/> Figure 4-1. Cytotoxicity of lead compounds against HepG2 cells.	115
Figure 4-2. Representative images of HepG2 cells grown in the presence of varying amounts of 2,6-dimethoxyquinone and control cells with no DMSO, with DMSO, or with tunicamycin.	116
Figure 4-3. Representation of ZIC®-HILIC stationary phase.	118

Figure 4-4. Calibration curves of sugar-standards with the ZIC®-HILIC column.	119
Figure 4-5. UPLC/MS chromatogram of UDP-GlcNAc detection in untreated HepG2 cells.	119
Figure 4-6. Measurement of UDP-GlcNAc levels as the relative response factor (RRF) over cell concentration in HepG2 cells treated with glucosamine (GlcN) for 24 hours.	121
Figure 4-7. UDP-GlcNAc levels in HepG2 cells following 24-hr treatment with amrinone.	122
Figure 4-8. UDP-GlcNAc levels in HepG2 cells following 24-hr treatment with alloxan.	122
Figure 4-9. UDP-GlcNAc levels in HepG2 cells following 24-hr treatment with lapachol.	123
Figure 4-10. Microwave assisted Pictet-Spengler/oxidation reaction for the synthesis of substituted isoquinolines.	125
Figure 4-11. SAR data of synthetic 6,7-dimethoxyisoquinoline derivatives.	125- 126
Figure 4-12. Hantzsch reaction for aminothiazole synthesis.	127
Figure 4-13. SAR data of aminothiazole derivatives.	128
Figure 4-14. Dose-response for aminothiazole TS-1-24.	129
Figure 4-15. Schematic of pyridinone focused library synthesis with microwave-assisted Suzuki cross-coupling reactions.	130
Figure 4-16. SAR data of pyridinone derivatives.	130- 131
Figure 4-17. Active and inactive quinones identified from the primary screen.	133
Figure 4-18. Schematic of substituted 1,4-naphthoquinones with lawsone precursor.	134
Figure 4-19. SAR data of quinone derivatives.	135- 137

Figure 4-20. Dose-response curve and structure of dehydroiso- β -lapachone, identified as a potent GFAT inhibitor.	137
Figure 4-21. Viability of HepG2 cells treated with dehydroiso- β -lapachone.	140
Figure 4-22. Effect of F6P on the dose-response and IC_{50} of dehydroiso- β -lapachone.	141
Figure 4-23. Effect of L-Gln on the dose-response and IC_{50} of dehydroiso- β -lapachone.	141
Figure 4-24. A representation of a reversible noncompetitive inhibitor.	142
<hr/>	
Figure 5-1. Benzoboroxole binding to a glycopyranoside under biological pH.	157
Figure 5-2. Schematic for the Alizarin Red S Assay.	159
Figure 5-3. Schematic of Magnetic-Bead (MB) pull-down assay with MS detection.	160
Figure 5-4. Comparison of ligand fishing for GFAT inhibitor EME-384.	162
Figure 5-5. ESI-MS/MS spectra of 5 bioactive mixtures with the MB pull-down assay.	163
Figure 5-6. Structure of solasodine.	164
Figure 5-7. Treatment of HepG2 cells with dehydroiso- β -lapachone and detection of UDP-GlcNAc <i>via</i> UPLC-MS.	165
Figure 5-8. β -lapachone derivative reaction scheme.	167
Figure 5-9. Synthetic scheme for <i>ortho</i> and <i>para</i> substituted 1,4-naphthoquinones.	168
<hr/>	
Equation 3-1. Z-factor.	64

List of Tables	Page
	#
Table 1-1. L-glutamate substrate and inhibitor derivatives.	15
Table 1-2. D-GlcN6P product and inhibitor derivatives.	16
Table 1-3. Non-substrate analog inhibitors of GFAT.	16
Table 2-1. Reagents used for PCR to isolate <i>hgfat1</i> -cDNA for use with Gateway® Cloning vector pDONR 221.	46
Table 2-2. Reagents used for PCR to insert 3 histidine codons at gene position 894 in <i>hgfat1</i> -cDNA within the pDONR221 entry clone.	51
Table 2-3. Buffer reagents required for complete GFAT purification, from cell lysis to enzyme storage.	53
Table 2-4. Stock solutions and reagents required for the Morgan-Elson assay with Ehrlich's reagent.	55
Table 3-1. Optimal enzyme concentration for the Morgan-Elson assay.	65
Table 3-2. Optimal incubation time for Ehrlich's Reagent with the modified Morgan-Elson assay.	67
Table 3-3. List of suppliers from the bioactive subset of the Canadian Compound Collection and academic labs comprising the small molecule libraries screened.	76
Table 3-4. Hit compounds selected for validation.	87-88
Table 3-5. Comparison of IC ₅₀ values from the primary and secondary dose-response screening and lead selection.	95
Table 3-6. Reagents present in incubation step of HTS-modified Morgan-Elson Assay.	98
Table 3-7. Reagents required for over-night acetylation reaction of HTS-modified Morgan-Elson Assay.	98
Table 3-8. Addition of Ehrlich's reagent to the HTS-modified Morgan-Elson assay for visualization of production of <i>N</i> -acetyl-glucosamine-6-phosphate.	99

Table 5-1. Mass spectrometry data for substrates and products of GFAT from the Finnigan LCQ Deca Mass Spectrometer.	156
Table 5-2: Mass Spectrometer Parameters for the AB Applied Biosystems MDS Sciex QTrap LC/MS/MS System with GFAT substrates F6P and L-gln.	156
Table 5-3. Reagents for Magnetic Bead Affinity Pull-Down assay with rhGFAT-His ₆ ²⁹⁸ .	174

List of Abbreviations and Symbols

aa: amino acid

A1C: glycated hemoglobin

AcSCoA: acetyl-coenzyme A

AMPO: arabinose-5-methylenephosphonate oxime

Amp^R: ampicillin resistant

ANOVA: analysis of variance

APO: arabinose-5-phosphate oxime

Arg: L-arginine

Asp: L-aspartic acid

att: attachment sites

BiP: binding protein

BDAP: *N*³-bromoacetyl-L-2,3-diaminopropanoic acid

BLAST: basic local alignment search tool

Boc-Asn-OH: *N*²-t-butoxycarbonyl-L-asparagine

Boc-Dap-OH: (5)-3-amino-2-(tert-butoxycarbonylamino)-propanoic acid

bp: base pairs

Cam^R: chloramphenicol resistant

cDNA: complementary DNA

CHOP: C/EBP (CCAAT/enhancer binding protein) homologous protein or DNA damage-inducible transcript 3

Cys: L-cysteine

DCM: dichloromethane

DMF: dimethylformamide

DMSO: dimethyl sulphoxide

DON: 6-diazo-5-oxo-L-norleucine

DPP-4: dipeptidyl peptidase-4 inhibitors

DSON: dimethylsulphonium salt

DTT: dithiothreitol

E.coli: Escherichia coli

EDCI: *N*-(3-dimethylaminopropyl)-*N*'-ethylcarbodiimide

EDTA: ethylenediaminetetraacetic acid

eIF2 α : translation initiation factor 2-alpha

EME-384: 6,7-dimethoxy-1-(naphthalen-2-yl)-isoquinoline

ER: endoplasmic reticulum

ERAD: endoplasmic reticulum associated degradation

ESI-MS/MS: Electrospray ionization – mass spectrometry

EtOAc: ethyl acetate

F6P: D-fructose-6-phosphate

FCDP: *N* ^{β} -fumarylcarboxyamido-L-2,3-diaminoproplonic acid

FMDP: *N*³-(4-methoxyfumaroyl)-L-2,3-diaminopropanoic acid

FPLC: fast protein liquid chromatography

FPG: Fasting plasma glucose

GALE: uridine-diphosphate-galactose-4-epimerase

GC: gas chromatography

GDP-Man: guanosine diphosphate mannose

Gfa: L-glutamine: D-fructose-6-phosphate amidotransferase (eukaryotic)

GFAT: L-glutamine: D-fructose-6-phosphate amidotransferase (mammalian)

Glc: glucose

Glc6P: D-glucose-6-phosphate

GlcN: D-glucosamine

GlcNAc: *N*-acetyl-D-glucosamine

GlcN1P: D-glucosamine-1-phosphate

GlcN6P: D-glucosamine-6-phosphate

GlcNAc1P: *N*-acetyl-D-glucosamine-1-phosphate

GlcNAc6P: *N*-acetyl-D-glucosamine-6-phosphate

GlmS: glucosamine-6-phosphate synthetase (prokaryotic)

Gln: L-glutamine

GLP-1: glucagon-like peptide-1 receptor agonists

Glu: L-glutamate

Gly: L-glycine

Gly-phe: glycine-phenylalanine

GPR119: G-protein coupled receptor 119

GRP78: glucose-regulated protein 78

GRP94: glucose-regulated protein 94

GSK-3 β : glycogen synthase kinase-3 β

HBP: Hexosamine Biosynthesis Pathway

HSCoA: coenzyme A

HepG2: human hepatocarcinoma cells

His: L-histidine

His₆: hexa-histidine affinity tag

HPLC: high-performance liquid chromatography

HTS: High-throughput screening

IC₅₀: half-maximal inhibitory concentration

IMAC: immobilized metal ion affinity chromatography

IPTG: isopropyl β -D-1-thiogalactopyranoside

Kan^R: kanamycin resistant

K_i: inhibition constant

K_M: Michaelis-Menten constant

Lys: L-lysine

MALDI-TOF-MS: matrix-assisted laser desorption ionization time-of-flight mass spectrometry

Met-tRNA: methionyl transfer ribonucleic acid

MPAH: 5-methylphosphono-D-arabino hydroximolactone

MOBIX: McMaster Institute for Molecular Biology and Biotechnology

MOI: mode of inhibition

MRM: multiple reaction monitoring

NIDDM: non-insulin dependent diabetes mellitus

O-glcNAc: O-linked *N*-acetyl glucosamine (on amino acid Ser or Thr)

OGT: Uridine diphospho-*N*-acetylglucosamine:polypeptide β -*N*-acetylglucosaminyltransferase

OGTT: Oral glucose tolerance test

PBS: phosphate buffered saline

PCR: polymerase chain reaction

PIDA: iodosobenzene diacetate

PIFA: bis[trifluoroacetoxy]-phenyliodine

PMSF: phenylmethylsulphonyl fluoride

rhGFAT1-His₆²⁹⁸: recombinant human L-glutamine:D-fructose-6-phosphate amidotransferase 1, internal hexa-histidine affinity tag at amino acid position 298

RRF: relative response factor

SAR: structure-activity relationship

SDS-PAGE: sodium dodecyl sulphate polyacrylamide gel electrophoresis

Ser: L-serine

SGLT2: sodium glucose cotransporter 2

TCEP-HCl: tris (2-carboxyethyl) phosphine hydrochloride

THF: tetrahydrofuran

Thr: L-threonine

TOF-MS: time-of-flight mass spectrometry

Trp: L-tryptophan

UDP: uridine diphosphate

UDP-G: uridine diphosphate glucose

UDP-GalNAc: uridine diphospho-*N*-acetyl-D-galactosamine

UDP-GlcNAc: uridine diphospho-*N*-acetyl-D-glucosamine

UPLC-TOF-MS: ultra high-performance liquid chromatography time-of-flight mass spectrometry

UPR: unfolded protein response

γ-GHM: gamma-glutamylhydroxamate

γ-Glu(P): DL-Methyl *N,N*-diethyl-[3-amino-3-methoxycarbonylpropyl]-*SR*-phosphonamidate.

γ-GSA: glutamate gamma-semi aldehyde

Z': Z-factor

ZIC[®]-HILIC: zwitterionic charge – hydrophilic interaction liquid chromatography

Chapter 1

L-glutamine:D-fructose-6-phosphate
amidotransferase (GFAT) and its role in the
secondary complications of diabetes

The socio-economic impact of Type 2 diabetes mellitus

Type 2 diabetes mellitus is a metabolic disorder characterized by hyperglycemia, a decrease in insulin production and/or a decrease in insulin sensitivity (Figure 1-1).¹ The total number of people with diabetes worldwide was estimated to be 171 million for 2000 and is projected to more than double by 2030.² In 2000, it was reported that 1.4 million Canadians were diagnosed with diabetes and that in 2016 this number will rise to 2.4 million. The cost of treatment for diabetes and related complications is expected to reach \$8.14 billion nationwide by 2016.³

As of 2007, in the United States, Type 2 diabetes was the sixth leading cause of death and the number one cause of kidney disease requiring dialysis. Type 2 diabetes is also a major cause of acquired blindness and lower-limb amputation unrelated to trauma. Diabetes is a major independent risk factor for cardiovascular disease and the majority of people with diabetes will die of cardiovascular complications.⁴ Costs of diabetes can be assessed in four areas: direct medical costs, including physician time and hospitalization for complications (dialysis, angioplasty, amputation, etc.); non-direct medical costs incurred by the patient; indirect costs to society including loss of productivity in the workforce; and other indefinable costs due to a decreased quality of life caused by complications.⁵ Having one or more complications can cause a significant economic impact due to the cost of treatment combined with loss of workplace productivity.⁶

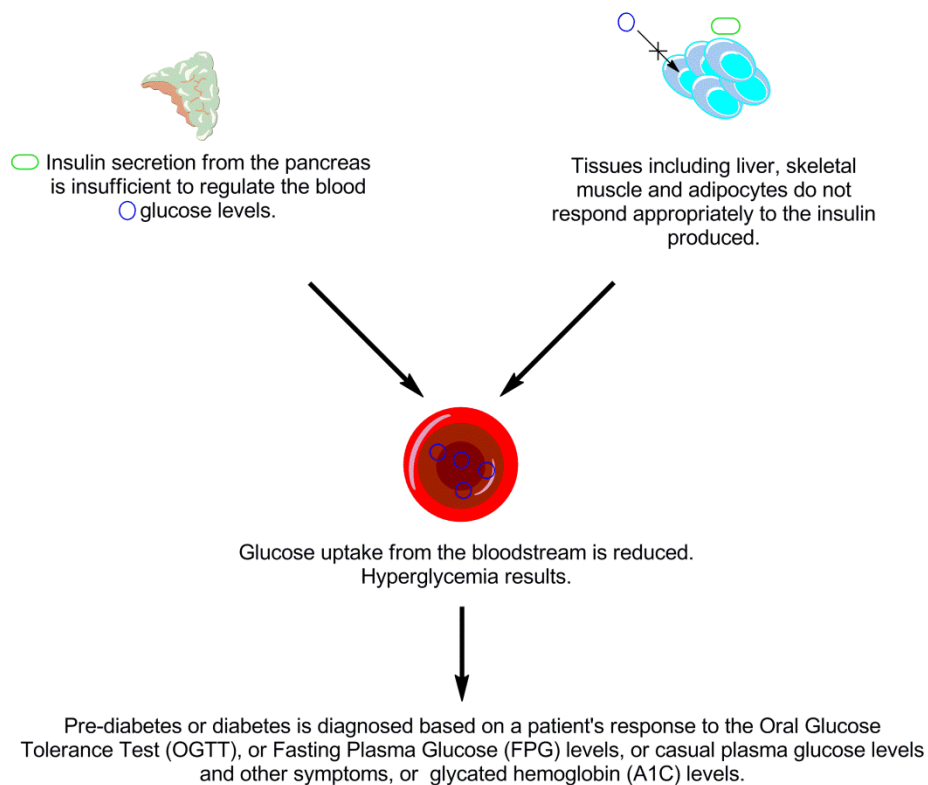


Figure 1-1. Overview of diabetes. Diabetes mellitus is a group of metabolic diseases identified by hyperglycemia as a result of defective or insufficient insulin secretion from the pancreas.⁷ In type 2 diabetes this is associated with insulin resistance in peripheral tissues. Pre-diabetes or diabetes are diagnosed based on glucose levels measured after diagnostic testing.⁸ Intervention is required to mediate the situation as chronic hyperglycemia is associated with long term damage and dysfunction of major organ systems.

Secondary complications resulting from diabetes are prevalent on the micro⁹ and macrovascular level.¹⁰ They include diabetic neuropathy,¹¹ nephropathy,¹² retinopathy,¹³ atherosclerosis,¹⁴ cardiovascular disease¹⁵ and heart failure.¹⁶ Other complications include erectile dysfunction¹⁷ and osteoporosis.¹⁸ Even after a patient is able to maintain tight glycemic control, often secondary complications persist. This situation is referred to as “metabolic memory” and high-lights the need for treatments to directly prevent diabetic complications.¹⁹

Current and future pharmaceutical treatments for Type II diabetes mellitus

There is no cure for diabetes. Treatment strategies focus upon controlling blood glucose levels and managing complications associated with diabetes. Current pharmaceutical treatments to manage non-insulin dependent Type 2 diabetes include: insulin secretagogues (sulphonylureas and rapid-acting prandial insulin releasers); α -glucosidase inhibitors; insulin sensitizers (metformin and thiazolidinediones);²⁰ and amylin analogues.²¹ However these medications are not without side-effects. Sulphonylureas can cause minor hypoglycaemia and weight gain, and some are not recommended for use in patients at high-risk of developing coronary artery disease.²⁰ α -glucosidase inhibitors can cause gastrointestinal discomfort and as a result some patients will discontinue use of the drug.²² Metformin has a risk of renal insufficiency.²⁰ Thiazolidinones can cause weight gain and rosiglitazone has been associated with an increased risk of myocardial infarction.²³

New pharmaceutical targets for Type 2 diabetes include glucagon-like peptide-1 receptor agonists (GLP-1), dipeptidyl peptidase-4 inhibitors (DPP-4),²⁴ sodium glucose cotransporter 2 (SGLT2) inhibitors,²⁵ and G-protein coupled receptor 119 agonists (GPR119).²⁶ GLP-1 agonists help with long-term glucose control while DPP-4 inhibitors primarily target postprandial hyperglycemia. SGLT2 inhibitors increase the urinary excretion of glucose and lower plasma glucose levels. Agonists of GPR119 are a potential non-peptidyl alternative to GLP-1 agonists.

Current pharmaceutical treatments have been effective in managing diabetes and new treatments show promise for tighter hyperglycemia control. Only a select few

have some benefit in treating complications.^{22, 27} There is a definite need for affordable, well-tolerated and easily administered medications to help combat the detrimental secondary side-effects of diabetes.²⁸

Introduction to the Hexosamine Biosynthesis Pathway, ER Stress and their role in diabetes and diabetic complications

The hexosamine biosynthesis pathway (HBP) is responsible for the synthesis of glucosamine-6-phosphate and glycoproteins for secondary protein modification. About 3% of the glucose which enters the glycolytic pathway is metabolized via the HBP.²⁹ The HBP appears to function as a nutrient sensor³⁰ and plays a role in pancreatic- β -cell function,³¹ insulin resistance and vascular complications of diabetes.²⁹ The enzyme L-glutamine: D-fructose-6-phosphate amidotransferase (GFAT) is involved in the first and rate limiting step of the HBP. GFAT activity has been implicated in the development of insulin resistance³² and diabetic complications.³³



Figure 1-2. The reaction catalyzed by L-glutamine:D-fructose-6-phosphate amidotransferase (GFAT). GFAT is an enzyme which catalyzes the irreversible reaction between L-glutamine and D-fructose-6-phosphate. The products D-glucosamine-6-phosphate and L-glutamate are the result. This is the first reaction in the hexosamine biosynthesis pathway (HBP).

Upon entering the cell, glucose is immediately phosphorylated to yield glucose-6-phosphate (Glc6P) which is subsequently converted to D-fructose-6-phosphate (F6P). GFAT catalyzes the reaction between F6P and L-glutamine (L-gln) to yield D-glucosamine-6-phosphate (GlcN6P) and L-glutamate (L-glu)(Figure 1-2).³⁴ The major end product of the HBP is uridine diphospho-*N*-acetyl-D-glucosamine (UDP-GlcNAc) which is

an allosteric feedback inhibitor of GFAT and therefore regulates glucose entry into the pathway. Prokaryotic forms of the enzyme are insensitive to feedback inhibition by UDP-GlcNAc. It is speculated that there is an additional allosteric binding site for UDP-GlcNAc in the eukaryotes. UDP-GlcNAc is a building block for proteoglycans, glycoproteins and glycolipids present in the endoplasmic reticulum (ER) and Golgi (Figure 1-3).

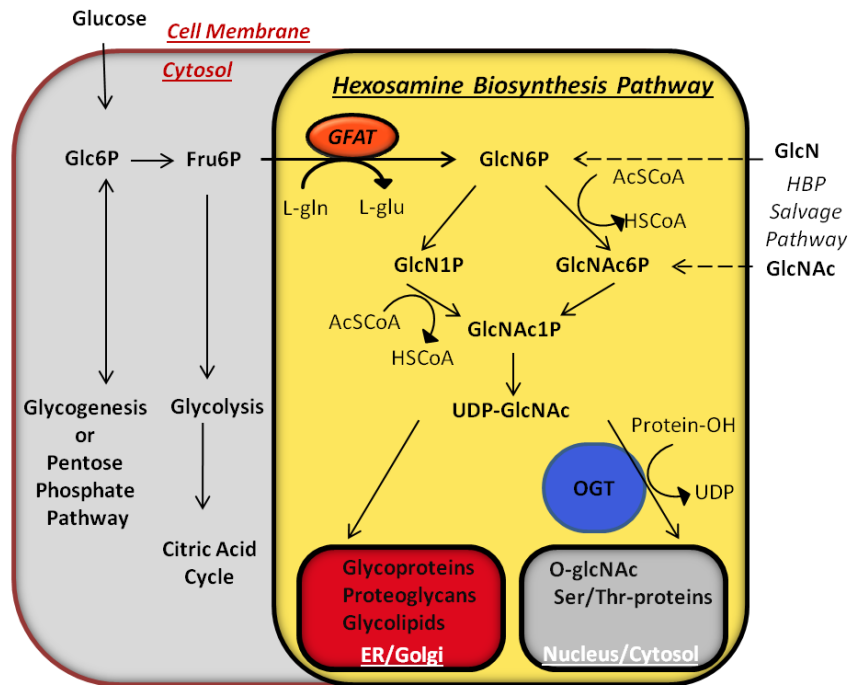


Figure 1-3. An adaptation of the Hexosamine Biosynthesis Pathway (HBP). About 3% of all glucose that enters the cell will enter the HBP where GFAT is the first and rate-limiting enzyme of the pathway. The glucose is ultimately converted into UDP-*N*-acetyl-glucosamine-6-phosphate (UDP-GlcNAc), a product which is used in the post-translational modification of proteins. In the ER, UDP-GlcNAc is used for *N*-linked glycosylation of proteins required for proper protein folding.³⁵ In the nucleus or cytosol, UDP-GlcNAc is used by uridine diphospho-*N*-acetylglucosamine:polypeptide β -*N*-acetylglucosaminyltransferase (OGT) for *O*-linked glycosylation involved in cell signaling.^{29,36}

Secondary diabetic complications have also been linked to endoplasmic reticulum (ER) stress, a state where unfolded or misfolded proteins accumulate in the ER.³⁷ The ER is an organelle responsible for lipid synthesis, protein folding and modification of

membrane proteins and proteins to be secreted.^{35,38} Post-translational modifications in the ER include glycosylation and the formation of intra and intermolecular disulphide bonds. Protein glycosylation is essential for the proper folding of many proteins³⁹ and UDP-GlcNAc is an essential substrate used for *N*-linked protein glycosylation in the ER.⁴⁰ Only correctly folded proteins will be directed to the Golgi complex, whereas unfolded proteins remain in the ER to complete folding or are targeted for degradation. When the protein-folding machinery is exhausted due to over-expression of native proteins, the concentration of unfolded proteins is increased. Unfolded proteins have their hydrophobic groups exposed and pose a risk of toxic aggregation.⁴¹ In this scenario the ER is stressed and the unfolded protein response (UPR) is initiated to return the ER to homeostasis.^{37, 42}

The first response to ER stress is a general inhibition of protein translation by phosphorylation of eIF2 α (translation initiation factor 2-alpha) which will effectively prevent binding of Met-tRNA to the ribosome. Second, there is a specific upregulation of the expression of ER chaperone proteins including glucose-regulated proteins (GRP)78 and (GRP)94. GRP78 is also known as Binding Protein (BiP). These proteins help to increase protein folding activity, avert any protein aggregation and are part of the UPR. Third, any unfolded or misfolded proteins which cannot be saved by the chaperone proteins are degraded. This process is referred to as ER-associated degradation (ERAD). Proteins are removed from the ER and transported to the cytosol to await degradation by the 26S proteasome. Lastly, if ER homeostasis is not re-established, ER stress has

been shown to stimulate apoptosis through induction of CHOP, a member of the family of C/EBP transcription factors (Figure 1-4).⁴³

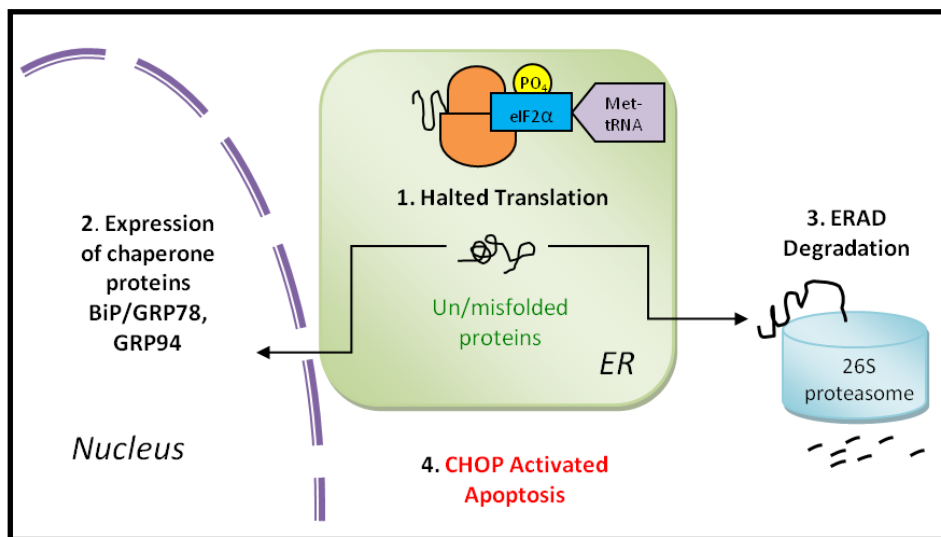


Figure 1-4. The unfolded protein response. Figure adapted from Araki *et al.*⁴³ 1) Further translation of proteins in the ribosome is halted, 2) ER chaperone protein transcription is induced, 3) Any proteins which remain misfolded despite presence of chaperone proteins are degraded, 4) If ER homeostasis is not reinstated and misfolded proteins continue to increase, CHOP will be induced in response to stress and promote apoptosis.

Evidence has shown a connection between ER stress and the development of the secondary side effects of Type 2 diabetes mellitus⁴¹ such as insulin degradation,⁴⁴ pancreatic β -cell death,⁴³ retinopathy,⁴⁵ atherosclerosis⁴⁶ and kidney disease.⁴⁷ The mechanisms linking HBP and ER stress are not known, but GFAT is an enzyme of interest in the matter. We have found over-expression of GFAT can induce ER-stress and inflammation,⁴⁸ and glucosamine-induced ER stress plays a role in atherogenesis.⁴⁹

Background to GFAT

GFAT is a relatively large enzyme ranging from 589 amino acids (aa) in *Methanobacterium*, to 716 aa in yeast.³⁴ Both prokaryotic and eukaryotic varieties have a distinct glutaminase N-terminal domain and an isomerase (F6P binding) C-terminal

domain. The N-terminal and C-terminal domains are relatively well conserved with roughly 49% sequence identity within eukaryotic species.³⁴

Human GFAT is expressed as 3 different variants, GFAT1, GFAT2⁵⁰ and splice isoform GFAT1-L.⁵¹ GFAT1 and GFAT2 have a 79% sequence identity, whereas the splice isoform has a 48-54 bp insert as compared to GFAT1. The enzymes have different expression profiles in tissues. In a mouse model, GFAT1 is expressed in the heart, placenta, lung, liver, skeletal muscle, kidney, pancreas, spleen, prostate, testis and colon, whereas GFAT2 has strong expression throughout the central nervous system and ovaries. The majority of GFAT1-L is expressed in skeletal muscle, along with the heart and brain. Due to the widespread expression of GFAT1, especially in pancreatic, liver, heart, and skeletal muscle tissues, our research efforts focus on this variant.

Human GFAT-1 (hGFAT1), EC 2.6.1.16, exists as a homotetramer comprised of 4 monomers of 681 amino acids in length and 77 kDa in mass.⁵² The gene, *gfpt1*, encodes the enzyme and is 3.1 kb in length and located at chromosome 2p13.⁵³ Regulation of GFAT appears to be largely controlled at the post-transcriptional level.⁵⁴ The enzyme has been demonstrated to be regulated by phosphorylation *in vitro*⁵⁵ and gene transcription is regulated by epidermal growth factor and glucose.⁵⁶ In terms of kinetics, hGFAT-1 has a Michaelis-Menten constant (K_M) of 0.007-0.41 mM for F6P and 0.26-0.61 mM for L-gln when catalyzing the synthase reaction to form glucosamine.⁵⁷

Enzyme mechanism of action and structural characteristics

The mechanism of action has only been studied in detail for the *E.coli* glucosamine-6-phosphate (GlmS) version of the enzyme and is based on X-ray

crystallography data. The enzyme action is irreversible; F6P cannot be formed from GlcN6P. It follows an ordered bi–bi process.⁵⁷ The reaction commences upon binding of F6P to the isomerase domain. This triggers a conformational change in the enzyme to accept glutamine binding at the glutaminase domain. The Cys1 thiol from the glutaminase domain is an activated nucleophile and is free to attack the amide carbon of L-gln to release ammonia. L-glu is the first released product. During this process the ammonia passes through a channel^{32b} to the isomerase domain where linearized F6P is waiting. A ketimine intermediate is formed, followed by ring-closure to yield the pyranose GlcN6P (Figure 1-5,6).⁵⁷

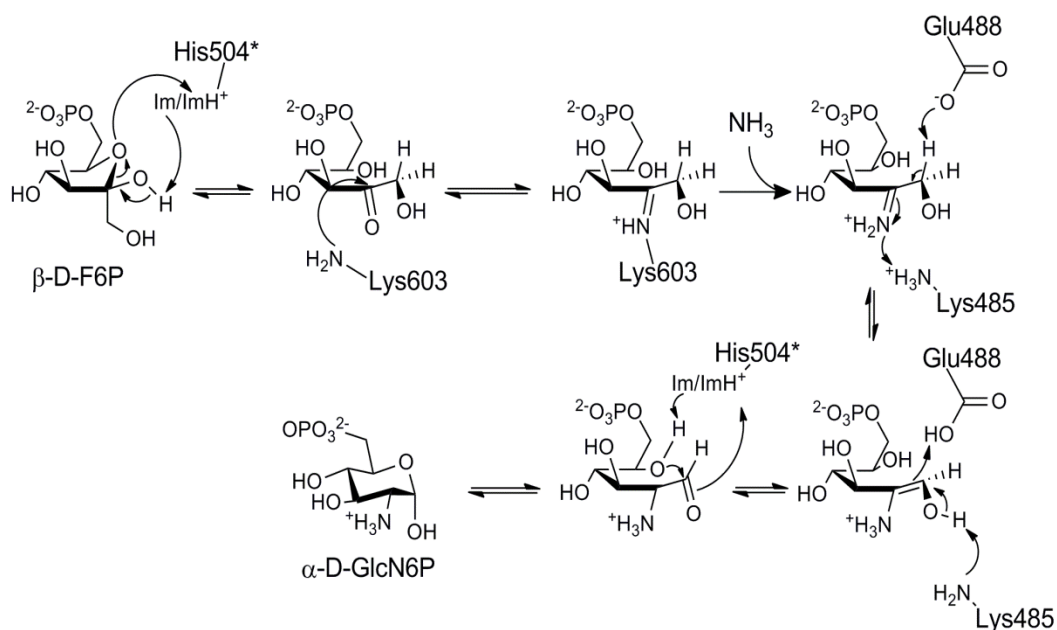


Figure 1-5. Proposed mechanism of F6P catalysis in *E. coli* GlmS. Adapted from Durand *et al.*⁵⁷ The amino acids which make up the C-terminal tail, residues 600-608, and the residues which make up the His loop (His 504, the asterisk indicates this amino acid is from an adjacent subunit) are mainly responsible for F6P catalysis. Following binding of the sugar, the pentose ring is opened and a Schiff base intermediate is formed with Lys603. NH₃ is a product of L-gln hydrolysis and reacts to form the ketimine intermediate. Ring closure is assisted with residues Glu488, Lys485, and His504. The hexosamine sugar is the final product and is released after L-glu.

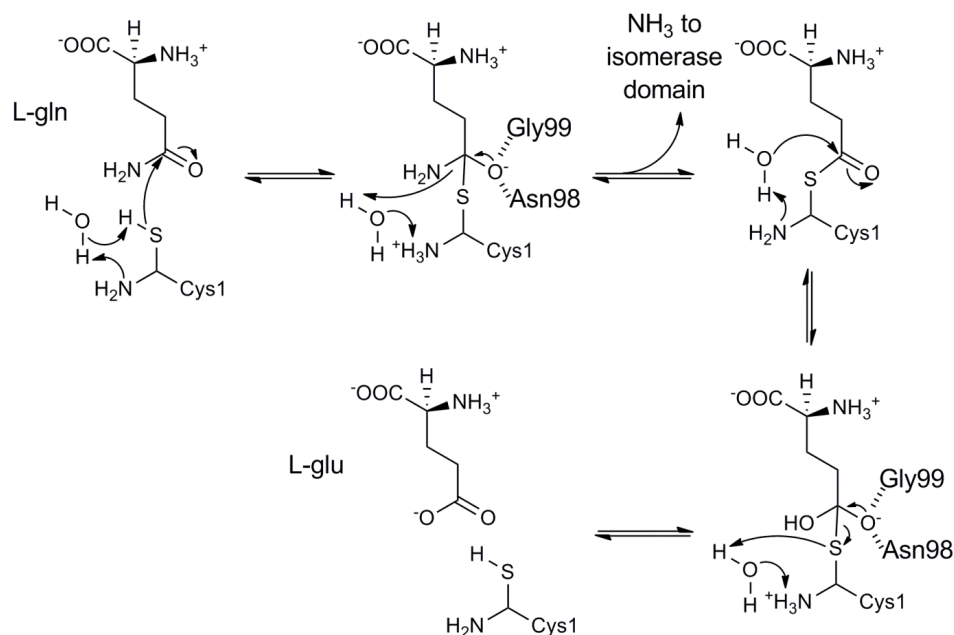


Figure 1-6. Proposed mechanism of L-gln hydrolysis in *E. coli* GlnS. Adapted from Durand *et al.*⁵⁷ The N-terminal Cys1 residue is the key factor in L-gln catalysis. With a water molecule, the reduced thiol of Cys1 is able to attack the carbonyl carbon of the amide. Gly99 and Asn98 help to stabilize the intermediate through hydrogen bonding. The NH₃ molecule is channeled towards the isomerase domain after cleavage. L-glu is formed following attack of a water molecule on the thioester intermediate. L-glu is released first before GlcN6P.

The crystal structure of *E. coli* GlnS has been elucidated,⁵⁸ as well as high-resolution images of the glutamine binding and isomerase domain.^{41, 59} The glutaminase domain shows a sandwich of anti-parallel β -sheets with layers of α -helices surrounding them. The active site for glutamine-binding is in the N-terminal end, and involves the Cys1 residue. There are two flexible loops on the glutamine binding site, residues 73-80 which make the Q-loop and residues 25-29, which are speculated to function as a lid which closes around the substrate after binding. The residues 25-29 are thought to rearrange after F6P has bound to the isomerase domain and this allows L-gln to be in the proper conformation for hydrolysis.

The isomerase domain is composed of two structurally identical subdomains within residues 241-424 and 425-592. These subdomains consist of an $\alpha\beta\alpha$ sandwich with a 5-stranded parallel β -sheet in between a set of α -helices. The domain also has an irregular loop at the C-tail between residues 593-608.

As for hGFAT-1, the structure of the isomerase domain has been partially characterized with cyclic Glc6P and linear GlcN6P.⁶⁰ This area contains a 43% sequence identity with the isomerase domain of *E.coli* GlmS, and also contains two similar subdomains of an $\alpha\beta\alpha$ sandwich. The study is also in agreement that the C-tail and His-loop are involved with substrate binding.

In vitro GFAT stability

Unfortunately, GFAT is not commercially available, is present in low abundance in natural sources, is unstable and difficult to purify.⁶¹ However, conditions have been identified by Broschat *et al* which help to stabilize the enzyme and preserve activity. Inclusion of F6P and reducing agent dithiothreitol (DTT) stabilize the enzyme for up to 350 hours when stored at 4 °C. UDP-GlcNAc and L-glutamine also help to slow the loss of enzyme activity but they are not as effective. With no additive, the half-life of hGFAT1 was 2 hours. Thus, when isolating hGFAT1 it was highly recommended to use F6P and DTT to retain enzyme activity.

Measurement of GFAT activity with the Morgan-Elson assay

There have been several assay methods published in which to study GFAT; indirectly using enzyme-coupled assays,⁶² radiometric assays,⁶³ HPLC⁶⁴ or GC⁶⁵ based

assays, or MALDI-TOF-MS.⁶⁶ The procedure most promising for our studies was a spectrophotometric end-point assay utilizing Morgan-Elson chromagens⁶⁷ for detection of glucosamine-6-phosphate. The Morgan-Elson endpoint assay utilizes Ehrlich's Reagent (an acidic solution of *p*-dimethylaminobenzaldehyde) which forms a chromophore measurable at 585 nm when in the presence of *N*-acetyl-glucosamine-6-phosphate (GlcNAc6P). The assay method, originally published in 1933 by Morgan and Elson for the detection of glucosamine and chondrosamine in dilute alkali solution,⁶⁸ has undergone several modifications. Reissig *et al* used a borate buffer which increased the colour development and shortened the reaction time.⁶⁹ Levy *et al* improved the acetylation step to enable detection of glucosamine,⁷⁰ while Richards and Greengard applied the method to hexosamine detection in tissues.⁷¹

The spectrophotometric assay utilized in the present thesis is adapted from the procedure described in European Patent Application EP 1 431 396 A1.^{67a} The assay has been formulated specifically for the detection of GFAT activity in a microwell plate format. The assay has several advantages over other assay methods, it is simple to perform and does not require any specialized equipment uncommon to a modern chemical biology laboratory, it measures the production of GlcN6P directly and it can be used with different tissues or enzyme extracts without any prior purification. All reagents for the assay are commercially available and the assay can be performed within a 2 hour time frame.

The assay takes place in three steps. First the tissue extract or GFAT preparation is incubated at 37 °C with its substrates, buffer, reducing agent, and with or without an

added inhibitor. This facilitates the production of GlcN6P, which is acetylated in the second step by heating acetic anhydride in alkali potassium tetraborate at 80 °C. *N*-acetyl-glucosamine-6-phosphate is readily detected after incubation at 37 °C with the acidic Ehrlich's Reagent, which results in production of a dark pink colour measurable at 585 nm.

The mechanism of the assay works by the base-catalyzed ring opening of the hemi-acetal of the *N*-acetylated glucosamine, which in the linearized form of the sugar a reducing aldehyde is present (Figure 1-7).^{67b} This changes to its enolic form and eliminates water with the formation of a heterocyclic ring with the adjacent amide. This oxazole structure is what condenses with *p*-dimethylaminobenzaldehyde and displays the pinkish-purple colour measurable at 585 nm.

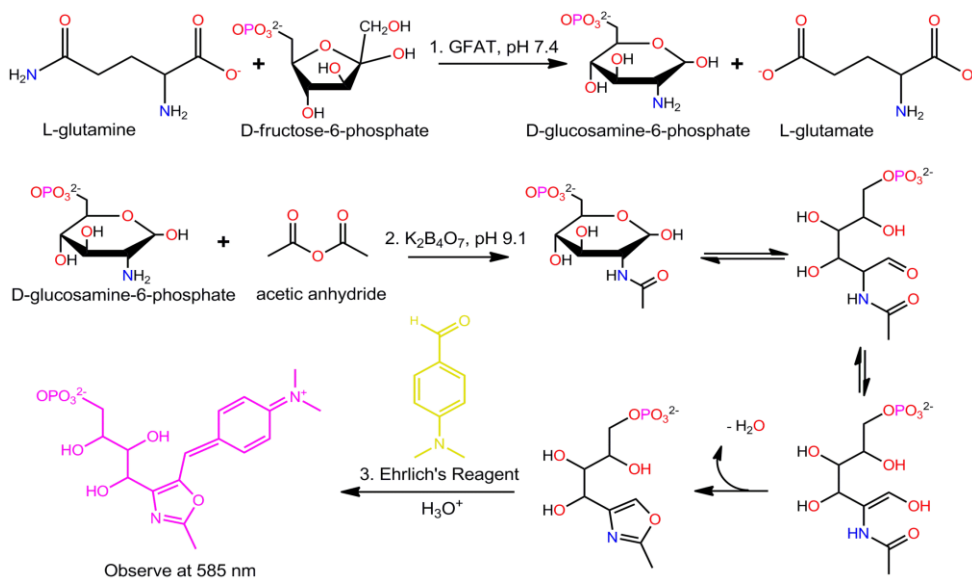


Figure 1-7. Morgan-Elson assay mechanism for detection of GlcN6P produced by GFAT. After the enzyme has produced GlcN6P, it is acetylated under basic conditions. This also initiates the formation of an oxazole ring which will condense with Ehrlich's reagent under acidic conditions to form a readily visible chromophore.

Known GFAT inhibitors

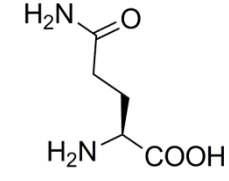
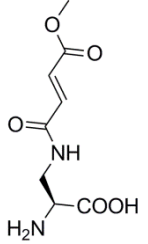
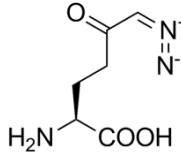
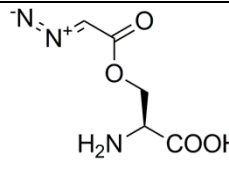
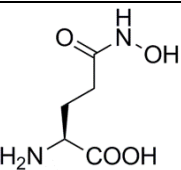
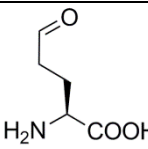
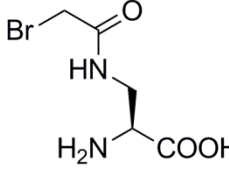
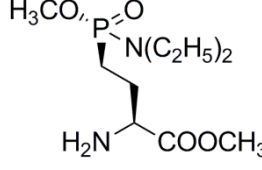
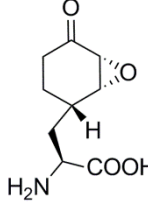
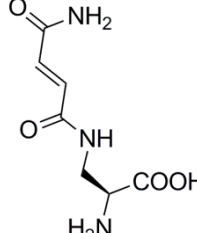
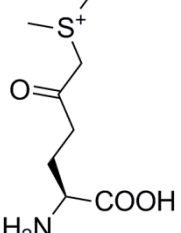
		
L-glutamine, substrate	FMDP, $IC_{50}=4 \mu M^{67a}$	DON, $IC_{50}=18 \mu M^{67a}$
		
Azaserine, $K_i=0.77 \text{ mM}^{72}$	γ -GHM, $K_i=95 \mu M^{72}$	γ -GSA, $K_i=23 \mu M^{73}$
		
BDAP, $IC_{50}=0.38 \mu M^{67a, 74}$	γ -Glu(P), $K_i=235 \mu M^{75}$	Anticapsin, $K_i=1 \mu M^{76}$
		
FCDP, $K_i=19 \mu M^{77}$	DSON, $K_i=0.37 \mu M^{78}$	

Table 1-1. L-glutamate substrate and inhibitor derivatives. Adapted from Milewski.³⁴ These are a variety of known inhibitors which are competitive for the glutaminase binding site. The majority have been assayed with *E.coli* or *S. typhimurium*^{72, 77} GlmS.

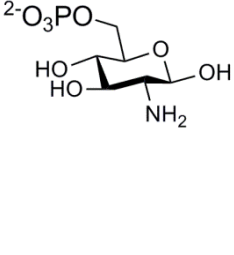
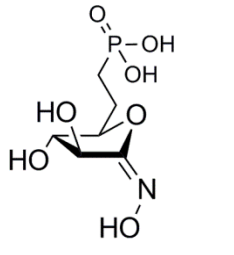
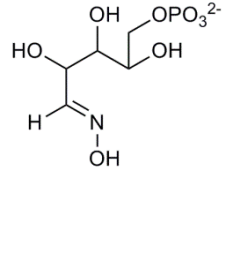
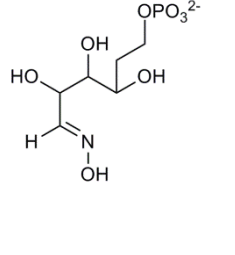
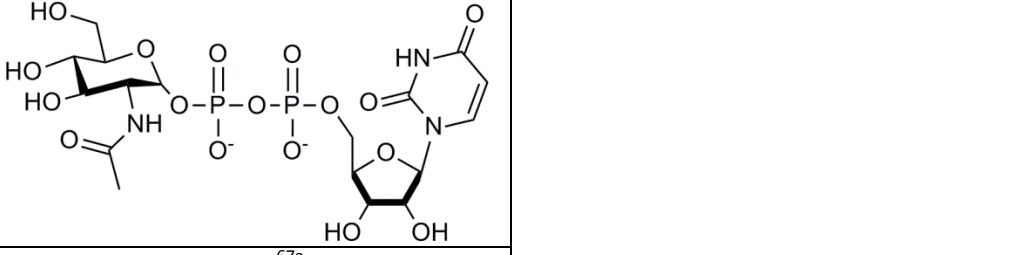
			
D-GlcN6P, $K_i=6 \mu\text{M}$ ⁷⁹	MPAH, $K_i=0.4 \text{ mM}$ ⁸⁰	APO, $K_i=14.3 \mu\text{M}$ ⁸¹	AMPO, $K_i=0.36 \text{ mM}$ ⁸¹
			
UDP-GlcNAc, $\text{IC}_{50}=8 \mu\text{M}$ ^{67a}			

Table 1-2. D-GlcN6P product and inhibitor derivatives. Adapted from Milewski.³⁴ The product D-GlcN6P exhibits feedback inhibition towards hGFAT-1, along with UDP-GlcNAc. The other inhibitors, MPAH, APO, and AMPO, are synthetic transition state mimics proposed to bind at the isomerase domain. They have been assayed with *E.coli* GlmS.

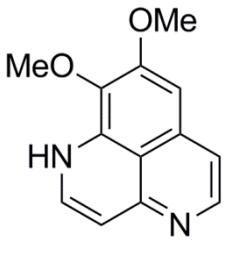
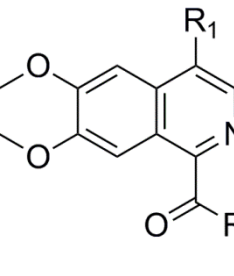
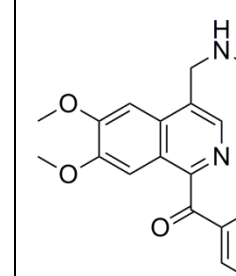
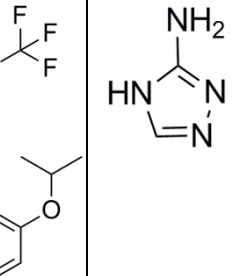
			
Aptamine, $\text{IC}_{50}=120 \mu\text{M}$ ⁸²	Patented GFAT inhibitor scaffold ⁸³	Compound 28, $\text{IC}_{50}=1 \mu\text{M}$ ⁸⁴	Amitrole, $\text{IC}_{50}=100 \mu\text{M}$ ⁸⁵

Table 1-3. Non-substrate analog inhibitors of GFAT. Aptamine is a natural product isolated from the sea sponge species *Aaptos*, discovered by Monsanto scientists in 2000. This natural product spawned the patent of 6,7-dimethoxyisoquinolines as GFAT inhibitors in 2005, and later in 2011, Compound 28 was identified. Amitrole was identified as an inhibitor of *E.coli* GlmS through docking simulations.

Presently, there are only a handful of known GFAT inhibitors, and most of these are substrate derivatives which are either toxic,⁸⁶ non-specific, poorly soluble or cell permeable and not ideal for *in vivo* studies.³⁴ Other inhibitors have been proposed via enzyme docking simulations (Table 1-1,2).^{85,87} The 1-arylcarbonyl-6,7-dimethoxyisoquinoline derivatives represent the most potent and only patented GFAT

inhibitors to date. This class of GFAT inhibitor was identified through separate efforts from Monsanto and Hoffmann-La Roche (Table 1-3).^{82-84, 88} Thus there is a need to discover and develop safe and effective *in vivo* GFAT inhibitors.

Rationale and Thesis Goals

There is substantial evidence that GFAT activity is involved in the development and progression of complications associated with diabetes and, as such, GFAT is an interesting target for therapeutic intervention. In addition, little is known about the effect of GFAT inhibition on complications such as atherosclerosis. Access to potent, selective, cell-permeable inhibitors of GFAT could be used as leads for new drugs as well as probes of GFAT biological function. The present thesis describes research aimed at identifying new inhibitors of GFAT using medium and high-throughput screening methods.

Objectives

1. *To isolate purified, active, GFAT enzyme from a renewable source in a scalable fashion, human GFAT 1 specifically*
2. *To establish an HTS-platform compatible Morgan-Elson assay for GFAT inhibitor discovery*
3. *To screen compound libraries for small molecules which inhibit GFAT in vitro*
4. *To validate inhibitors in vitro with a dose-response assay*
5. *To synthesize libraries of derivatives identified from the screen, perform a structure-activity relationship analysis and identify inhibitors with high potency*

6. *To test the most promising GFAT inhibitors in established cell culture models to determine the effect of perturbation on the HBP*
7. *To determine the mode of inhibition of the most potent and least toxic inhibitor*

References

1. Reaven, G. M., Insulin-Independent Diabetes Mellitus: Metabolic Characteristics. *Metab. Clin. Exp.* **1980**, *29* (5), 445-454.
2. Wild, S.; Roglic, G.; Green, A.; Sicree, R.; King, H., Global Prevalence of Diabetes: Estimates for the year 2000 and projections for 2030. *Diabetes Care* **2004**, *27* (5), 1047-1053.
3. Ohinmaa, A.; Jacobs, P.; Simpson, S.; Johnson, J. A., The Projection of Prevalence and Cost of Diabetes in Canada: 2000 to 2016. *Can. J. Diabetes* **2004**, *28* (2), 1-8.
4. Fisher, M. L.; Kapustin, J. F., A Practical Guide for Aggressive Management of Type 2 Diabetes. *J. Nurse Pract.* **2007**, *3* (4), 259-270.
5. Williams, R.; Van Gaal, L.; Lucioni, C., Assessing the impact of complications on the costs of Type II diabetes. *Diabetologia* **2002**, *45* (7), S13-S17.
6. Breton, M.-C.; Guénette, L.; Amiche, M. A.; Kayibanda, J.-F.; Grégoire, J.-P.; Moisan, J., Burden of Diabetes on the Ability to Work: A Systematic Review. *Diabetes Care* **2013**, *36* (3), 740-749.
7. Diagnosis and Classification of Diabetes Mellitus. *Diabetes Care* **2006**, *29* (suppl 1), S43-S48.
8. Goldenberg, R. M.; Cheng, A. Y. Y.; Punthakee, Z.; Clement, M., Use of Glycated Hemoglobin (A1C) in the Diagnosis of Type 2 Diabetes Mellitus in Adults. *Can. J. Diabetes* **2011**, *July*, 247-249.
9. Sheetz M.J; L., K. G., Molecular Understanding of Hyperglycemia's Adverse Effects for Diabetic Complications. *JAMA* **2002**, *288* (20), 2579-2588.
10. Fowler, M. J., Microvascular and Macrovascular Complications of Diabetes. *Clin. Diabetes* **2011**, *29* (3), 116-122.
11. Tracy, J. A.; Dyck, P. J. B., The Spectrum of Diabetic Neuropathies. *Phys. Med. Rehabil. Clin.* **2008**, *19* (1), 1-26.
12. Gross, J. L.; de Azevedo, M. J.; Silveiro, S. P.; Canani, L. H.; Caramori, M. L.; Zelmanovitz, T., Diabetic Nephropathy: Diagnosis, Prevention, and Treatment. *Diabetes Care* **2005**, *28* (1), 164-176.
13. Association, A. D., Diabetic Retinopathy. *Clin. Diabetes* **2001**, *19* (1), 29-32.
14. Yeboah, J.; Bertoni, A. G.; Herrington, D. M.; Post, W. S.; Burke, G. L., Impaired Fasting Glucose and the Risk of Incident Diabetes Mellitus and Cardiovascular Events in an Adult Population: MESA (Multi-Ethnic Study of Atherosclerosis). *J. Am. Coll. Cardiol.* **2011**, *58* (2), 140-146.
15. Matheus, A. S. d. M.; Tannus, L. R. M.; Cobas, R. A.; Palma, C. C. S.; Negrato, C. A.; Gomes, M. d. B., Impact of Diabetes on Cardiovascular Disease: An Update. *Int. J. Hypertens.* **2013**, *2013*, Article ID: 653789, 15 pages.
16. Bell, D. S. H., Heart Failure: A Serious and Common Comorbidity of Diabetes. *Clin. Diabetes* **2004**, *22* (2), 61-65.
17. Thethi, T. K.; Asafu-Adjaye, N. O.; Fonseca, V. A., Erectile Dysfunction. *Clin. Diabetes* **2005**, *23* (3), 105-113.
18. Brown, S. A.; Sharpless, J. L., Osteoporosis: An Under-Appreciated Complication of Diabetes. *Clin. Diabetes* **2004**, *22* (1), 10-20.

19. (a) Bailey, C. J.; Day, C., Glycaemic memory. *Br. J. Diabetes Vasc. Dis.* **2008**, *8* (5), 242-247; (b) Ceriello, A.; Ihnat, M. A.; Thorpe, J. E., The “Metabolic Memory”: Is More Than Just Tight Glucose Control Necessary to Prevent Diabetic Complications? *J. Clin. Endocrinol. Metab.* **2009**, *94* (2), 410-415.
20. Krentz, A.; Bailey, C., Oral Antidiabetic Agents. *Drugs* **2005**, *65* (3), 385-411.
21. Schmitz, O.; Brock, B.; Rungby, J., Amylin Agonists: A Novel Approach in the Treatment of Diabetes. *Diabetes* **2004**, *53* (suppl 3), S233-S238.
22. Hanefeld, M., Cardiovascular Benefits and Safety Profile of Acarbose Therapy in Prediabetes and Established Type 2 Diabetes. *Cardiovasc. Diabetol.* **2007**, *6*, 1-20.
23. Nissen Se, W. K., Rosiglitazone Revisited: An Updated Meta-Analysis of Risk for Myocardial Infarction and Cardiovascular Mortality. *Arch. Intern. Med.* **2010**, *170* (14), 1191-1201.
24. Krentz, A.; Patel, M.; Bailey, C., New Drugs for Type 2 Diabetes Mellitus. *Drugs* **2008**, *68* (15), 2131-2162.
25. Ghosh, R. K.; Ghosh, S. M.; Chawla, S.; Jasdanwala, S. A., SGLT2 Inhibitors: A New Emerging Therapeutic Class in the Treatment of Type 2 Diabetes Mellitus. *J. Clin. Pharmacol.* **2012**, *52* (4), 457-463.
26. Semple, G.; Fioravanti, B.; Pereira, G.; Calderon, I.; Uy, J.; Choi, K.; Xiong, Y.; Ren, A.; Morgan, M.; Dave, V.; Thomsen, W.; Unett, D. J.; Xing, C.; Bossie, S.; Carroll, C.; Chu, Z.-L.; Grottick, A. J.; Hauser, E. K.; Leonard, J.; Jones, R. M., Discovery of the First Potent and Orally Efficacious Agonist of the Orphan G-Protein Coupled Receptor 119. *J. Med. Chem.* **2008**, *51* (17), 5172-5175.
27. (a) Cariou, B.; Charbonnel, B.; Staels, B., Thiazolidinediones and PPAR γ Agonists: Time for a Reassessment. *Trends Endocrin. Met.* **2012**, *23* (5), 205-215; (b) Millar, J. S., Novel Benefits of Peroxisome Proliferator-Activated Receptors on Cardiovascular Risk. *Curr. Opin. Lipidol.* **2013**, *24* (3), 233-238.
28. Bottomley, J. M.; Raymond, F. D., Pharmaco-Economic Issues for Diabetes Therapy. *Best Pract Res Clin Endocrinol Metab* **2007**, *21* (4), 657-685.
29. Buse, M. G., Hexosamines, Insulin Resistance, and the Complications of Diabetes: Current Status. *Am. J. Physiol.-Endoc. M.* **2006**, *290* (1), E1-E8.
30. Rossetti, L., Perspective: Hexosamines and Nutrient Sensing. *Endocrinology* **2000**, *141* (6), 1922-1925.
31. Kaneto, H.; Xu, G.; Song, K. H.; Suzuma, K.; Bonner-Weir, S.; Sharma, A.; Weir, G. C., Activation of the Hexosamine Pathway Leads to Deterioration of Pancreatic Beta-Cell Function Through the Induction of Oxidative Stress. *J. Biol. Chem.* **2001**, *276* (33), 31099-31104.
32. (a) Hebert, L. F.; Daniels, M. C.; Zhou, J.; Crook, E. D.; Turner, R. L.; Simmons, S. T.; Neidigh, J. L.; Zhu, J. S.; Baron, A. D.; McClain, D. A., Overexpression of Glutamine:fructose-6-phosphate amidotransferase in Transgenic Mice Leads to Insulin Resistance. *J. Clin. Invest.* **1996**, *98* (4), 930-936; (b) Floquet, N.; Durand, P.; Maigret, B.; Badet, B.; Badet-Denisot, M.-A.; Perahia, D., Collective motions in Glucosamine-6-phosphate Synthase: Influence of Ligand Binding and role in Ammonia Channelling and Opening of the Fructose-6-Phosphate Binding Site. *J. Mol. Biol.* **2009**, *385* (2), 653-664.
33. Srinivasan, V.; Sandhya, N.; Sampathkumar, R.; Farooq, S.; Mohan, V.; Balasubramanyam, M., Glutamine fructose-6-phosphate amidotransferase (GFAT) Gene

- Expression and Activity in Patients with Type 2 Diabetes: Inter-Relationships with Hyperglycaemia and Oxidative Stress. *Clin. Biochem.* **2007**, *40* (13-14), 952-957.
34. Milewski, S., Glucosamine-6-phosphate Synthase—the Multi-Facets Enzyme. *BBA-Protein Struct. M.* **2002**, *1597* (2), 173-192.
35. Helenius, A., How N-linked Oligosaccharides Affect Glycoprotein Folding in the Endoplasmic Reticulum. *Mol. Biol. Cell* **1994**, *5* (3), 253-265.
36. (a) Dias, W. B.; Hart, G. W., O-GlcNAc Modification in Diabetes and Alzheimer's Disease. *Mol. Biosyst.* **2007**, *3* (11), 766-772; (b) Hanover, J. A., Glycan-dependent signaling: O-linked N-acetylglucosamine. *FASEB J.* **2001**, *15* (11), 1865-1876.
37. (a) Ron, D.; Walter, P., Signal Integration in the Endoplasmic Reticulum Unfolded Protein Response. *Nat. Rev. Mol. Cell Biol.* **2007**, *8* (7), 519-29; (b) Schroder, M.; Kaufman, R. J., ER Stress and the Unfolded Protein Response. *Mutat. Res.* **2005**, *569* (1-2), 29-63.
38. Araki, K.; Nagata, K., Protein Folding and Quality Control in the ER. *Cold Spring Harb. Perspect. Biol.* **2011**, *3* (11), a007526.
39. Helenius, A.; Aebi, Markus, Intracellular Functions of N-Linked Glycans. *Science* **2001**, *291* (5512), 2364-2369.
40. Helenius, A.; Aebi, M., Roles of N-linked Glycans in the Endoplasmic Reticulum. *Annu. Rev. Biochem.* **2004**, *73* (1), 1019-1049.
41. Yoshida, H., ER stress and Diseases. *FEBS J.* **2007**, *274* (3), 630-658.
42. (a) Hebert, D. N.; Molinari, M., In and Out of the ER: Protein Folding, Quality Control, Degradation, and Related Human Diseases. *Physiol. Rev.* **2007**, *87* (4), 1377-1408; (b) Pahl, H. L., Signal Transduction From the Endoplasmic Reticulum to the Cell Nucleus. *Physiol. Rev.* **1999**, *79* (3), 683-701.
43. Araki, E.; Oyadomari, S.; Mori, M., Impact of Endoplasmic Reticulum Stress Pathway on Pancreatic β -Cells and Diabetes Mellitus. *Exp. Biol. Med.* **2003**, *228* (10), 1213-1217.
44. Allen, J. R.; Nguyen, L. X.; Sargent, K. E.; Lipson, K. L.; Hackett, A.; Urano, F., High ER stress in Beta-Cells Stimulates Intracellular Degradation of Misfolded Insulin. *Biochem. Biophys. Res. Commun.* **2004**, *324* (1), 166-170.
45. Ikesugi, K.; Mulhern, M. L.; Madson, C. J.; Hosoya, K.; Terasaki, T.; Kador, P. F.; Shinohara, T., Induction of Endoplasmic Reticulum Stress in Retinal Pericytes by Glucose Deprivation. *Curr. Eye Res.* **2006**, *31* (11), 947-953.
46. Werstuck, G. H.; Khan, M. I.; Femia, G.; Kim, A. J.; Tedesco, V.; Trigatti, B.; Shi, Y., Glucosamine-Induced Endoplasmic Reticulum Dysfunction Is Associated with Accelerated Atherosclerosis in a Hyperglycemic Mouse Model. *Diabetes* **2006**, *55* (1), 93-101.
47. Liu, G.; Sun, Y.; Li, Z.; Song, T.; Wang, H.; Zhang, Y.; Ge, Z., Apoptosis Induced by Endoplasmic Reticulum Stress Involved in Diabetic Kidney Disease. *Biochem. Biophys. Res. Commun.* **2008**, *370* (4), 651-656.
48. Sage, A. T.; Walter, L. A.; Shi, Y.; Khan, M. I.; Kaneto, H.; Capretta, A.; Werstuck, G. H., Hexosamine Biosynthesis Pathway Flux Promotes Endoplasmic Reticulum Stress, Lipid Accumulation, and Inflammatory Gene Expression in Hepatic Cells *Am. J. Physiol.-Endoc. M.* **2010**, *298* (3), E499-E510.

49. Beriault, D. R.; Werstuck, G. H., The Role of Glucosamine-Induced ER Stress in Diabetic Atherogenesis. *Exp. Diabetes Res.* **2012**, *2012*, 1-11.
50. Oki, T.; Yamazaki, K.; Kuromitsu, J.; Okada, M.; Tanaka, I., cDNA Cloning and Mapping of a Novel Subtype of Glutamine:fructose-6-phosphate Amidotransferase (GFAT2) in Human and Mouse. *Genomics* **1999**, *57* (2), 227-234.
51. (a) Niimi, M.; Ogawara, T.; Yamashita, T.; Yamamoto, Y.; Ueyama, A.; Kambe, T.; Okamoto, T.; Ban, T.; Tamanoi, H.; Ozaki, K.; Fujiwara, T.; Fukui, H.; Takahashi, E.; Kyushiki, H.; Tanigami, A., Identification of GFAT1-L, a Novel Splice Variant of Human Glutamine: Fructose-6-Phosphate Amidotransferase (GFAT1) that is Expressed Abundantly in Skeletal Muscle. *J. Hum. Genet.* **2001**, *46* (10), 566-571; (b) DeHaven, J. E.; Robinson, K. A.; Nelson, B. A.; Buse, M. G., A Novel Variant of Glutamine: Fructose-6-Phosphate Amidotransferase-1 (GFAT1) mRNA Is Selectively Expressed in Striated Muscle. *Diabetes* **2001**, *50* (11), 2419-2424.
52. McKnight, G. L.; Mudri, S. L.; Mathewes, S. L.; Traxinger, R. R.; Marshall, S.; Sheppard, P. O.; O'Hara, P. J., Molecular cloning, cDNA sequence, and Bacterial Expression of Human Glutamine:Fructose-6-Phosphate Amidotransferase. *J. Biol. Chem.* **1992**, *267* (35), 25208-25212.
53. Whitmore, T. E.; Mudri, S. L.; McKnight, G. L., Physical Mapping of the Human Glutamine:Fructose-6-Phosphate Amidotransferase Gene (GFPT) to Chromosome 2p13. *Genomics* **1995**, *26* (2), 422-423.
54. Burt, D.; Brodbeck, K.; Haring, H. U.; Schleicher, E. D.; Weigert, C., Partial Characterisation of the Human GFAT Promoter: Effect of Single Nucleotide Polymorphisms on Promoter Function. *Biochim. Biophys. Acta* **2005**, *1740* (1), 85-90.
55. (a) Li, Y.; Roux, C.; Lazereg, S.; LeCaer, J. P.; Laprevote, O.; Badet, B.; Badet-Denisot, M. A., Identification of a Novel Serine Phosphorylation Site in Human Glutamine:Fructose-6-Phosphate Amidotransferase Isoform 1. *Biochemistry* **2007**, *46* (45), 13163-13169; (b) Chang, Q.; Su, K.; Baker, J. R.; Yang, X.; Paterson, A. J.; Kudlow, J. E., Phosphorylation of Human Glutamine:Fructose-6-Phosphate Amidotransferase by cAMP-dependent Protein Kinase at Serine 205 Blocks the Enzyme Activity. *J. Biol. Chem.* **2000**, *275* (29), 21981-21987.
56. Paterson, A. J.; Kudlow, J. E., Regulation of Glutamine:Fructose-6-Phosphate Amidotransferase gene Transcription by Epidermal Growth Factor and Glucose. *Endocrinology* **1995**, *136* (7), 2809-2816.
57. Durand, P.; Golinelli-Pimpaneau, B.; Mouilleron, S.; Badet, B.; Badet-Denisot, M. A., Highlights of Glucosamine-6P Synthase Catalysis. *Arch. Biochem. Biophys.* **2008**, *474* (2), 302-317.
58. Teplyakov, A.; Obmolova, G.; Badet, B.; Badet-Denisot, M.-A., Channeling of Ammonia in Glucosamine-6-Phosphate Synthase. *J. Mol. Biol.* **2001**, *313* (5), 1093-1102.
59. Teplyakov, A.; Obmolova, G.; Badet-Denisot, M.-A.; Badet, B.; Polikarpov, I., Involvement of the C terminus in Intramolecular Nitrogen Channeling in Glucosamine- 6-Phosphate Synthase: Evidence from a 1.6 Å Crystal Structure of the Isomerase Domain. *Structure* **1998**, *6* (8), 1047-1055.
60. Nakaishi, Y.; Bando, M.; Shimizu, H.; Watanabe, K.; Goto, F.; Tsuge, H.; Kondo, K.; Komatsu, M., Structural Analysis of Human Glutamine:Fructose-6-Phosphate Amidotransferase, a Key Regulator in Type 2 Diabetes. *FEBS Lett.* **2009**, *583* (1), 163-167.

61. (a) Huynh, Q. K.; Gulve, E. A.; Dian, T., Purification and Characterization of Glutamine:Fructose 6-Phosphate Amidotransferase from Rat Liver. *Arch. Biochem. Biophys.* **2000**, *379* (2), 307-13; (b) Kornfeld, R., Studies on L-Glutamine d-Fructose 6-Phosphate Amidotransferase : I. Feedback Inhibition by Uridine Diphosphate-N-Acetylglucosamine. *J. Biol. Chem.* **1967**, *242* (13), 3135-3141; (c) Winterburn, P. J.; Phelps, C. F., Studies on the Control of Hexosamine Biosynthesis by Glucosamine Synthetase. *Biochem. J.* **1971**, *121* (4), 711-720; (d) Winterburn, P. J.; Phelps, C. F., Purification and Some Kinetic Properties of Rat Liver Glucosamine Synthetase. *Biochem. J.* **1971**, *121* (4), 701-709.
62. (a) Li, Y.; Lopez, P.; Durand, P.; Ouazzani, J.; Badet, B.; Badet-Denisot, M. A., An Enzyme-Coupled Assay for Amidotransferase Activity of Glucosamine-6-Phosphate Synthase. *Anal. Biochem.* **2007**, *370* (2), 142-146; (b) Ye, F.; Maegawa, H.; Morino, K.; Kashiwagi, A.; Kikkawa, R.; Xie, M.; Shen, Z., A Simple and Sensitive Method for Glutamine:Fructose-6-Phosphate Amidotransferase Assay. *J. Biochem. Biophys. Meth.* **2004**, *59* (3), 201-208.
63. (a) Broschat, K. O.; Gorka, C.; Kasten, T. P.; Gulve, E. A.; Kilpatrick, B., A Radiometric Assay for Glutamine:Fructose-6-Phosphate Amidotransferase. *Anal. Biochem.* **2002**, *305* (1), 10-15; (b) Callahan, M.; Tourian, A.; Hung, W.-Y., A Sensitive, Specific Radioisotope Assay for L-glutamine-D-fructose-6-phosphate Aminotransferase. *Anal. Biochem.* **1981**, *115* (2), 347-352.
64. (a) Span, P. N.; Pouwels, M.-J. J. M.; Olthaar, A. J.; Bosch, R. R.; Hermus, A. R. M. M.; Sweep, C. G. J., Assay for Hexosamine Pathway Intermediates (Uridine Diphosphate-N-Acetyl Amino Sugars) in Small Samples of Human Muscle Tissue. *Clin. Chem.* **2001**, *47* (5), 944-946;
65. (a) Biondi, P. A.; Manca, F.; Negri, A.; Tedeschi, G.; Secchi, C., Gas Chromatographic Determination of Glycoprotein Amino Sugars as O-pentafluorobenzoyloxime Acetates. *J. Chromatogr. A* **1989**, *467*, 315-320; (b) Sonesson, A.; Bryn, K.; Jantzen, E.; Larsson, L., Gas Chromatographic Determination of (phosphorylated) 2-keto-3-deoxyoctonic acid, Heptoses and Glucosamine in Bacterial Lipopolysaccharides after Treatment with Hydrofluoric Acid, Methanolysis and Trifluoroacetylation. *J. Chromatogr. B: Biomed. Sci. Appl.* **1989**, *487*, 1-7.
66. Maillard, L. T.; Guerineau, V.; Badet-Denisot, M. A.; Badet, B.; Laprevote, O.; Durand, P., Monitoring Enzyme-Catalyzed Production of Glucosamine-6P by Matrix-Assisted Laser Desorption/Ionization Time-of-Flight Mass Spectrometry: a New Enzymatic Assay for Glucosamine-6P Synthase. *Rapid Commun. Mass Spectrom.* **2006**, *20* (4), 666-72.
67. (a) Burghardt, C.; Kochan, J. Method for Measuring Glucosamine-6-Phosphate. EP 1 431 396 A1. 2004; (b) Morgan, W. T. J.; Elson, L. A., A Colorimetric Method for the Determination of N-acetylglucosamine and N-acetylchondrosamine. *Biochem. J.* **1934**, *28* (3), 988-995.
68. Elson, L. A.; Morgan, W. T. J., A Colorimetric Method for the Determination of Glucosamine and Chondrosamine. *Biochem J.* **1933**, *27* (6), 1824-1827.
69. Reissig, J. L.; Strominger, J. L.; Leloir, L. F., A Modified Colorimetric Method for the Estimation of N-Acetyl amino Sugars. *The Journal of biological chemistry* **1955**, *217*, 959-966.

70. Levvy, G. A.; McAllan, A., The N-acetylation and Estimation of Hexosamines. *Biochem J.* **1959**, *73* (1), 127-132.
71. Richards, T. C.; Greengard, O., Distribution of Glutamine Hexosephosphate Aminotransferase in Rat Tissues; Changes with State of Differentiation. *Biochem. Biophys. Acta.* **1973**, *304*, 842-850.
72. Chmara, H.; Andruszkiewicz, R.; Borowski, E., Inactivation of Glucosamine-6-Phosphate Synthetase from Salmonella typhimurium LT2 by Fumaroyl Diaminopropanoic acid Derivatives, a Novel Group of Glutamine Analogs. *BBA Protein Struct. M.* **1986**, *870* (2), 357-366.
73. Badet-Denisot, M.-A.; Leriche, C.; Massière, F.; Badet, B., Nitrogen Transfer in E. coli Glucosamine-6P Synthase. Investigations Using Substrate and Bisubstrate Analogs. *Bioorg. Med. Chem. Lett.* **1995**, *5* (8), 815-820.
74. Milewski, S.; Chmara, H.; Andruszkiewicz, R.; Borowski, E., N3-haloacetyl Derivatives of l-2,3-diaminopropanoic acid: Novel Inactivators of Glucosamine-6-Phosphate Synthase. *Biochimica et Biophysica Acta (BBA) - General Subjects* **1992**, *1115* (3), 225-229.
75. Milewski, S.; Hoffmann, M.; Andruszkiewicz, R.; Borowski, E., Investigation of Mechanism of Nitrogen Transfer in Glucosamine 6-Phosphate Synthase with the Use of Transition State Analogs. *Bioorganic Chemistry* **1997**, *25* (5–6), 283-296.
76. Chmara, H.; Zahner, H.; Borowski, E.; Milewski, S., Inhibition of Glucosamine-6-Phosphate Synthetase from Bacteria by Anticapsin. *J. Antibiot.* **1984**, *37* (6), 652-657.
77. Chmara, H.; Andruszkiewicz, R.; Borowski, E., Inactivation of Glucosamine-6-Phosphate Synthetase from Salmonella typhimurium LT 2 SL 1027 by N β -fumarylcarboxyamido-L-2,3-diaminopropionic acid. *Biochem. Bioph. Res. Co.* **1984**, *120* (3), 865-872.
78. Walker, B.; Brown, M. F.; Lynas, J. F.; Martin, S. L.; McDowell, A.; Badet, B.; Hill, A. J., Inhibition of Escherichia coli Glucosamine Synthetase by Novel Electrophilic Analogues of Glutamine—Comparison with 6-diazo-5-oxo-norleucine. *Bioorg. Med. Chem. Lett.* **2000**, *10* (24), 2795-2798.
79. Broschat, K. O.; Gorka, C.; Page, J. D.; Martin-Berger, C. L.; Davies, M. S.; Huang Hc, H. C.; Gulve, E. A.; Salsgiver, W. J.; Kasten, T. P., Kinetic Characterization of Human Glutamine-Fructose-6-Phosphate Amidotransferase I: Potent Feedback Inhibition by Glucosamine 6-Phosphate. *J. Biol. Chem.* **2002**, *277* (17), 14764-14770.
80. Le Camus, C.; Chassagne, A.; Badet-Denisot, M.-A.; Badet, B., Stereoselective Synthesis of 5-methylphosphono-D-arabino hydroximolactone, Inhibitor of Glucosamine-6-Phosphate Synthase and Phosphoglucose Isomerase. *Tetrahedron Lett.* **1998**, *39* (3–4), 287-288.
81. Le Camus, C.; Badet-Denisot, M.-A.; Badet, B., Arabinose-5-phosphate oxime vs its Methylene phosphonate Mimetic as High Energy Intermediate of the Glucosamine-6P Synthase Catalyzed Reaction. *Tetrahedron Lett.* **1998**, *39* (17), 2571-2572.
82. Bobzin, S. C.; Yang, S.; Kasten, T. P., Application of Liquid Chromatography–Nuclear Magnetic Resonance Spectroscopy to the Identification of Natural Products. *J. Chromatogr. B: Biomed. Sci. Appl.* **2000**, *748* (1), 259-267.
83. Bolin, D.; Chen, S.; Mischke, S.; Qian, Y. Glutamine Fructose-6-Phosphate Amidotransferase (GFAT) Inhibitors. WO 2005/040150 A2, 6 May 2005.

84. Qian, Y.; Ahmad, M.; Chen, S.; Gillespie, P.; Le, N.; Mennona, F.; Mischke, S.; So, S.-S.; Wang, H.; Burghardt, C.; Tannu, S.; Conde-Knape, K.; Kochan, J.; Bolin, D., Discovery of 1-arylcarbonyl-6,7-dimethoxyisoquinoline Derivatives as Glutamine Fructose-6-Phosphate Amidotransferase (GFAT) Inhibitors. *Bioorg. Med. Chem. Lett.* **2011**, *21* (21), 6264-6269.
85. Floquet, N.; Richez, C.; Durand, P.; Maigret, B.; Badet, B.; Badet-Denisot, M. A., Discovering New Inhibitors of Bacterial Glucosamine-6P Synthase (GlmS) by Docking Simulations. *Bioorg. Med. Chem. Lett.* **2007**, *17* (7), 1966-1970.
86. (a) Longnecker, D. S.; Curphey, T. J., Adenocarcinoma of the Pancreas in Azaserine-treated Rats. *Cancer Res.* **1975**, *35* (8), 2249-2257; (b) Krakoff, I. H.; Karnofsky, D. A., Inhibition of Uric Acid Biosynthesis in Birds by o-Diazoacetyl-L-Serine (Azaserine) and 6-Diazo-5-Oxo-L-Norleucine (DON). *Am. J. Physiol.* **1958**, *195* (1), 244-250.
87. Vennilaa, J. P.; Thiruvadigalb, D. J.; Kavitha, H. P., Antibacterial Evaluation of Some Organic Compounds as Potential Inhibitors for Glucosamine-6-Phosphate Synthase. *J. Pharm. Res.* **2012**, *5* (4), 1963-1966.
88. Bobzin, S. C.; Yang, S.; Kasten, T. P., LC-NMR: a New Tool to Expedite the Dereplication and Identification of Natural Products. *J. Ind. Microbiol. Biot.* **2000**, *25* (6), 342-345.

Chapter 2

Cloning, Expression and Large-Scale Purification of rhGFAT1-His₆²⁹⁸

Preface

The work described in this chapter was carried out with the assistance of Naresh Balachandran & Dr. Paul Berti (Dept. of Chemistry & Chemical Biology, McMaster University), and Susan McCusker (Center for Microbial Chemical Biology, McMaster University). Dr. Berti allowed use of his lab to perform the cloning and expression techniques necessary to produce GFAT, while Naresh provided his knowledge and expertise in microbiology and biochemistry. Susan McCusker assisted with FPLC training and the large-scale protein expression techniques.

Abstract

Human L-glutamine:D-fructose-6-phosphate amidotransferase 1 (hGFAT1) has been successfully cloned, expressed and purified *via* the introduction of an internal hexahistidine affinity tag at gene position 894. The internal affinity tag allows the recombinant GFAT to maintain its enzymatic activity as it does not interfere with catalytic sites of the enzyme located at both the N- and C- termini. To generate sufficient amounts of enzyme, large-scale protein expression techniques were developed and employed. A viable and renewable source of enzyme allowed us to pursue a screening campaign to discover novel inhibitors for this rate-limiting enzyme of the hexosamine biosynthesis pathway (HBP).

Introduction

With the identification of GFAT as a viable target for therapeutic intervention,¹ there has been an increasing interest in discovering inhibitors to probe and modulate the target. Overall, however, GFAT has been a relatively under-evaluated medicinal target primarily due to the difficulty associated with obtaining a reliably pure² and active³ form of the enzyme. While GFAT is expressed in every prokaryotic (as GlmS) and eukaryotic (as Gfa or GFAT for mammalian species) organism in nature, it is found in low abundance.⁴ Isolating the enzyme from a natural source is also complicated as GFAT loses activity rapidly if not in the presence of its substrate (F6P) or exposed to oxidizing conditions.²⁻³ Once the Cysteine1 (Cys1) at the glutaminase domain is oxidized, GFAT loses all enzymatic activity. Large scale production of the enzyme using recombinant methods are further complicated by the fact that the catalytic sites of the enzyme are both located at the N- and C- termini. As a result, any modification of the ends of the enzyme with an affinity tag would result in a loss of activity.

Badet-Denisot *et al* have described the construction of a recombinant prokaryotic (*E.coli* GlmS) and recombinant human GFAT1 system containing an internal hexa-histidine tag (His₆).⁵ *E.coli* GlmS was used as a model system to find the best place to situate the histidine tag and the studies indicated that insertion of the hexa-histidine tag at amino acid position 225 through sub-cloning maintained enzyme activity (Figure 2-1). This information was applied to a human GFAT construct and, following sequence alignment, the His₆-tag was inserted at position 298 (nucleotide position 894). This

construct was expressed in SF9 insect cells and purified on a Ni²⁺-charged Sepharose column.

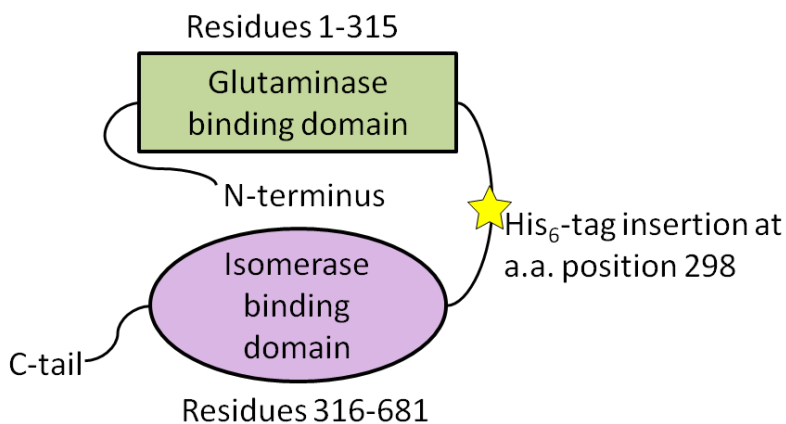


Figure 2-1. A representation of the rhGFAT-1 monomer identifying the glutaminase and isomerase binding domains along with the affinity tag insertion site. hGFAT-1 is active as a homotetramer; here a monomer is depicted for simplicity. The glutaminase binding domain begins at the N-terminus and encompasses amino acids 1-315. Cys1 is largely responsible for the catalytic activity of this domain; addition of an affinity-tag here would render the enzyme inactive as has been shown in models involving GlmS. The C-terminus tail has been identified as properly ordered and conserved amongst species and is used in substrate binding. The His₆-tag has been inserted at a position which connects the two domains and is not involved in the catalytic processes of either glutaminase or isomerase domains.

The cloning strategy described by Badet-Denisot is limited by the availability and location of unique restriction sites within the gene of interest and the expression vector. As a result, we have cloned a recombinant form of hGFAT1 with an internal hexahistidine tag from human *gfat1*-cDNA by site-directed mutagenesis *via* PCR. The Gateway[®] cloning technology (Invitrogen, Life Technologies Corporation) was utilized to generate the expression plasmid and is based on the lambda bacteriophage site-specific recombination system which facilitates the integration of lambda into the *E.coli* genome.⁶

Gateway® cloning has three key features: it has site-specific DNA recombination sequences (attachment sites or *att* sites) which prevent gene inversion; it does not require restriction enzymes or ligases; and the Gateway® vectors can be used in several different expression systems. The recombination enzymes BP and LR clonases only recognize a 25-30 bp attachment site unique to each enzyme and this prevents non-specific recombination.

To take advantage of the lambda site-specific recombination for Gateway® cloning, a series of circularized vectors are commercially available for either cloning or expression which contain specific *att* sites (Figure 2-2). A gene of interest can be PCR amplified and flanked with *att* specific sequences on either end of the gene. When the vector is combined with the *att*-flanked gene along with the clonase enzyme mix, the gene of interest will be inserted into the vector. To encourage selection of only successful recombination reactions, the Gateway® vectors contain the *ccdB* gene inserted between the *att* recombination sites. The *ccdB* protein interferes with *E.coli* DNA gyrase and is lethal to most strains of *E.coli*.⁷ Also, antibiotic resistance genes are present within the Gateway® vectors for increased selectivity.

We also chose to express hGFAT-1 in *E.coli* BL21 Rosetta™ pRARE2 (EMD4Biosciences, EMD Millipore Canada) chemically competent cells to ensure consistent expression of the human gene in a prokaryotic host. Rosetta 2™ *E.coli* are BL21 derivatives containing the pRARE2 plasmid which can enhance expression of eukaryotic proteins in prokaryotic systems since they contain the corresponding tRNA's for the 7 rare codons typically not used in prokaryotes.⁸

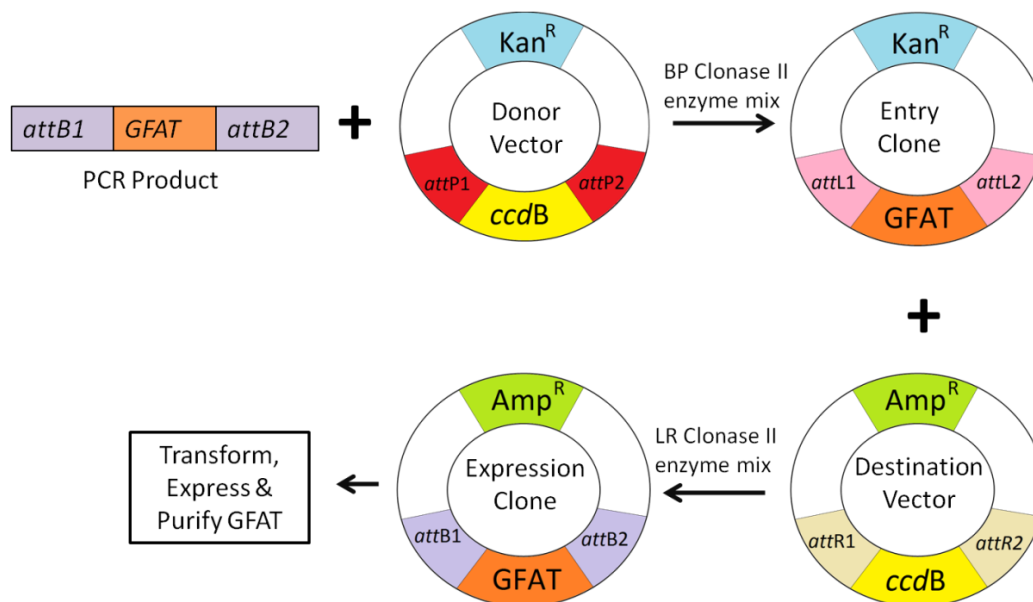


Figure 2-2. Schematic of Gateway® Cloning procedure. Generation of an entry clone with a recombination reaction between an *attB*-flanked gene of interest and a Donor Vector with *attP* sites catalyzed by BP Clonase II enzyme mix. The resulting Entry Clone contains an *attL* site which is a combination of sequences from both *attB* and *attP* sites. To create an Expression Clone, a recombination reaction catalyzed by the LR Clonase II enzyme mix with the entry clone and a destination vector containing the *ccdB* gene flanked by *attR* sites is initiated. The final plasmid is viable for protein expression when transformed into an appropriate *E. coli* strain.

Results & Discussion

Generation of a recombinant human GFAT1 protein expression vector utilizing Multi-Site Gateway® cloning technology

In order to facilitate the Gateway® cloning procedure, *hgfat1*-cDNA must first be PCR amplified to include specific *att* recombination sites. A plasmid harbouring the gene of interest (pCIS-GFAT, containing a 3.1 kb *EcoRI/PvuI* fragment encoding the cDNA for human GFAT 1) was obtained from Michael J. Quon.⁹ The gene was PCR amplified with a forward primer containing the *attB1* site along with a start codon and a Shine-Dalgarno sequence.¹⁰ The reverse primer contained the *attB2* site and a stop codon. The *hgfat1*-cDNA fragment with the added features necessary for Gateway® Cloning and protein expression was successfully amplified by PCR as evidenced by the fragment between

2500 and 2000 bp visible on the agarose gel (Figure 2-3) and by DNA sequencing analysis.

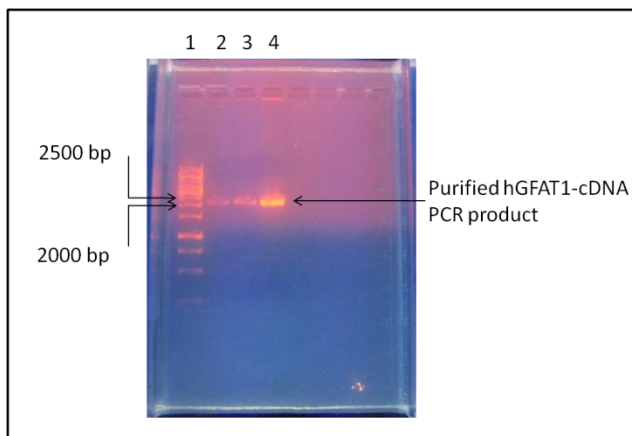


Figure 2-3. Photograph of agarose gel with purified *hgfat1*-cDNA PCR amplified samples. The gene for *hgfat1*-cDNA amplified from the pCIS-GFAT vector was 2122 base pairs in length from start codon to stop codon with *attB* sites added for Gateway® cloning recombination with the pDONR 221 vector. Lane 1, Gene Ruler™ 1kb DNA ladder (Fermentas), Lane 2, 25 ng *hgfat1*-cDNA, Lane 3, 50 ng *hgfat1*-cDNA, Lane 4 125 ng *hgfat1*-cDNA.

The pDONR 221 vector and the pET301/CT-DEST vector (Invitrogen, Life Technologies) were selected for the cloning and expression of hGFAT1, respectively. The pDONR 221 vector features M13 forward and reverse priming sites, *attP1* and P2 recombination sequences, the *ccdB* gene in between the *attP* sites for negative selection, a kanamycin resistance marker and was 4761 nucleotides in size. The pET301/CT-DEST vector was 7382 nucleotides in size and features a T7 promoter and terminator site, a *lac* operator for IPTG inducible expression, *attR1* and R2 sites, a *ccdB* gene in between the *attR* sites, an ampicillin resistance marker, and a C-terminus hexahistidine tag. However, given the catalytic sequences at the N- and C- termini of hGFAT1, a stop codon was included at the end of the *hgfat1*-cDNA PCR-amplified sequence to prevent the intrinsic His₆-tag on the vector from being added to the termini of the

enzyme. As well, the pET301/CT-DEST lacked a prokaryotic ribosome binding sequence (Shine-Dalgarno sequence) and this was incorporated into the vector to ensure optimal levels of protein expression.

The next step involved insertion of the *hgfat1*-cDNA into a Donor Vector to generate an Entry Clone. This was catalyzed by the BP Clonase II enzyme mix. The BP Clonase II enzyme mix would only catalyze a reaction between *attB* and *attP* sites. Also recombination only occurred between *attB1* x *attP1* and likewise for the latter recombination sites which ensured no inversion of the gene sequence. Once the recombination reaction was complete, the *hgfat1*-cDNA was contained in an entry clone flanked by *attL* sites which contained sequences from both *attB* and *attP* recombination sites. The entry clone was used to insert the gene of interest into a destination vector which contained *attR* sites. The LR Clonase enzyme mix catalyzed the reaction between *attL* and *attR* sites and resulted in reformation of the *attB* site in the new expression vector once the reaction was complete.

To confirm that the cloning procedure was successful, the GFAT expression clone pET301/CT-DEST *hgfat1*-cDNA was used to transform One Shot[®] Top10 chemically competent *E.coli* (Invitrogen, Life Technologies Corporation) and successful transformants were selected from LB/agar/ampicillin Petri dishes. Well-spaced colonies were selected for plasmid isolation and DNA sequencing at the McMaster Institute for Molecular Biology and Biotechnology (MOBIX, McMaster University, Hamilton, ON) using T7 Promoter and T7 Terminator as primers. BLAST analysis confirmed the presence of *hgfat1*-cDNA within the pET301/CT-DEST expression clone along with Start

and Stop codons and the Shine-Dalgarno sequence in the correct locations. This confirmed that the PCR method developed to amplify *hgfat1*-cDNA from pCIS-GFAT and Gateway® Cloning technology was successful at creating a protein expression vector.

To confirm the new construct was expressed, the isolated expression vector pET301/CT-DEST/*hgfat1*-cDNA was used to transform chemically competent *E.coli* BL21 cells. Expression was induced with 0.3 mM of isopropyl β -D-1-thiogalactopyranoside (IPTG) and the culture was further incubated for another 5 hours. The cell pellet was resuspended in GFAT lysis buffer and lysed with an Avestin Emulsiflex-C5 homogenizer. The cell lysate was tested for GFAT protein expression and was confirmed with SDS-PAGE (Figure 2-4).

Insertion of an internal hexa-histidine tag into hgfat1-cDNA genetic position 894

Work was then directed to the introduction of an internal hexa-histidine affinity tag to allow for ease of purification of the enzyme. The polymerase chain reaction (PCR) was selected as a viable method to introduce the affinity tag while *hgfat1*-cDNA was present within a vector.¹¹ Site-directed mutagenesis using PCR allowed firm control over where the tag was placed and increased reproducibility over sub-cloning procedures. The affinity-tag insertion was performed with *hgfat1*-cDNA present in the entry clone pDONR 221. Performing the His-tag insertion with *hgfat1*-cDNA already in the expression vector (pET301-CT/DEST) would have saved an extra step in the procedure. However, with larger plasmid sizes more mutations can be likely as nucleotides are used unevenly from the PCR reaction mixture. We found several unwanted mutations when we tried to insert the His-tag while *hgfat-1* was present in this vector. The plasmid size

of the expression clone and gene combined was 9600 bp, but combined with the entry clone the size was closer to 7000 bp. Performing the His-tag insertion with the entry clone did not afford us any complications.

Forward and reverse primers (FWDHIS3L, REVHIS3L, respectively) were designed with nine extra base pairs in the middle corresponding to three of the six codons to be inserted. The primers overlapped around gene position 894 and three histidine codons were inserted following one round of PCR. A second set of forward and reverse primers (FWDHISL, REVHISL, respectively) were designed which contained eighteen extra base pairs corresponding to six histidine codons flanked by the sequence for GFAT on either side. These were used in a second round of PCR under the same reaction conditions. It should be noted that attempts to insert all eighteen base pairs within one round of PCR resulted in several undesired mutations.

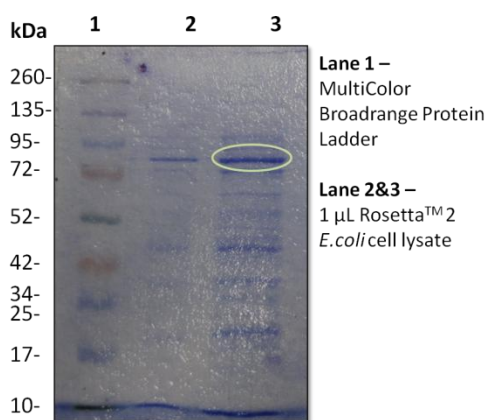


Figure 2-4. Photograph of SDS-PAGE gel (4% stacking, 10% resolving) stained with Coomassie Blue. Lane 1, MultiColor broadrange protein ladder (Fermentas Canada Inc., Burlington, ON), Lanes 2 and 3, 1 µL sample of Rosetta 2™ *E.coli* cell lysate transformed with pET301/CT-DEST/*hgfat1*-cDNA and expression induced with IPTG. A dark blue band, highlighted in Lane 3 by an ellipse, was a protein with a MW in the range of 72-95 kDa. This was proposed to be the hGFAT-1 monomer, which had a MW of 77 kDa.

Following the PCR, the newly formed *hgfat1*-cDNA His₆⁸⁹⁴ was sequenced using M13 forward and reverse primers along with a primer (LW5HISUP) designed especially to view the affinity-tag insertion (Figure 2-5). Sequencing confirmed successful insertion of the tag and no unwanted mutations (Figure 2-6). *hgfat1*-cDNA His₆⁸⁹⁴ was re-inserted into the pET301/CT-DEST expression clone.

Protein expression and purification of rhGFAT1-His₆²⁹⁸

Protein expression levels of rhGFAT1-His₆²⁹⁸ were optimized by adjusting the amount of inducing agent used (IPTG), time allowed for expression, culture density and temperature. Chemically competent Rosetta 2TM *E.coli* was transformed with the pET-301/CT-DEST *hgfat1*-His₆⁸⁹⁴ expression clone. Optimal GFAT expression was found to occur when cultures were induced with 0.5 mM IPTG at OD₆₀₀ = 0.4-0.6 and allowed to incubate for 3 hours at 37 °C before harvesting (Figure 2-7).

rhGFAT1-His₆²⁹⁸ was purified in one step by immobilized metal affinity chromatography (IMAC) on a Fast Protein Liquid Chromatography (FPLC) system. The His₆-tagged GFAT bound favourably to a Ni (II) Sepharose chelating column while all other proteins were eluted. rhGFAT1-His₆²⁹⁸ was found to elute from the column when 200-500 mM imidazole was applied. Fractions containing GFAT were pooled together and concentrated using a spin-column (or centrifugal filter unit). This device allows for concentration of the enzyme while also performing a buffer exchange to remove excess imidazole.

atg tgt ggt ata ttt gct tac tta aac tac cat gtt cct cga acg aga
 cga gaa atc ctg gag acc cta atc aaa ggc ctt cag aga ctg gag tac
 aga gga tat gat tct gct ggt gtg gga ttt gat gga ggc aat gat aaa
 gat tgg gaa gcc aat gcc tgc aaa acc cag ctt att aag aag aaa gga
 aaa gtt aag gca ctg gat gaa gaa gtt cac aag caa caa gat atg gat
 ttg gat ata gaa ttt gat gta cac ctt gga ata gct cat acc cgt tgg
 gca aca cat gga gaa ccc agt cct gtc aat agc cac ccc cag cgc tct
 gat aaa aat aat gaa ttt atc gtt att cac aat gga atc atc acc aac
 tac aaa gac ttg aaa aag ttt ttg gaa agc aaa ggc tat gac ttc gaa
 tct gaa aca gac aca gag aca att gcc aag ctc gtt aag tat atg tat
 gac aat cgg gaa agt caa gat acc agc ttt act acc ttg gtg gag aga
 gtt atc caa caa ttg gaa ggt gct ttt gca ctt gtg ttt aaa agt gtt
 cat ttt **ccc ggg caa gca gtt ggc aca agg cga ggt agc** cct ctg ttg
 att ggt gta cgg agt gaa cat aaa ctt tct act gat cac att cct ata
 ctc tac aga aca ggc aaa gac aag aaa gga agc tgc aat ctc tct cgt
 gtg gac agc aca acc tgc ctt ttc ccg gtg gaa gaa aaa gca gtg gag
 tat tac ttt gct tct gat gca agt gct gtc ata gaa cac acc aat cgc
 gtc atc ttt ctg gaa gat gat gat gtt gca gca gta gtg gat gga cgt
 ctt tct atc cat cga att aaa cga act gca **CAC CAC CAC CAC CAC CAC**
 gga gat cac ccc gga cga gct gtg caa aca ctc cag atg gaa ctc cag
 cag atc atg aag ggc aac ttc agt tca ttt atg cag aag gaa ata ttt
 gag cag cca gag tct gtc gtg aac aca atg aga gga aga gtc aac ttt
 gat gac tat act gtg aat ttg ggt ggt ttg aag gat cac ata aag gag
 atc cag aga tgc cgg cgt ttg att ctt att gct tgt gga aca agt tac
 cat gct ggt gta gca aca cgt caa gtt ctt gag gag ctg act gag ttg
 cct gtg atg gtg gaa cta gca agt gac ttc ctg gac aga aac aca cca
 gtc ttt cga gat gat gtt tgc ttt ttc ctt agt caa tca ggt gag aca
 gca gat act ttg atg ggt ctt cgt tac tgt aag gag aga gga gct tta
 act gtg ggg atc aca aac aca gtt ggc agt tcc ata tca cgg gag aca
 gat tgt gga gtt cat att aat gct ggt cct gag att ggt gtg gcc agt
 aca aag gct tat acc agc cag ttt gta tcc ctt gtg atg ttt gcc ctt
 atg atg tgt gat gat cgg atc tcc atg caa gaa aga cgc aaa gag atc
 atg ctt gga ttg aaa cgg ctg cct gat ttg att aag gaa gta ctg agc
 atg gat gac gaa att cag aaa cta gca aca gaa ctt tat cat cag aag
 tca gtt ctg ata atg gga cga ggc tat cat tat gct act tgt ctt gaa
 ggg gca ctg aaa atc aaa gaa att act tat atg cac tct gaa ggc atc
 ctt gct ggt gaa ttg aaa cat ggc cct ctg gct ttg gtg gat aaa ttg
 atg cct gtg atc atg atc atc atg aga gat cac act tat gcc aag tgt
 cag aat gct ctt cag caa gtg gtt gct cgg cag ggg cgg cct gtg gta
 att tgt gat aag gag gat act gag acc att aag aac aca aaa aga acg
 atc aag gtg ccc cac tca gtg gac tgc ttg cag ggc att ctc agc gtg
 atc cct tta cag ttg ctg gct ttc cac ctt gct gtg ctg aga ggc tat
 gat gtt gat ttc cca cgg aat ctt gcc aaa tct gtg act gta gag **tga**

Figure 2-5. *hgfat1*-cDNA genetic sequence with hexa-histidine insertion at position 894. The location of the 18 desired hexa-histidine nucleotides are identified with bolded and capitalized letters. The start and stop codons are identified by bolded letters. Without the insert, *hgfat1*-cDNA was 2046 bp in length, with the insert the length was 2064 bp. The underlined and bolded letters indicate the base pairs used to design primer LW5HISUP. This 30 bp long primer was designed upstream of the His₆-tag insert at position 585 to allow for sequencing analysis.

```

a agc tgc aat ctc tct cgt gtg gac agc aca acc tgc ctt ttc ccg
gtg gaa gaa aaa gca gtg gag tat tac ttt gct tct gat gca agt gct
gtc ata gaa cac acc aat cgc gtc atc ttt ctg gaa gat gat gat gtt
gca gca gta gtg gat gga cgt ctt tct atc cat cga att aaa cga act
gca CAC CAC CAC CAC CAC CAC gga gat cac ccc gga cga gct gtg caa
aca ctc cag atg gaa ctc cag cag atc atg aag ggc aac ttc agt tca
ttt atg cag aag gaa ata ttt gag cag cca gag tct gtc gtg aac aca
atg aga gga aga gtc aac ttt gat gac tat act gtg aat ttg ggt ggt
ttg aag gat cac ata aag gag atc cag aga tgt cgg cgt ttg att ctt
att gct tgt gga aca agt tac cat gct ggt gta gca aca cgt caa gtt
ctt gag gag ctg act gag ttg cct gtg atg gtg gaa cta gca agt gac
ttc ctg gac aga aac aca cca gtc ttt cga gat gat gtt tgc ttt ttc
ctt agt caa tca ggt gag aca gca gca gat act ttg atg ggt ctt cgt tac
tgt aag gag aga gga gct tta act gtg ggg atc aca aac aca gtt ggc
agt tcc ata tca cgg gag aca gat tgt gga gtt cat att aat gct ggt
cct gag att ggt gtg gcc agt aca aag gct tat acc agc cag ttt gta
tcc ctt gtg atg ttt gcc ctt atg atg tgt gat gat cgg atc tcc atg
caa gaa aga cgc aaa gag atc atg ctt gga tt
    
```

Figure 2-6. Sequencing of the His₆-tag insert at position 894 with upstream primer LW5HISUP. The sequence shown was a fragment of *hgfat1*-cDNA located in the pET 301/CT-DEST expression clone. The 846 bp fragment began at position 702 and confirmed the presence of the His₆-tag insert. Sequencing was performed by MOBIX and the construct was confirmed to be *hgfat1*-cDNA by BLAST analysis (NCBI Reference Sequence: NM_001244710.1).

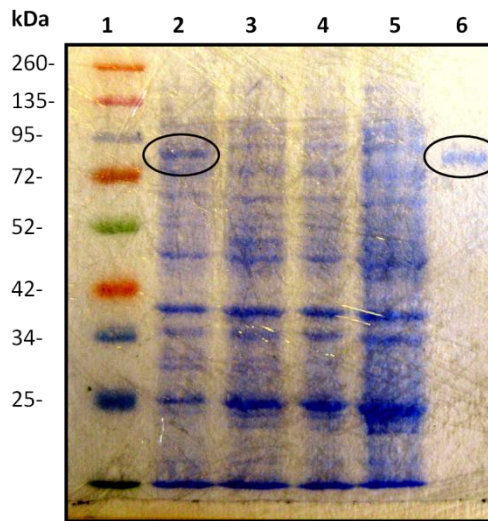


Figure 2-7. Photograph of SDS-PAGE gel (4% stacking, 10% resolving) with pET-301/CT-DEST *hgfat1*-His₆⁸⁹⁴ transformed Rosetta 2™ *E.coli* cell cultures. Lane 1: Spectra Broad Range Molecular Weight Multi-Colour Protein Marker (Fermentas Canada Inc, Burlington, ON), Lane 2: IPTG induced culture, harvested at 3 hrs, Lane 3: Non-IPTG induced culture, harvested at 3 hrs, Lane 4: IPTG-induced cell culture, harvested after 22 hrs, Lane 5: Non-IPTG induced cell culture, harvested after 22 hrs, Lane 6: Previously purified rhGFAT-His₆²⁹⁸. The hGFAT1 monomer had a molecular weight of 77 kDa.

Purified GFAT was characterized with the Morgan-Elson Assay, SDS-PAGE (Figure 2-8), and the Bio-RAD Protein Assay Kit (Bio-RAD, CA) to determine activity, purity and concentration of the enzyme. On average, 4 L of cell culture or 8 g of cell pellet yielded 1.2-1.8 mg of highly pure and active GFAT.

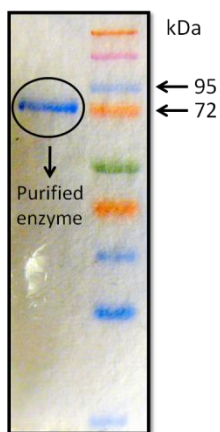


Figure 2-8. SDS-PAGE gel (8% stacking, 16% resolving) of FPLC purified rhGFAT-His₆²⁹⁸, purified with a 5 mL HisTrap FF Ni (II) column (GE Healthcare) on an ÄKTA 100 Purifier FPLC™ system (GE Healthcare). The gel was run for 40 min at constant 200 V and stained with Coomassie Brilliant Blue. The lane on the right featured the Spectra Broad Range Molecular Weight Multi-Colour Protein Marker (Fermentas Canada Inc., Burlington, ON) while the lane on the left featured a purified sample of rhGFAT-His₆²⁹⁸, 0.8 µg.

To ensure GFAT maintained enzymatic activity, it was necessary to purify the enzyme at 4 °C and store it in the presence of its substrate, 1 mM F6P, along with a reducing agent, 2 mM Tris (2-carboxyethyl) phosphine hydrochloride.³ Using these additives, recombinant human GFAT retained activity for at least 3 years when stored at -80°C.

Overall, we found it difficult to achieve high-levels of protein expression with this system, as compared to the method employed by the Badet-Denisot group.^{5b} On average we expressed 0.19 mg protein/g cell pellet, whereas Badet-Denisot had levels around 0.5-1 mg protein/g cell pellet. This was possibly due to the large size of *hgfat1*-cDNA (2.1 kb) and GFAT expression clone combined (10 kb). Badet-Denisot utilized a

pET28a(+) vector, 5.4 kb in length, or 7.5 kb with *hgfat1*-cDNA. Given the modest levels of protein expression, a method for large-scale protein production was developed.

Large-Scale GFAT Expression

Given the enzyme quantities required for the planned HTS campaign, a process for large-scale protein expression was developed. The Mobile Pilot Plant Fermentor (New Brunswick Scientific) was employed to grow 20 – 22 L of GFAT expression culture at one time. The fermentor could hold up to 32 L, self-autoclaved any media, self-sterilized sample valves, and could incubate culture from 18 °C to 37 °C. Cell pellets were harvested directly from the fermentor in tandem with a pump that delivered the culture to a centrifuge. Each large scale fermentation produced 32 - 40 g of cell pellet effectively quadrupling the amount obtained using the smaller scale fermentations described above. We estimated that 40 mg of enzyme would be sufficient to complete a screen of 3950 bioactive compounds in duplicate, including controls, a pilot screen, hit-validation studies, and instrument dead volume and, as such, five large-scale fermentations were carried out.

Characterization of rhGFAT1-His₆²⁹⁸

While agarose gel electrophoresis and DNA sequencing confirmed the presence of *hgfat1*-cDNA, and SDS-PAGE confirmed expression of the protein, enzyme activity was determined using the Morgan – Elson Assay.¹² Figure 2-9 and Figure 2-10 confirmed that recombinant human GFAT1 was able to retain catalytic activity despite being expressed in a prokaryotic system, following cell-lysis, and after insertion of a hexa-

histidine affinity tag and the IMAC purification process. rhGFAT1-His₆²⁹⁸ also displayed similar Michaelis-Menten kinetics compared to literature values as evident in Figure 2-11. Comparing the effect of known amidotransferase inhibitor 6-diazo-5-oxo-L-norleucine (DON)⁴ to native and recombinant GFAT produced similar results as well indicating that competitive inhibitors for the recombinant enzyme should behave analogous to the native enzyme (Figure 2-12).

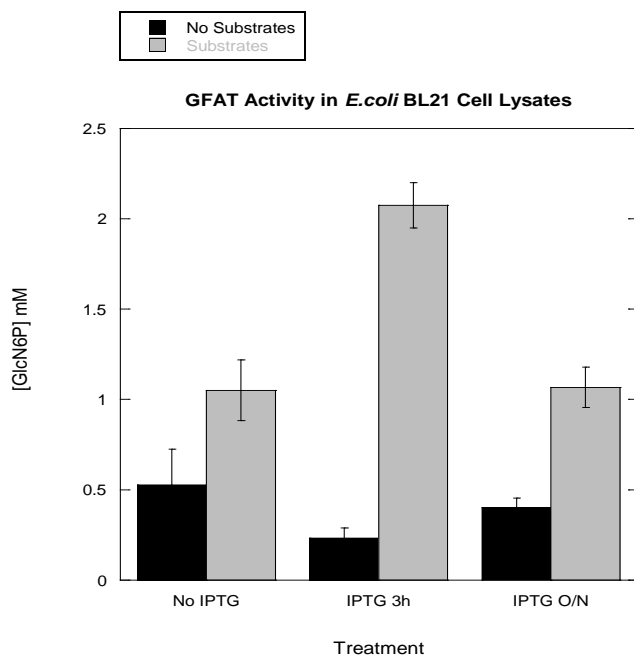


Figure 2-9. Comparison of GFAT activity measured in Rosetta 2™ *E.coli* cell lysates with the pET-301/CT-DEST *hGFAT1*-His₆⁸⁹⁴ protein expression clone. Cells were treated with either no IPTG before harvesting, (No IPTG), harvested after induction for 3 hours (IPTG 3 h), or after overnight incubation (IPTG O/N). Equal volumes of lysate were tested for GFAT activity with the Morgan-Elson assay in either the presence or absence of 10 mM GFAT substrates F6P and L-gln. Following a One-Way ANOVA with Tukey's All-Pairs Comparison (KaleidaGraph, v4.1), treatment with IPTG for 3 h when tested with substrates was significant as compared to no treatment or overnight treatment ($p=0.0002$, $p=0.0003$ respectively). No significant difference was found between samples not assayed with substrates.

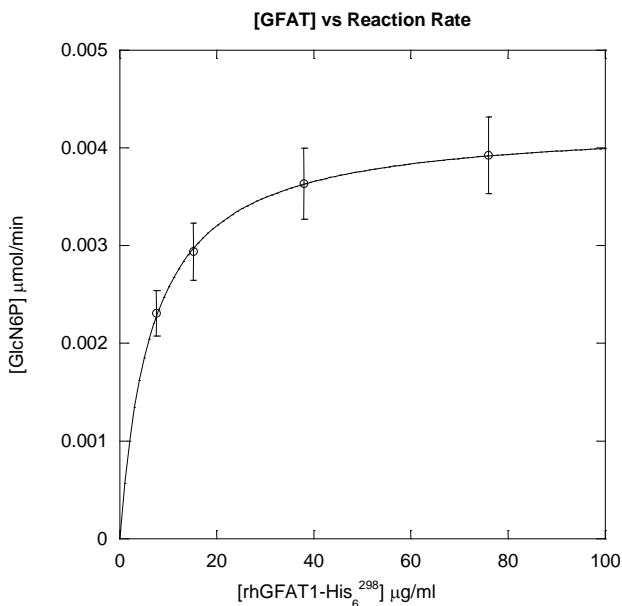


Figure 2-10. Determining the activity of rhGFAT-His₆²⁹⁸ following protein purification and buffer exchange assessed by the Morgan-Elson assay. Initially, there was an increase in the rate of GlcN6P production with increasing enzyme concentration, which eventually reached its maximum velocity.

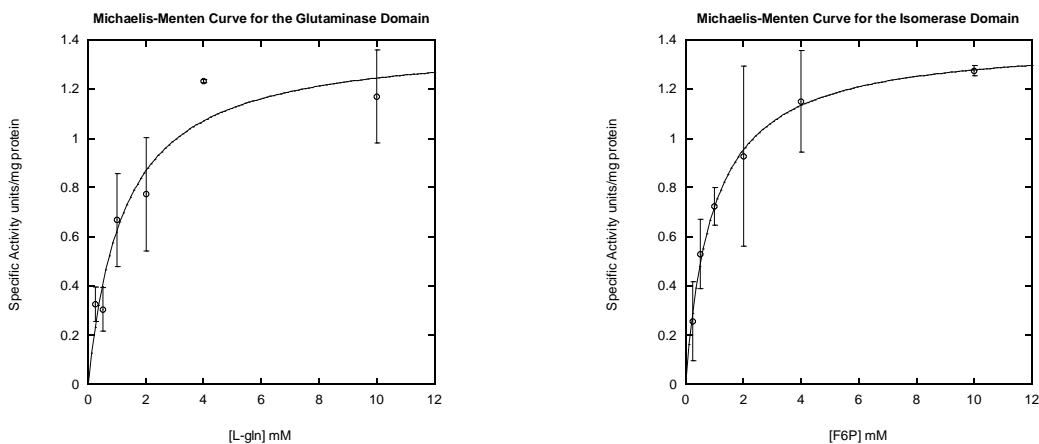


Figure 2-11. Michaelis-Menten kinetics for the glutaminase and isomerase domains of rhGFAT-His₆²⁹⁸. Michaelis-Menten kinetics was observed with the Morgan-Elson assay varying one substrate while keeping the other in excess at 10 mM. The K_M for the glutaminase domain was 0.83 – 1.59 mM, and for the isomerase domain the K_M was 0.66 - 1.2 mM. Both of these numbers were in good agreement within error with the literature values of 0.8-0.84 mM and 0.98-1.04 mM for the glutaminase and isomerase domains respectively.¹³ One unit is defined as 1 µmol of GlcN6P produced per minute.

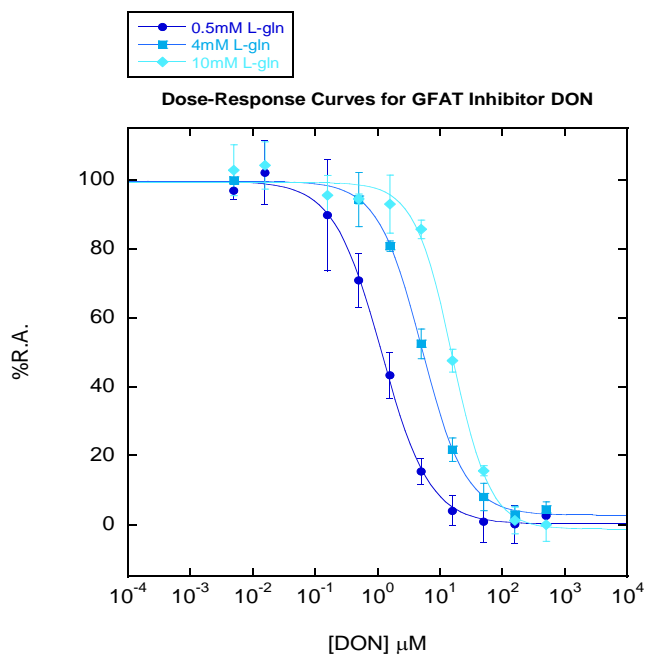


Figure 2-12. Dose-Response curves for GFAT inhibitor 6-diazo-5-oxo-L-norleucine (DON). DON exhibits competitive inhibition with substrate L-gln, as demonstrated experimentally by an increase in IC_{50} with an increase in substrate. Inhibitory activity was tested at various levels of L-gln with constant 20 mM F6P. rhGFAT1-His₆²⁹⁸ expressed in SF9 insect cells had an IC_{50} for DON of 18 μM with 10 mM L-gln and F6P^{5a} which was similar to the IC_{50} found here 15.7 \pm 1.7 μM at the same L-gln concentration. At the 0.5 and 4 mM levels, the IC_{50} was 1.16 \pm 0.08 μM and 5.13 \pm 0.18 μM respectively. This corresponds to a 4.4 and 13.4 fold increase in IC_{50} from the 0.5 mM L-gln concentration. Dose-response curves were fit using KaleidaGraph 4.1 and the four-point parameter Hill-equation.

Conclusion

An insertion of an internal affinity tag in hGFAT-1 by site-directed mutagenesis *via* PCR was demonstrated to be more straight-forward and facile than the method presented by Richez *et al.*^{5a} A reliable and reproducible method was developed for the large scale expression and purification of functional recombinant human GFAT. A procedure for large-scale expression was included which was necessary if the user wishes to perform a high-throughput screen for the enzyme or structural X-ray crystallography studies. The enzyme produced under these conditions was utilized for probe-discovery and further lead characterization.

Materials & Methods:

GFAT Cloning: Multi-Site Gateway® Cloning Technology

*i) PCR amplification of *hgfat1*-cDNA*

A plasmid (pCIS-GFAT) encoding human *gfat1*-cDNA was donated by Michael J. Quon. The *hgfat1*-cDNA fragment from the pCIS-GFAT vector was amplified and flanked with *attB1* and *attB2* sites for recombination with the *attP* sites in the pDONR 221 vector. The forward primer was designed as follows, Forward: 5`- GGGG ACA AGT TTG TAC AAA AAA GCA GGC **TTC GAA GGA GAT ATA CAT *ATG TGT GGT ATA TTT GCT TAC TTA AAC TAC C*** -3`. The *attB1* sequence is underlined, the *hgfat1*-cDNA sequence is bolded, the start codon is italicized and bolded, the Shine-Dalgarno sequence is underlined and italicized. The reverse primer consisted of the following sequence, Reverse: 5`- GGG GAC CAC TTT GTA CAA GAA AGC TGG GTC TCA CTC TAC AGT CAC AGA TTT GGC AAG -3`. The underlined region indicates the *attB2* site, the italicized region indicates the stop codon in the reverse primer and the bolded region indicates the *hgfat1*-cDNA genetic code.

Reagent:	Volume:
10x Pfu polymerase buffer + MgSO ₄	5 µL
Forward Primer-GFATFWD (1 mM)	2 µL
Reverse Primer-GFATREV (1 mM)	2 µL
dNTP mix (4 mM)	2.5 µL
pCIS-GFAT (100 ng/µL)	1 µL
ddH ₂ O	36.5 µL
Pfu polymerase	1 µL
Total Reaction Volume:	50 µL

Table 2-1. Reagents used for PCR to isolate *hgfat1*-cDNA for use with Gateway® Cloning vector pDONR 221. Forward and Reverse primers were obtained from MOBIX (McMaster University, Hamilton, ON), Fermentas Pfu DNA Polymerase (recombinant) and buffer was from Thermo Scientific Life Science Research (Cat. No. EP0501), along with the 10 mM dNTP mix (#R0191) which was diluted before use.

PCR was performed under the following reaction conditions (Table 2-1): 1 cycle at 95 °C for 1 min, 30 cycles of 95 °C for 1 min, 54 °C for 1 min, and 72 °C for 5 min, followed by 1 cycle of 72 °C for 10 min, and a final hold at 4 °C for a total of 32 cycles. The success of the PCR reaction was confirmed by running the DNA fragment (1,2, and 5 µL samples) alongside a 1 kb DNA ladder (Gene Ruler™ 1 kb Ready-to-use DNA ladder, Fermentas) *via* 1% TAE (40 mM Tris, 20 mM acetic acid, 1 mM EDTA, pH 8.0) agarose gel electrophoresis for 45 minutes at constant 115 V. The PCR amplified fragment was purified by a QIAGEN QIAquick Gel Extraction Kit 50 (Cat. No. 28704, QIAGEN, Toronto, ON), sequenced and analyzed with Basic Local Alignment Search Tool (BLAST).

ii) *Creation of the hgfat1-cDNA entry clone*

The PCR-amplified fragment containing *hgfat1* was inserted into the donor vector (pDONR221) using the BP Clonase II reaction (pDONR Vectors Manual, Version E, Cat. No. 11798-014, Invitrogen, Life Technologies). An equimolar amount of PCR product and donor vector was preferred, ideally 50 femtomoles of each. In a 10 µL total reaction volume, 6 µL of PCR product was combined with 1 µL of pDONR221 vector, 1 µL TE buffer, pH 8.0, and 2 µL of BP Clonase II enzyme mix. After one hour incubation at r.t., 1 µL of 2 µg/mL Proteinase K solution was added and incubation continued for 10 minutes at 37 °C. Once the incubation time was complete, the Donor Vector was used to transform chemically competent *E.coli* One Shot® Top 10 cells (Invitrogen, Life Technologies). The *E. coli* cells were transformed with 2 µL of the BP cloning reaction and were incubated on ice for 20 minutes. The cells were heat shocked at 42 °C for 2 minutes and cooled on ice for 2 minutes before adding 900 µL of SOC media and incubating for 1 hour at 37 °C/200 rpm. The cells were cultured on pre-warmed Luria-

Bertani media (LB)/Agar/ 50 µg/mL kanamycin Petri dishes and incubated overnight at 37 °C to select desired transformants. A well-spaced colony was selected for plasmid isolation and sequencing analysis. Isolation of plasmid DNA was performed according to manufacturer's instructions (Qiagen QIAprep Spin MiniPrep Kit 50, Cat. No. 27104). Isolated plasmid DNA was analyzed *via* sequencing (MOBIX) and BLAST analysis using M13 forward and reverse primers. Presence of *hgfat1*-cDNA was confirmed (ref. NM 002056.1), along with the inserted Shine-Dalgarno sequence. All antibiotics used were purchased from BioShop Canada (Burlington, ON).

iii) Creation of the hgfat1-cDNA expression clone

To generate the expression clone from the entry clone (pDONR221-*hgfat1*) and destination vector (pET301/CT-DEST), the LR recombination reaction was performed according to the manufacturer's instructions. The purified plasmid DNA of the entry clone was resuspended in TE buffer to yield a final concentration of 150 ng/µL, likewise for the destination vector. The LR Clonase II enzyme mix was used to catalyze the recombination reaction between the entry clone and the destination vector to yield the expression clone. The cloning reaction was used to transform chemically competent *E. coli* Top10 cells and successful transformants were selected on LB/Agar/100 µg/mL ampicillin Petri dishes. A well-spaced colony was selected for plasmid isolation and DNA sequencing. Isolated plasmid DNA samples were sequenced using T7 Promoter and T7 Terminator as primers. BLAST analysis confirmed the presence of *hgfat1*-cDNA (ref NM 002056.1) within the pET301/CT-DEST expression clone.

Induced protein expression with Rosetta 2™ E.coli transformed with the hgfat1-cDNA expression clone

The isolated expression clone (pET301/CT-DEST/hgfat1-cDNA) was used to transform chemically competent Rosetta 2™ *E.coli* (71402-3, EMD 4 Biosciences, EMD Millipore, San Diego CA). Positive transformants were selected on LB/Agar/50 µg/mL ampicillin/34 µg/mL chloramphenicol pre-warmed Petri dishes (ampicillin was used to select for the pET301/CT-DEST hGFAT1 expression plasmid and chloramphenicol to select for the pRARE2 plasmid). An isolated colony was selected to induce expression. The transformant was cultured in 5 mL of LB broth overnight with 50 µg/mL ampicillin and 34 µg/mL chloramphenicol with shaking and heating at 37 °C. The 5 mL seed stock was transferred to a sterile 1 L stock of LB broth with the same antibiotics. The culture was grown until OD₆₀₀ reached 0.55. Expression was induced with 0.3 mM IPTG and the culture was further incubated for another 5 hrs. The cells were harvested in a temperature controlled centrifuge (5000 rpm, 4 °C, 20 min). The cell pellet was collected and stored at -80 °C.

SDS-PAGE of E.coli cell lysates following protein expression of rhGFAT-1

The cell pellet was resuspended in 25 mL of lysis buffer (50 mM Tris-HCl, pH 7.8, 200 mM NaCl, 1 mM F6P, 1 mM DTT, 1 mM PMSF, 10% glycerol) and lysed with an Avestin Emulsiflex-C5 homogenizer. The lysed cells were centrifuged (4000 rpm, 4 °C, 10 min) to remove any insoluble material. The cell lysate was kept on ice and subjected to SDS-PAGE. A 4% stacking gel and 10% resolving gel was used and was run at 200 V for 50 minutes. A Spectra Multi-Colour Broadrange Protein Ladder (Fermentas, Thermo

Scientific, Ottawa, ON) was used as a standard and 1 µL samples of lysate were applied to the gel. The gel was stained with Coomassie Blue.

Entry clone hexa-histidine tag insertion by site-directed mutagenesis via PCR

After successful expression of rhGFAT-1 from the expression clone, six histidine codons were inserted at gene position 894 by two-rounds of site-directed mutagenesis *via* PCR. The entry clone plasmid was selected as the genetic source to perform the insertion. In between PCR rounds, the plasmid DNA was transformed and propagated in chemically competent *E.coli* One Shot® Top 10 cells. The plasmid DNA was isolated with the QIAGEN QIAprep Spin MiniPrep Kit (Cat. No. 27104, QIAGEN, Toronto, ON) before the addition of the remaining histidine codons. Two sets of primers were designed as follows: Primer Design Pair 1, Forward (FWDHIS3L): 5`-CCATCGAATTAAACGAACTGCA **CACCACCAC**GGAGATCA CCCC GGACGAGC -3`, Reverse (REVHIS3L): 5`- GCTCGTCCG GGGTGATCTCC**GTGGTGGTGT**GCAGTTCGTTTAATTCGATGG-3`, Primer Design Pair 2, Forward (FWDHISL): 5`-CCATCGAATTAAACGAACTGCA**CACCACCACCACCACCAC**GGAG ATCACCCCGGACGAGC -3`, Reverse (REVHISL): 5`- GCTCGTCCGGGGTGATCTCC**GTGGTGTGGTGTGGTGTGGTGT**GCAGTTCGTTTAATTCGATGG-3`. The bolded regions refer to the inserted histidine codons.

PCR was performed under the following reaction conditions (Table 2-2): 1 cycle at 95 °C for 5 minutes, 18 cycles of 95 °C for 1 min, 53 °C for 1 min, and 68 °C for 14 minutes, and a final hold at 4 °C. Parent DNA was digested with 1 µL DpN1 10 U/µL (ER1705, Fermentas, Thermo Scientific Life Science Research) and incubation at 37 °C for one hour. The successful hexa-histidine codon insertion within the entry clone was

confirmed with DNA sequencing (MOBIX Lab, McMaster University) using M13 primers to see the start and end of the *rhgfat1* gene as well as a primer designed especially for sequencing (LW5HISUP) just upstream of the inserted histidine codons.

Reagent:	Volume:
10X Pfu polymerase buffer + MgSO ₄	5 µL
Forward Primer-FWDHIS3L or FWDHISL (1 mM)	1 µL
Reverse Primer-REVHIS3L or REVHISL(1 mM)	1 µL
dNTP mix (4 mM)	4 µL
pDONR221- <i>hgfat1</i> (100 ng/µL)	1 µL
ddH ₂ O	37 µL
Pfu polymerase	1 µL
Total Reaction Volume:	50 µL

Table 2-2. Reagents used for PCR to insert 3 histidine codons at gene position 894 in *hgfat1*-cDNA within the pDONR221 entry clone. Primers were obtained from MOBIX, all other reagents from Thermo Scientific Life Science Research.

After successful insertion of the histidine codons, an expression vector was generated by cloning *hgfat1*-His₆⁸⁹⁴ cDNA into the destination vector, pET301/CT-DEST plasmid using the LR recombination reaction. A 10 µL reaction mixture containing 2 µL of 70 ng/µL of Entry Clone, 1 µL of 150 ng/µL Destination Vector, 5 µL of 1xTE buffer pH 8.0, and 2 µL of the LR Clonase II enzyme mix was incubated for 1 hour at r.t. To this solution, 1 µL of Proteinase K solution was incubated for 10 min at 37 °C. This expression vector was propagated and isolated from *E.coli* One Shot[®] Top 10 cells before transformation into Rosetta 2[™] *E. coli*.

Optimizing protein expression of recombinant human GFAT1-His₆²⁹⁸

Transformed Rosetta 2[™] glycerol stocks with the pET301/CT-DEST *hgfat1*-His₆⁸⁹⁴ cDNA expression clone were thawed, and sterile 4x50 mL LB broth flasks were inoculated. Antibiotics were added to a final concentration of 50 µg/mL ampicillin and 34 µg/mL chloramphenicol. Seed cultures were incubated with shaking (200 rpm)

overnight at 37 °C. The seed cultures were transferred to 4x1 L sterile LB stock with the same antibiotics. Flasks were incubated with shaking at 37 °C. When $OD_{600} = 0.4-0.6$, IPTG was added to a final working concentration of 0.5 mM. Cultures were incubated for 3 hrs or overnight before harvesting by centrifugation (5000 rpm for 20 min at 4 °C). Cell pellets were harvested, weighed and stored at -80 °C until ready for lysis and SDS-PAGE analysis. Samples were run on a 4% stacking, 10% resolving gel at 200 V for 40 min and stained with Coomassie blue.

Purification of rhGFAT1-His₆²⁹⁸ by Immobilized Metal Affinity Chromatography (IMAC) via FPLC

About 6-8 g of expression pellet was thawed on ice and resuspended 3:1 (mL of buffer to gram of pellet) in GFAT Lysis Buffer (Table 2-3). Cells were lysed by cell disruption at 20 kpsi, 4 °C (Cell disrupter with continuous flow head, Constant Systems, Ltd., UK). Benzonase® Nuclease HC, Purity >90% (Cat. No. 71205, Merck4Biosciences, EMD Millipore, Billerica, MA) was added to the cell lysate on ice at a final concentration of 25 U/mL and allowed to incubate for one hour. Phenylmethyl sulfonyl fluoride (PMSF, PMS123, BioShop Canada Inc., Burlington, ON) was also added. Following DNA degradation, imidazole (IMD510, BioShop Canada Inc., Burlington, ON) was added to the cell lysate to a final concentration of 10 mM. The cell lysate was centrifuged at 21,000 rpm at 4 °C for 30 minutes and filtered through 0.22 µm sterile filters to remove insoluble material. The rhGFAT1-His₆²⁹⁸ was purified *via* FPLC (ÄKTA 100 Purifier FPLC™, GE Healthcare Life Sciences) on a 5 mL HisTrap FF column (17-5255-01, GE Healthcare Life Sciences) using GFAT Wash Buffer for removing unwanted proteins and GFAT Elution buffer to elute the enzyme. Fractions containing active GFAT were pooled

together, concentrated and buffer exchanged with GFAT Storage Buffer using Amicon Ultra-15 Centrifugal Filter Units with Ultracel-30 Membrane (Millipore, Billerica, MA). Concentrated enzyme (0.4 mg/mL) was stored at -80 °C until further use. GFAT enzyme prepared in this manner was stable for up to 3+ years.

Components**	GFAT Lysis Buffer	GFAT Wash*	GFAT Elution*	GFAT Storage Buffer
50 mM Tris-HCl, pH 7.8	Yes	Yes	Yes	Yes
[NaCl] mM	20	200	200	200
[Imidazole] mM [§]	0-10	10	500	0
1 mM F6P	Yes	Yes	Yes	Yes
2 mM TCEP	Yes	Yes	Yes	Yes
10% Glycerol	Yes	Yes	Yes	Yes
1 mM PMSF	Yes [#]	Yes	Yes	Yes
2 mM MgCl ₂	Yes	No	No	No

Table 2-3. Buffer reagents required for complete GFAT purification, from cell lysis to enzyme storage. A few conditions must be observed for the best results: * Wash and Elution buffers were filtered through a 0.45-0.22 µm vacuum filter before use on the FPLC, **For long-term storage, buffers were kept at -20 °C, for short term storage they were kept at 4 °C, [§]Imidazole concentration in cell lysate was increased just prior to FPLC purification, # Was not added directly to prepared lysis buffer, was added immediately after cells were lysed *via* cell disruption or foaming may occur. All buffers contained the reducing agent tris (2-carboxyethyl) phosphine hydrochloride or TCEP (TCE101, BioShop Canada, Burlington, ON). This reducing agent was compatible with the His-Trap FF column.

Large-scale expression of rhGFAT1-His₆²⁹⁸ with industrial fermentor & tandem centrifuge

Two 200 mL seed cultures with pET301/CT-DEST *hgfat1*-His₆⁸⁹⁴ expression clone transformed Rosetta 2TM glycerol stocks were prepared with appropriate antibiotics for overnight incubation. LB broth for 22 L of culture was prepared for use with the Mobile Pilot Plant Fermentor and Centrifuge (MPP-40 Mobile Fermentation Pilot Plant system with gas overlay kit, New Brunswick Scientific). The media was autoclaved within the fermentor and overnight pET301/CT-DEST *hgfat1*-His₆⁸⁹⁴ *E.coli* seed cultures were added once the sterilization cycle was finished and the media had cooled to 37 °C. Protein

expression was induced with 0.5 mM IPTG when OD_{600} reached 0.4. Cells were harvested after a 3 hr incubation period in tandem by centrifuge. Cell pellets were stored at $-80\text{ }^{\circ}\text{C}$ until ready for purification.

Standard Morgan-Elson Assay for Detection of GFAT Activity

The assay was performed within a polystyrene 96-well plate with a total assay volume of 290 μL . The assay was performed in 3 steps; incubation of enzyme and substrates; acetylation of GlcN6P; and visualization with Ehrlich's reagent. The 100 μL incubation mixture consisted of: 10 mM L-glutamine (L-gln, G3126, Sigma Aldrich, Oakville, ON), 10 mM fructose-6-phosphate disodium salt hydrate (F6P, F3627, Sigma-Aldrich, Oakville, ON), 1x phosphate buffered saline (PBS), 5 mM ethylenediaminetetraacetic acid (EDTA), 1 mM dithiothreitol (DTT, DTT002, BioShop Canada Inc., Burlington, ON), inhibitor solution, and the GFAT enzyme preparation or tissue extract. Distilled deionized water was used to fill the remaining assay volume when necessary. The incubation volume was mixed thoroughly and the assay plate was sealed with aluminum plate-sealing film (Aluminum Seal film, PCR-AS-200, Axygen Scientific, VWR Canada, Mississauga, ON), and placed in a $37\text{ }^{\circ}\text{C}$ water bath for 1 hour. A 1.5% acetic anhydride solution in acetone (10 μL) and 200 mM potassium tetraborate (50 μL) were added to the incubation mixture and it was doubly sealed followed by heating in a water bath at $80\text{ }^{\circ}\text{C}$ for 25 min. The plate was cooled on ice for 5 minutes before Ehrlich's reagent (*p*-dimethylaminobenzaldehyde, 156477, Sigma Aldrich, Oakville, ON) was added. Ehrlich's reagent was diluted 2:1 in acetic acid directly before use. The plate was sealed and heated in a water bath for 20 min at $37\text{ }^{\circ}\text{C}$. The plate was

cooled to room temperature before absorbance was measured at 585 nm. When the plate could not be read the same day, it was stored at -20 °C. Samples to create a standard curve of GlcN6P (G5509, Sigma Aldrich, Oakville, ON) were added after the incubation procedure. Buffer was added in place of enzyme in these samples (Table 2-4).

Purpose	Reagent	[Stock] Solutions	Volume added to well	[Final] in assay
Starting Materials	L-Glutamine	100 mM	10 µL	10 mM
Starting Materials	Fructose 6-Phosphate	100 mM	10 µL	10 mM
Buffer, pH 7.45	PBS	10X	10 µL	1X
Chelating Agent	EDTA	50 mM	10 µL	5 mM
Reducing Agent	DTT	10 mM	10 µL	1 mM
	Water		Up to 100 µL	
Enzyme Source	GFAT enzyme or Lysate preparation		0.25-50 µL	
Inhibits Enzyme	+/- Inhibitor		10 µL	
Standards	GlcN6P standards	0, 2.5, 5, 10, 20, 30 mM	10 µL	0-3 mM
Acetylating Agent	Acetic Anhydride	1.5% acetic anhydride in acetone	10 µL	0.09%
pH-Stabilizer/ Acetylating Agent	Potassium Tetraborate	200 mM	50 µL	62.5 mM
Indicator	Ehrlich's reagent	2 g <i>p</i> -dimethylaminobenzaldehyde /0.3 mL water + 2.2 mL conc. HCl/17.4 mL acetic acid (dilute 1:2 in acetic acid before use)	130 µL	100.4 mM

Table 2-4. Stock solutions and reagents required for the Morgan-Elson assay with Ehrlich's reagent.

Ehrlich's reagent was an acidic solution of *p*-dimethylaminobenzaldehyde. The preparation of the stock kept for 2-3 months when stored away from light at 4 °C.

Measurement of rhGFAT1-His₆²⁹⁸ activity in E.coli cell lysates

Three 5 mL seed cultures of the Rosetta 2™ GFAT expression strain were incubated overnight in LB broth at 37 °C with shaking. Each seed culture was transferred

to a 1 L flask of sterile LB with 50 µg/mL ampicillin and 34 µg/mL chloramphenicol and continued to incubate with shaking. Once $OD_{600} = 0.4-0.6$, protein expression was induced with 0.5 mM IPTG. Cells were harvested after 3 hrs and overnight induction. A 1 L non-induced sample was also harvested. Cell pellets were weighed and resuspended in 5 mL of Lysis Buffer per gram of cell pellet. Cells were lysed with an Avestin Emulsiflex-C5 homogenizer. The lysed cells were centrifuged (4000 rpm, 4 °C, 10 min) to remove any insoluble material. The cell lysate was kept on ice and 50 µL samples were tested in triplicate for GFAT activity with the standard Morgan-Elson assay. Samples were also tested without added substrates to compare background levels of GlcN6P production.

Determination of Michaelis-Menten Kinetics of rhGFAT1-His₆²⁹⁸

The Morgan-Elson assay was performed under standard conditions with 7 nM rhGFAT1-His₆²⁹⁸ enzyme per well. A set of GlcN standards which did not contain enzyme were included in triplicate as well to form a calibration curve. The rate of GFAT activity was measured by quenching the enzyme reaction with acetic anhydride after 5, 10, 20 and 30 minutes of incubation. The rates were measured in duplicate under varying substrate conditions from 0.25, 5, 1, 2, 4, 10 mM of either L-Gln or F6P while keeping the second substrate constant at 10 mM. The acetylation and visualization steps were performed as normal.

Determination of the Inhibitory Effect of DON on rhGFAT1-His₆²⁹⁸

The half-maximal inhibitory concentration (IC₅₀) for 6-diazo-5-oxo-L-norleucine or DON (D2141, Sigma Aldrich, Oakville, ON) was measured using the Morgan-Elson assay under standard conditions with 7 nM rhGFAT1-His₆²⁹⁸ enzyme per well. A half-log dilution series from 500 to 0.005 μM of DON in ddH₂O was used. Enzyme activity was measured in triplicate at various L-gln levels (0.5, 4, 10 mM) while keeping F6P constant at 20 mM in assay solution. A positive control containing enzyme but no inhibitor was used along with a negative control containing no enzyme or added inhibitor.

References

1. Chou, K.-C., Molecular Therapeutic Target for Type-2 Diabetes. *J. Proteome Res.* **2004**, *3* (6), 1284-1288.
2. Huynh, Q. K.; Gulve, E. A.; Dian, T., Purification and Characterization of Glutamine:Fructose 6-Phosphate Amidotransferase from Rat Liver. *Arch. Biochem. Biophys.* **2000**, *379* (2), 307-313.
3. Broschat, K. O.; Gorka, C.; Page, J. D.; Martin-Berger, C. L.; Davies, M. S.; Huang Hc, H. C.; Gulve, E. A.; Salsgiver, W. J.; Kasten, T. P., Kinetic Characterization of Human Glutamine-Fructose-6-Phosphate Amidotransferase I: Potent Feedback Inhibition by Glucosamine 6-Phosphate. *J. Biol. Chem.* **2002**, *277* (17), 14764-14770.
4. Milewski, S., Glucosamine-6-Phosphate Synthase—the Multi-Facets Enzyme. *BBA-Protein Struct. M.* **2002**, *1597* (2), 173-192.
5. (a) Richez, C.; Boetzel, J.; Floquet, N.; Koteswar, K.; Stevens, J.; Badet, B.; Badet-Denisot, M. A., Expression and Purification of Active Human Internal His(6)-tagged L-glutamine: D-Fructose-6P Amidotransferase I. *Protein Express. Purif.* **2007**, *54* (1), 45-53; (b) Li, Y.; Roux, C.; Lazereg, S.; LeCaer, J. P.; Laprevote, O.; Badet, B.; Badet-Denisot, M. A., Identification of a Novel Serine Phosphorylation Site in Human Glutamine:Fructose-6-Phosphate Amidotransferase Isoform 1. *Biochemistry* **2007**, *46* (45), 13163-13169.
6. Landy, A., Dynamic, Structural, and Regulatory Aspects of Lambda Site-Specific Recombination. *Ann. Rev. Biochem.* **1989**, *58* (1), 913-941.
7. Kaneko, T.; Mizushima, T.; Ohtsuka, Y.; Kurokawa, K.; Kataoka, K.; Miki, T.; Sekimizu, K., Co-induction of DNA Relaxation and Synthesis of DnaK and GroEL Proteins in Escherichia coli by Expression of LetD (CcdB) Protein, an Inhibitor of DNA Gyrase Encoded by the F factor. *Molec. Gen. Genet.* **1996**, *250* (5), 593-600.
8. Tegel, H.; Tourle, S.; Ottosson, J.; Persson, A., Increased Levels of Recombinant Human Proteins with the Escherichia coli Strain Rosetta(DE3). *Protein Express. Purif.* **2010**, *69* (2), 159-167.
9. Chen, H.; Ing, B. L.; Robinson, K. A.; Feagin, A. C.; Buse, M. G.; Quon, M. J., Effects of Overexpression of Glutamine:Fructose-6-Phosphate Amidotransferase (GFAT) and Glucosamine Treatment on Translocation of GLUT4 in Rat Adipose Cells. *Mol. Cell. Endocrinol.* **1997**, *135* (1), 67-77.
10. Jin, H.; Zhao, Q.; Gonzalez de Valdivia, E. I.; Ardell, D. H.; Stenström, M.; Isaksson, L. A., Influences on Gene Expression in vivo by a Shine–Dalgarno Sequence. *Mol. Microbiol.* **2006**, *60* (2), 480-492.
11. Qi, D.; Scholthof, K. B., A One-Step PCR-based Method for Rapid and Efficient Site-Directed Fragment Deletion, Insertion, and Substitution Mutagenesis. *J. Virol. Methods* **2008**, *149* (1), 85-90.
12. Elson, L. A.; Morgan, W. T. J., A Colorimetric Method for the Determination of Glucosamine and Chondrosamine. *Biochem J.* **1933**, *27* (6), 1824-1827.
13. Durand, P.; Golinelli-Pimpaneau, B.; Mouilleron, S.; Badet, B.; Badet-Denisot, M. A., Highlights of Glucosamine-6P Synthase Catalysis. *Arch. Biochem. Biophys.* **2008**, *474* (2), 302-17.

Chapter 3

Identification of GFAT Inhibitors: Assay Development and High-Throughput Screening Campaign

Preface

This work was completed with the assistance of Jan Blanchard and Jenny Wang, both from the High-Throughput Screening facility at the Center for Microbial Chemical Biology at McMaster University. Dr. Emelia Awuah synthesized the isoquinoline compound described.

Abstract

A high-throughput screen to discover novel inhibitors for human L-glutamine:D-fructose-6-phosphate amidotransferase 1 (hGFAT1) has been successfully completed. A 3950 compound bioactive library was tested for inhibitory activity in duplicate against GFAT using a semi-automated and modified Morgan-Elson assay. From the primary screen, 58 compounds were identified as 'hits', showing 73% or less residual GFAT activity compared to controls. After secondary validation involving dose-response determination, 13 compounds were validated hits and 9 of these were selected as leads for further study.

Introduction

As outlined in the Introduction Chapter, there are only a handful of known GFAT inhibitors. Most of these are substrate derivatives and not ideal for *in vivo* studies showing relatively high toxicity, poor solubility and cell permeability.¹ Given the new source of GFAT, this Chapter describes the development and execution of a high-throughput screen (HTS) aimed at discovering new GFAT inhibitor leads with improved potency and pharmacokinetic properties.

High-throughput screening was originally developed as a tool by the pharmaceutical industry to increase the rate of lead discovery and drug generation.² In academia, HTS is used as a tool for probe development, particularly in new areas of research where little is known about a biological target.³ The rationale behind HTS relies on statistics – the more compounds tested, the more leads will be discovered. Automation by liquid-handler platforms and micro assay volumes are used to increase throughput, while chemical libraries consist of thousands to hundreds of thousands of compounds for screening.

However, recent debate has stated that HTS is not producing drug compounds in the pharmaceutical industry at the increased rate that was promised.⁴ HTS cannot be perceived as the start and end-point of a drug or probe discovery program, it realistically lies somewhere in the middle. After a specific biologic target of interest has been identified, validated and a source has been obtained, the next challenge is developing or modifying assay capabilities for an HTS platform. An HTS assay must be sensitive, reproducible, accurate, and economical.⁵ Any hits identified from the primary screen are

only the beginning. They require follow up with dose-response assays, a second, complementary assay, and further refinement of the chemical scaffold to improve activity. Whether drug/probe discovery is initiated with HTS, a “grind and find” approach from a natural product source,⁶ or a virtual screen,⁷ the downstream follow-up processes remain the same, regardless of which method was used.

Since a natural-products screen⁸ and a couple of virtual screens⁹ have already been performed, we ventured to perform the first HTS campaign to unveil novel GFAT inhibitors or hexosamine biosynthesis pathway chemical probes.

Results & Discussion

Modification and Optimization of the Morgan-Elson Assay for a High-Throughput Screening Platform

The Morgan-Elson assay had been used reliably on the bench top to monitor GFAT activity. However, some modifications and compromises were necessary in order to take advantage of the High-Throughput Screening (HTS) facility available at the McMaster University Center for Microbial Chemical Biology (CMCB).

As a method to compare variable changes in the assay or to measure the overall robustness of an assay, the Z-factor was employed. The Z-factor (Z') is a statistical parameter used to judge whether or not an assay will be useful for inhibitor screening (Equation 3-1).¹⁰ A Z-factor of 0 or less means the assay is unsuitable for screening, 0-0.5 indicates a marginal assay, 0.5-1 indicates a good assay, and a score of 1 would be ideal. Our goal was to achieve a Z' of 0.5 or better.

$$Z' = 1 - \frac{3(\sigma_p + \sigma_n)}{|\mu_p - \mu_n|} \quad \text{Eq. 3-1}$$

Where: σ_p = standard deviation of positive controls

σ_n = standard deviation of negative controls

μ_p = mean of positive controls

μ_n = mean of negative controls

The first step of the assay was enzyme incubation. How much enzyme to use in the assay and how long the incubation period should take were two questions we needed to answer. We found that an enzyme concentration of 0.04 mg/mL and an

incubation time of one hour were optimal for our screening purposes (Figure 3-1, Table 3-1).

[GFAT] mg/mL	Z-factor
0.09	0.68
0.04	0.75
0.03	0.67

Table 3-1. Optimal enzyme concentration for the Morgan-Elson assay. The Z-factor was used to judge to suitability of an assay for HTS (Eq. 3.1). A Z-score of 0.5 or higher indicated a good assay, while 1 would be ideal. We found 0.04 mg/mL was the best concentration of enzyme to use under the modified assay conditions. At the higher enzyme concentration, more error may occur due to the increased viscosity of the stock solution.

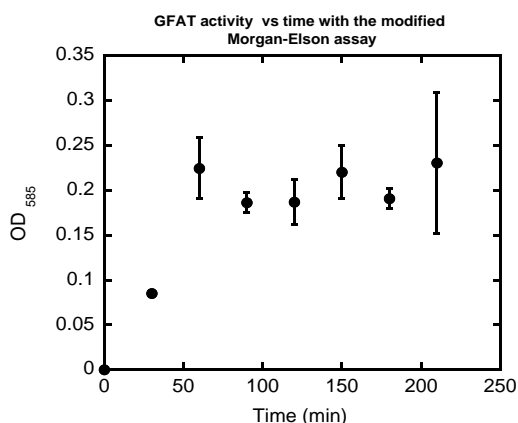


Figure 3-1. Optimal enzyme incubation time for the Morgan-Elson assay. Enzyme activity was quenched after the addition of acetic anhydride at 30 minute intervals. After 60 minutes of incubation, no increase in enzyme activity was observed.

The assay was usually performed with acetone during the acetylation step while concentrated acetic acid was present in Ehrlich’s reagent. Due to the vapour pressure of acetone, the solvent could “leak out” from micro-pipette tips used on the HTS platform causing errors in its dispensing into a microwell plate. Thus, each well may have a different volume of acetylating reagent and this would affect the consistency of the

results. Acetonitrile, which is much less volatile, was found to be an acceptable substitute to replace acetone without affecting assay sensitivity (Figure 3-2).

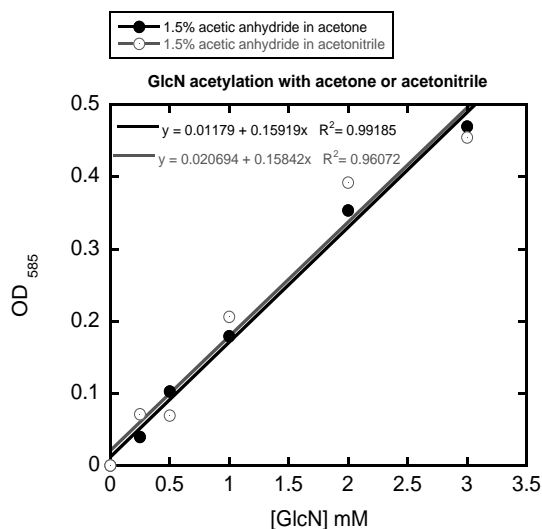


Figure 3-2. Use of acetone and acetonitrile solvents in the Morgan-Elson assay. Glucosamine standards were acetylated with a 1.5% acetic anhydride solution prepared in acetone (black circles) or acetonitrile (white circles). The slopes of each line were very similar which indicated that acetonitrile solvent did not affect the assay sensitivity.

Ehrlich's reagent is a concentrated solution of *para*-dimethylaminobenzaldehyde dissolved in acetic acid, hydrochloric acid and water. Its addition was generally carried out in a fume hood and could not be used directly on the HTS robotic platform. As a result, the addition of Ehrlich's reagent was performed manually off-line. Unfortunately, this downgraded the screen from fully- to semi-automated.

The incubation step with enzyme was usually performed at 37 °C in a water bath, the acetylation step was performed at 80 °C in a water bath, and the visualization step was performed at 37 °C in a water bath. Fortunately, one of the HTS robotic systems was equipped with a 37 °C incubator which allowed for incubation of biological

samples only. Unfortunately, the rest of the assay involved solvents, and there was not an online option to heat the microwell plates to the specified temperature after the acetylation and visualization reagents were added. Thus, these two steps were modified so that they could be performed at room temperature, albeit with a much longer incubation period. Typically acetylation at 80 °C took 25 minutes for reaction completion, at room temperature the reaction was allowed to incubate for 20 hours. The visualization step would previously take 25 minutes at 37 °C, at room temperature it was found that a 4 hour incubation time gave optimal results (Table 3-2).

Time (hours)	Z-factor
1	0.48
2	0.67
3	0.74
4	0.75
5	0.75

Table 3-2. Optimal incubation time for Ehrlich's Reagent with the modified Morgan-Elson assay. Upon the addition of Ehrlich's reagent, an incubation time of 4 hrs at room temperature was found to be optimal, yielding a Z' of 0.75. Extending the incubation time to 5 hrs did not increase the Z'.

Last but not least, the Morgan-Elson assay was performed on the bench top in a 96-well microtiter plate format. In order to increase throughput as well as decrease costs for reagents, materials and instrument time, 384-well microtiter plates were utilized for the screen. This decreased the total assay volume from 300 μ L to 90 μ L per well and decreased the total absorbance measured (Figure 3-3).

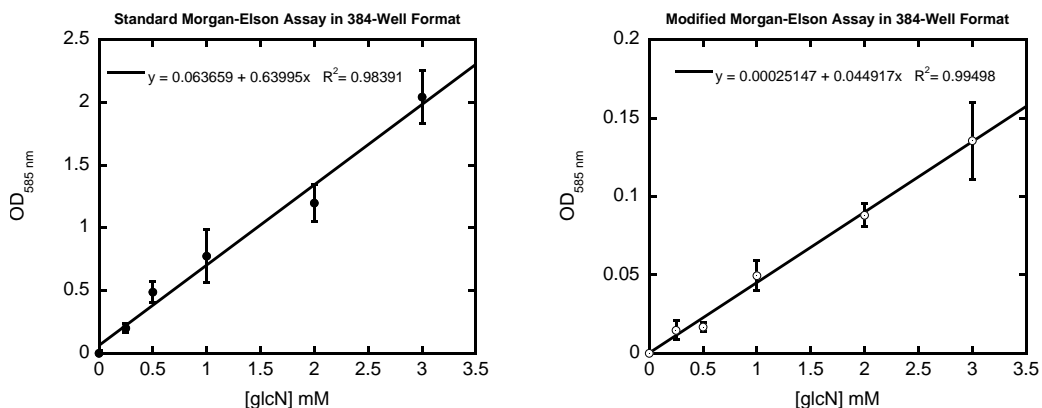


Figure 3-3. Standard curve with the Morgan-Elson assay, comparison of the “standard” versus the modified method. Glucosamine standards were tested with the Morgan-Elson assay utilizing the “standard” method (left) and following the change in solvents and increase in assay time (right). While there was a decrease in the level of absorbance achieved compared to the standard assay protocol, the modified assay still had an effective range over 0.25 mM-3 mM levels of glucosamine. The standard curves were performed manually in 384-well format.

The overall Z-factor was determined by performing the modified assay on the HTS-platform in a 384-well format using half of the wells for positive controls (enzyme, substrates, DMSO) and the other half as negative controls (buffer in place of enzyme, substrates, DMSO). The Z-factor for the HTS-modified Morgan-Elson assay was found to be 0.6 (Figure 3-5) which was slightly less than the Z-factor for the standard 96-well plate assay at 0.7 (Figure 3-4).

Controls and reference inhibitors for the HTS Screen

In addition to high controls (enzyme, substrates, DMSO) and low controls (substrates, DMSO, and buffer in place of enzyme) for the screening campaign, a reference inhibitor was also desired as a control. While azaserine and 6-diazo-5-oxo-L-norleucine (DON) were commercially available inhibitors, they had poor solubility in DMSO unlike the compound libraries available for screening.

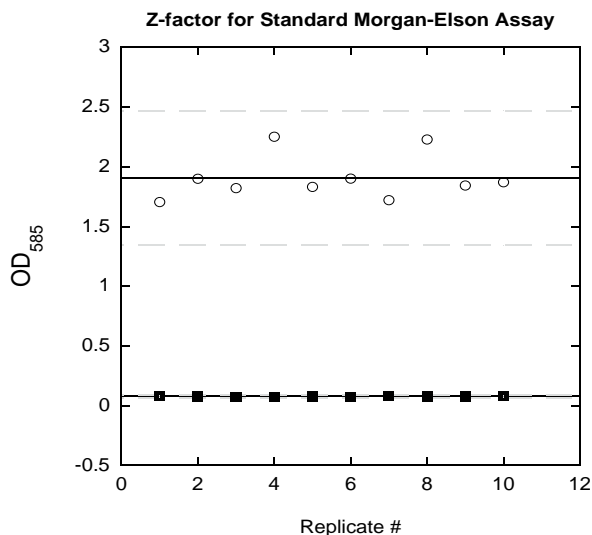


Figure 3-4. Z-factor determination for the standard Morgan-Elson assay. The assay was performed as described previously in a 96-well plate format. The Z-factor was calculated using Eq. 3.1 and was determined to be 0.7 for the assay under these conditions. The positive controls (white circles), included enzyme, substrates and DMSO while the negative controls (black squares), included buffer in place of enzyme, substrates and DMSO. The solid black lines represent the average of the controls while the dashed grey lines are 3 standard deviations away from the average of the controls.

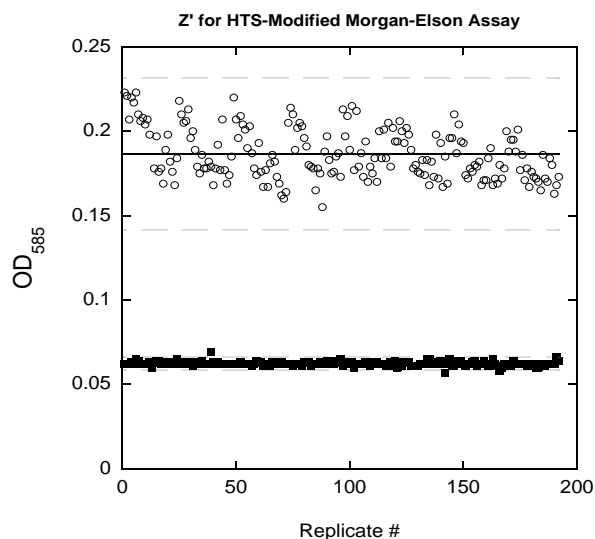


Figure 3-5. Z-factor determination for HTS-modified Morgan-Elson assay. Following the modifications made to make the Morgan-Elson assay HTS compatible, the Z-factor was determined for a 384-well microtiter plate by using half of the wells on the plate as positive controls (white circles) and the other half for negative controls (black squares). The black solid lines indicate the average absorbance while the grey dashed lines indicate three standard deviations away from the average. The Z-factor calculated using Eq. 3-1 was 0.6 for this assay, which meant the signal-to-noise ratio was acceptable for screening. The assay was performed on the HTS-platform.

We decided to synthesize *N*³-(4-methoxyfumaroyl)-L-2,3-diaminopropanoic acid (FMDP), a known GFAT inhibitor and peptide derivative similar to azaserine and DON.¹¹ FMDP had a reported IC₅₀ of 4 μM for hGFAT-1 and was synthesized in 5 steps from dimethyl fumarate and *N*²-(tert-butoxycarbonyl)-L-asparagine (Boc-Asn-OH) (Figure 3-6). We proceeded with a convergent synthesis and utilized the activated ester of monomethyl fumarate to couple with a protected amino acid derivative to yield the product. Unfortunately we did not find it to be as potent as was reported. We obtained an IC₅₀ of 23.3±7.5 μM when FMDP was assayed under similar conditions to the reported value (Figure 3-7). Like azaserine and DON, we also found FMDP to have poor solubility in DMSO.

Efforts were then directed to the preparation¹² of 6,7-dimethoxy-1-(naphthalen-2-yl)-isoquinoline (or EME 384), a patented GFAT inhibitor.¹³ As mentioned in Chapter 1, these 1-arylcarbonyl-6,7-dimethoxyisoquinoline compounds have been previously explored as GFAT inhibitors by Hoffmann-La Roche Inc. Dr. Emelia Awuah performed the synthesis utilizing a microwave-assisted Bischler-Napieralski reaction with β-arylethylamines and aryl acetic acid precursors (Figure 3-8). EME 384 had increased solubility in DMSO and showed greater potency over FMDP. When performed under the same assay conditions as FMDP with substrates at 10xK_M, EME 384 had an IC₅₀ of 1.85±0.33 μM (Figure 3-9). Thus, EME 384 was included as a control throughout the screen to ensure that potent inhibitors could be detected under the HTS-compatible assay conditions.

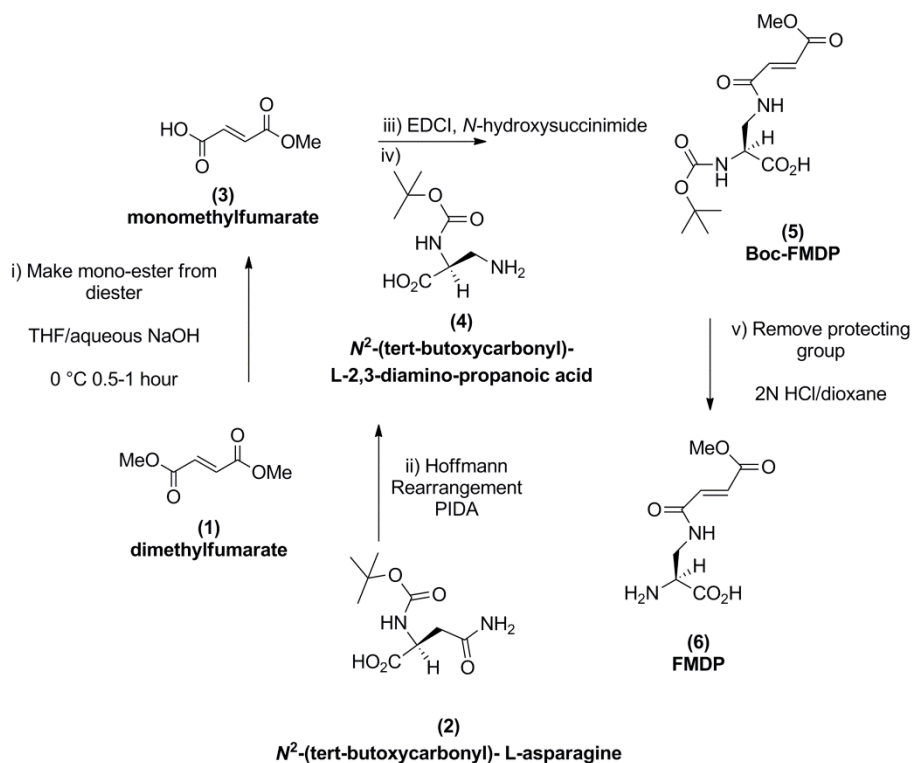


Figure 3-6. Synthesis of GFAT inhibitor FMDP. i) Hydrolysis of dimethyl fumarate to monomethyl fumarate gave a 60% yield and was purified by silica gel column chromatography.¹⁴ ii) The Hoffman rearrangement was performed with iodosobenzene diacetate (PIDA) and *N*²-(tert-butoxycarbonyl)-L-asparagine and gave a yield of 55% *N*²-(tert-butoxycarbonyl)-L-2,3-diaminopropanoic acid.¹⁵ iii) The *N*-succinimoyl ester of monomethyl fumarate was synthesized with *N*-(3-dimethylaminopropyl)-*N*'-ethylcarbodiimide (EDCI) and gave a 51% yield. iv) The activated ester was coupled with (4) to yield (5). v) Following removal of the BOC protecting group, FMDP was produced with 54% yield.¹⁶

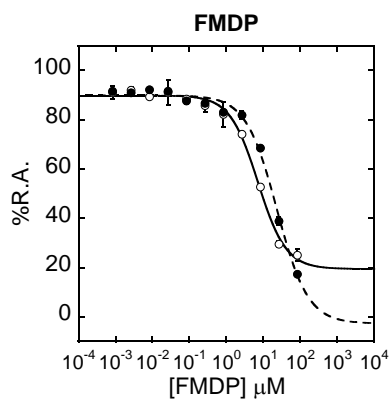


Figure 3-7. Dose-response of FMDP. Performed with the Morgan-Elson Assay at 1xK_M (white circles) and 10xK_M (black circles). FMDP had an IC₅₀ of 7.1 ± 1.0 and 23.3 ± 7.5 at the low and high substrate concentrations respectively. Fitted with the 4-point parameter Hill equation (KaleidaGraph v.4.1).

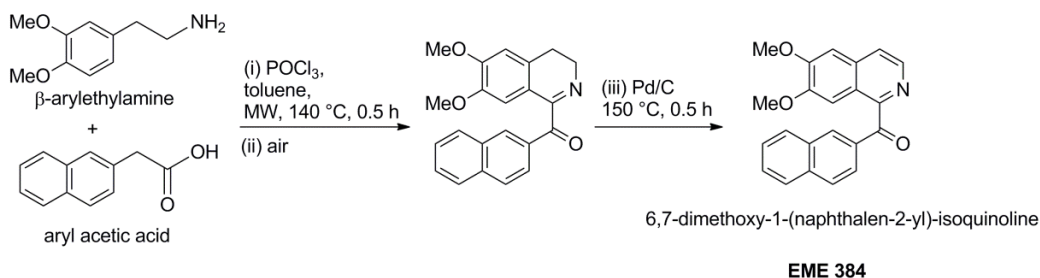


Figure 3-8. Microwave-assisted Bischler-Napieralski reaction scheme to synthesize 6,7-dimethoxy-1-(naphthalen-2-yl)-isoquinoline or EME 384. Adapted from Awuah *et al.* The Bischler-Napieralski reaction performed with phosphoryl chloride, combined with oxidation resulted in the dihydroisoquinoline intermediate which was subsequently dehydrated to form the final isoquinoline product. Yields ranged from 55-80%.

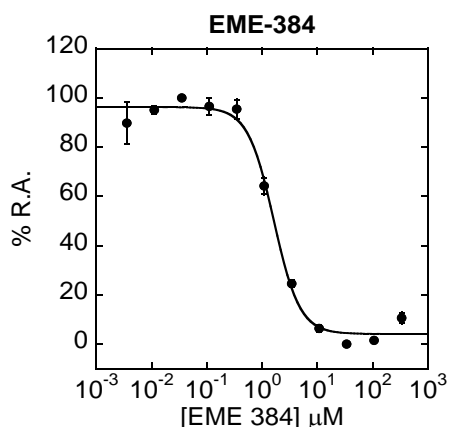


Figure 3-9. GFAT inhibitor EME 384 dose-response. A dose-response curve was generated with the use of the standard Morgan-Elson assay with substrates both at $10 \times K_M$. The IC_{50} for EME 384 under these conditions was $1.85 \pm 0.33 \mu M$. Fitted with the 4-point parameter Hill equation (KaleidaGraph v.4.1).

HTS Pilot Screen with the Modified Morgan-Elson Assay

A pilot screen was performed in duplicate with four 96-well compound plates (or two 384-well assay plates) out of the Bioactive Collection (P1000 library #9-12) at the CMCB. There was some variation between the controls of the first and second assay plates of the pilot screen (Figure 3-10). The first plate showed a tighter assay window (Z-factor of 0.55 for plate 1 versus 0.31 for plate 2) than the second assay plate. This might have been due to insufficient cleaning of the pipette tips used to dispense the enzyme in

between assay plates. Standard procedures in the HTS lab at McMaster had the tips reused 3 times in order to help lower overall screening costs. Since the enzyme stock used in the screen was concentrated (0.4 mg/mL) and fructose-6-phosphate was included in the enzyme preparation, this solution was quite “sticky” and could not be removed completely from the pipette tips during the washing steps. It was important that the tips were thoroughly cleaned between steps so that there was no carryover of reagents to the next assay plate. Due to the large decrease in the Z-factor in the second assay plate, a new set of pipette tips was used each time the enzyme was dispensed. All other reagents re-used tips up to 3 times.

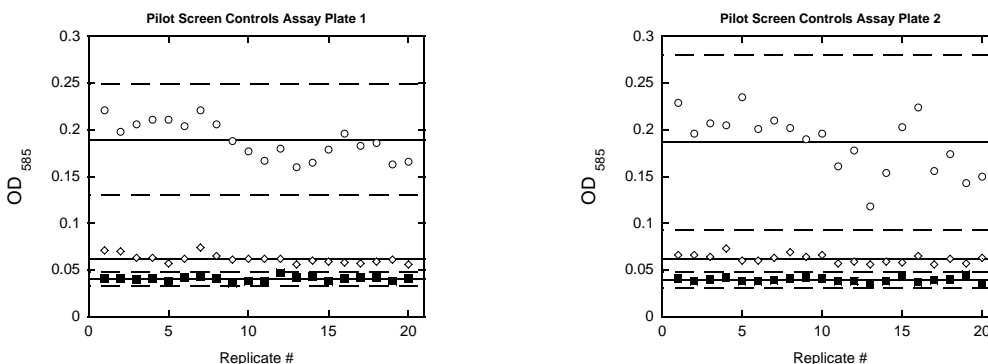


Figure 3-10. Control data from the pilot screen. Two 384-well assay plates were used to perform a test screen of 320 compounds using the HTS-modified Morgan-Elson assay on the HTS robotic platform. Comparing the positive (white circles) and negative (black squares) controls between the first and second assay plates of the pilot screen, the first plate had a much tighter screening window than the second plate. The reference compound, EME 384 (white diamonds), displayed GFAT inhibition under the modified assay conditions.

Surprisingly, one inhibitor was discovered in the pilot screen among the 320 compounds tested (Figure 3-11). An aminothiazole, N1(8Hindeno[1,2d][1,3]thiazol2yl) decanamide, from the Maybridge collection, ID #: RH01165 (MAC ID: MAC-0000673) (Figure 3-12). The compound displayed 35% residual enzyme activity and it was investigated further by creating a dose-response curve to confirm if it was a validated hit

(Figure 3-13). This compound had an IC_{50} of $38 \pm 6 \mu\text{M}$ when tested with the standard Morgan-Elson assay, substrates at $10xK_M$. Aminothiazoles had not been previously reported to have any inhibitory activity against GFAT.

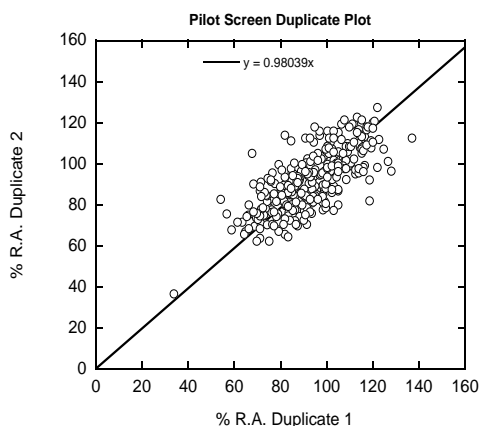


Figure 3-11. Duplicate plot of the compounds tested for GFAT inhibitory activity in the pilot screen. From the pilot screen, 320 bioactive compounds were tested in duplicate. A perfect screen would have a duplicate plot with a slope of 1, we had obtained a slope of 0.98, indicating that the assay was being performed with high-accuracy on the robotic platform. The duplicate plot also indicated that all compounds were being dispensed from the 96-well compound plates to the 384-well assay plates reliably. Any outliers, such as the point at 34,36, may be a sign of an inhibitor.

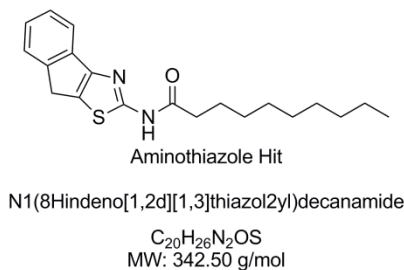


Figure 3-12. Structure, name, molecular formula and molecular weight of lead compound identified from pilot screen. This compound was a lead from the Maybridge collection, ID #: RH01165, MAC ID# MAC-0000673. It had not been previously reported as a GFAT inhibitor.

Following the results obtained from the pilot screen, we had an assay in hand suitable for screening small molecule libraries on a robotic platform, a reference compound used to gauge the reliability of the assay and the efficacy of any lead compounds, and had identified a novel GFAT inhibitor. We were now prepared to complete the HTS campaign.

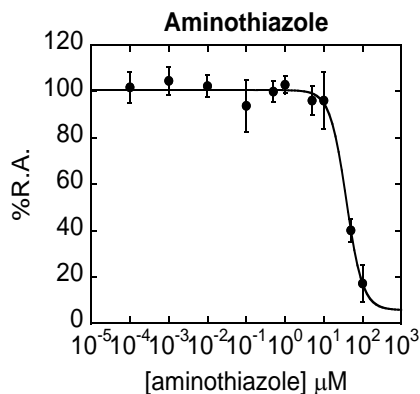


Figure 3-13. Dose-response for the aminothiazole hit identified from the pilot screen. The lead compound was tested with the standard Morgan-Elson assay to determine if it was a positive hit. The half-maximal inhibitory concentration was determined to be $38 \pm 6 \mu\text{M}$ and it displayed a sigmoidal shaped dose-response curve indicating that it was a veritable and novel GFAT inhibitor.

GFAT hits identified from the HTS

The primary screen at the HTS facility at the Center for Microbial Chemical Biology at McMaster University was performed on a Biomek Fx platform utilizing two Cytomat hotels to hold reagents, assay plates and compound plates. The first two steps of the assay were performed online while the last visualization step was performed manually off-line in a fume-hood. Each compound was tested in duplicate, and 64 wells were reserved for controls on every assay plate. A total of 33 assay plates were used in the primary screen, and about 6 assay plates, or 960 compounds, could be processed per day.

Our screening library consisted of 3950 known bioactive compounds from commercial suppliers (Prestwick, Microsource, Sigma-Aldrich, BIOMOL Research Laboratories, Maybridge) and a handful from academic laboratories (Hall Lab, University of Alberta, McNulty & Capretta Labs, McMaster University, Table 3-3). The statistically active threshold for 'hit' compounds was determined to be 73% or less of relative

activity compared to the high controls, which was 3 standard deviations below the average of the high controls. Compounds falling within this range were projected to demonstrate inhibitory activity against GFAT.

Subset (Distributor)	# of compounds	Details
Prestwick Chemical Library (Prestwick Chemical, Plymouth Meeting, PA, USA)	1,120	Off-patent small molecules; >85% FDA approved Average MW = 385 g/mol
Natural Products Library (BIOMOL International, L.P., Plymouth Meeting, PA, USA)	361	Natural Products Average MW = 350 g/mol
Lopac 1280 (International Version) (Sigma-Aldrich Canada Ltd., Oakville, ON, CA)	885	Pharmacologically active small molecules Average MW = 350 g/mol
Spectrum Collection (Microsource Discovery Systems, Inc., Gaylordsville, CT, USA)	1,214	Natural products and bioactives Average MW = 350 g/mol
Total Bioactives	3,580	
Academic Labs (Capretta, McNulty, D.G. Hall)	370	Synthetic natural product derivatives
TOTAL # Screened	3,950	

Table 3-3. List of suppliers from the bioactive subset of the Canadian Compound Collection and academic labs comprising the small molecule libraries screened. The Canadian Compound Collection is a library of small molecules available for screening at the Center for Microbial Chemical Biology at McMaster University. A total of 3580 bioactive compounds were tested, plus 370 synthetic natural product derivatives supplied by academic labs. The structures of compounds supplied by the McNulty and Hall labs were unknown. The bioactive subset was chosen to increase our chances of finding inhibitors.

The Z-factor for the screen was found to be 0.63 overall, which indicated a good assay (Figure 3-14). A duplicate plot of the entire screen also demonstrated the quality of the screening experiment (Figure 3-15). Perfect replicates would lie directly along the line. Fifty-eight compounds were identified as inhibitors, yielding a primary hit rate of 1.5%. This hit rate may be considered high compared to most high-throughput screens, but our compound library was biased since it contained only small molecules which had displayed some form of biological activity previously.

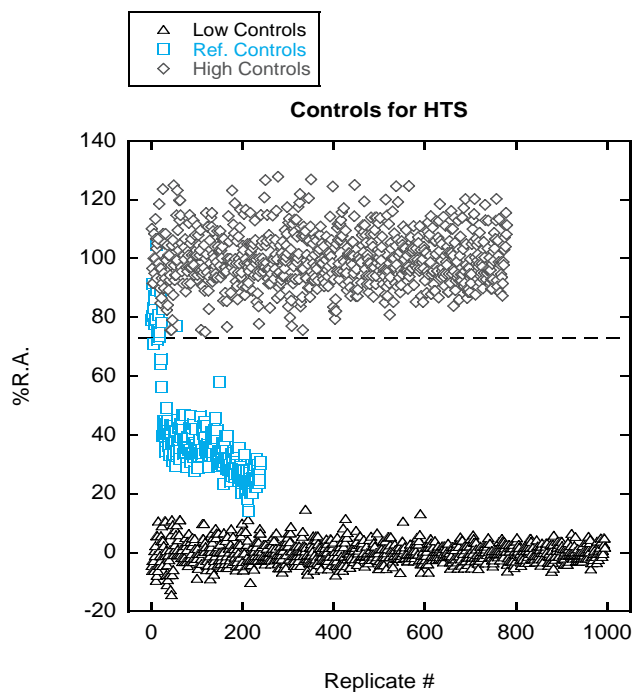


Figure 3-14. Controls for the complete HTS of 3950 compounds. The dashed line indicates the statistically active threshold at 73%, which was 3 standard deviations below the average of the high controls. Any compounds which displayed 73% or less enzyme activity were deemed to be lead compounds.

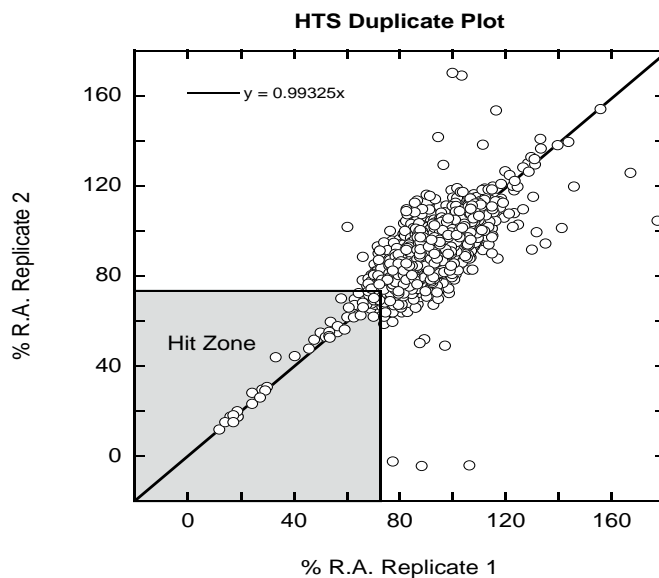


Figure 3-15. Duplicate plot of compounds from the primary screen. The grey area indicates the "Hit Zone", or compounds which fall below 73% residual activity. 58 leads were identified in the "Hit Zone".

Following the screen, the initial 58 hits were followed up with a primary dose-response screen performed with the HTS-modified assay to validate hit compounds or reveal false positives (Figures 3-16, a-h). From here, we identified that 22 of the 58 primary hits exhibited a dose-response relationship.

Validation of hits via secondary dose-response screening

To ensure the compounds being tested had not been degraded or mislabeled, a select number of the hits were purchased and used to perform a secondary set of dose-response assays. The reference inhibitor, EME 384, was included as a control compound in the secondary dose-response screen to ensure the assay and robotic system were functioning properly, and as a benchmark to compare the other leads. These assays were performed under high ($10 \times K_M$) and low ($1 \times K_M$) substrate concentrations to determine compound potency. Any IC_{50} values in the high nM to low μ M range were considered very potent, from 5-50 μ M potency was considered to be good, and above 50 μ M potency was considered to be modest.

The lead selection was narrowed down for further testing after investigating the known biological activity, toxicity, structure, availability and cost of the compounds (Table 3-4). Homidium bromide (57), acriflavinium HCl (43), propidium iodide (3), coralyne chloride hydrate (2), and primaquine diphosphate (16) were selected for purchase because they all contained an isoquinoline as part of their core structure, similar to EME 384.

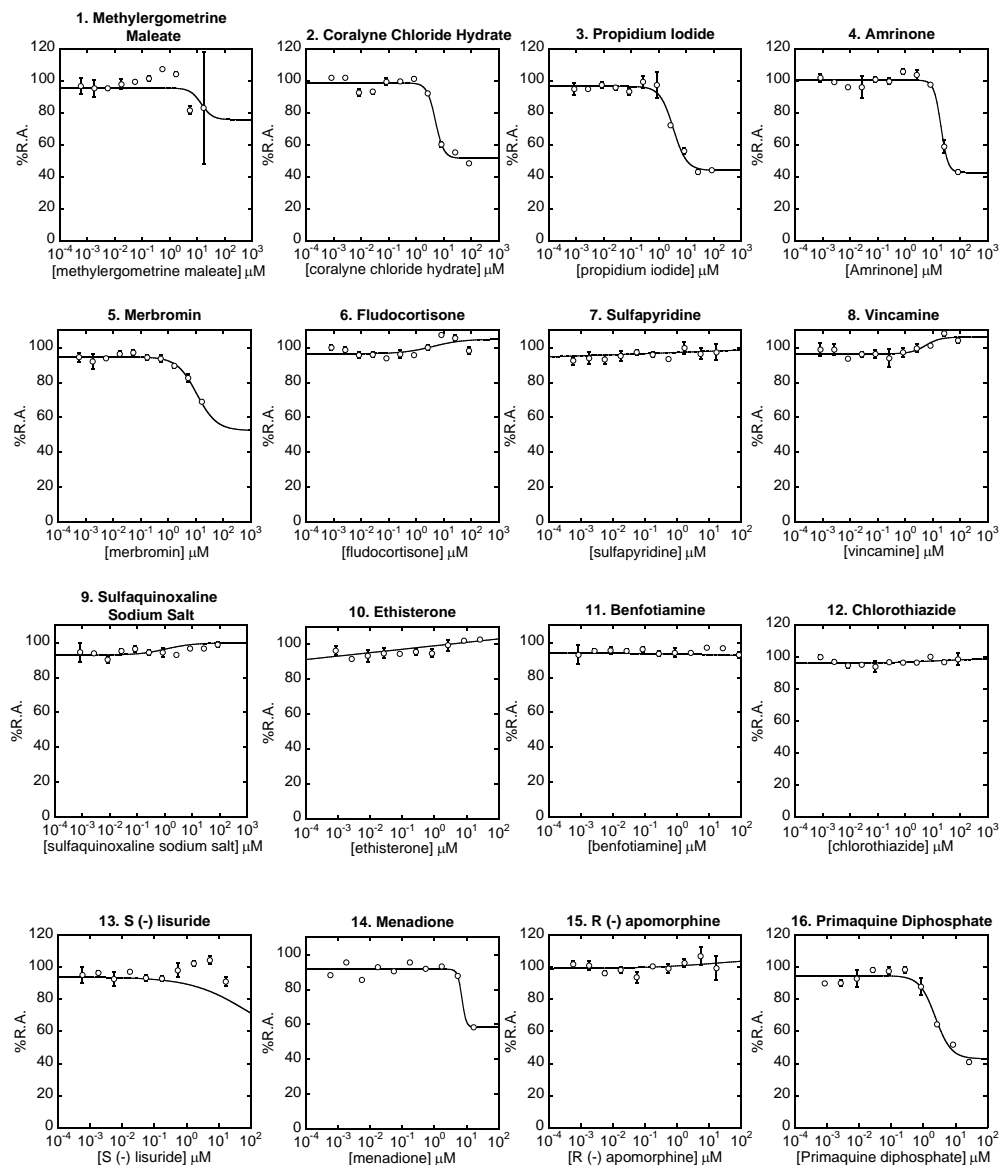


Figure 3-16a. Dose-response curves for hit compounds 1-16 out of 58. The four-point parameter Hill equation was used to fit the curves (KaleidaGraph v4.1) and determine the half-maximal inhibitory concentration if applicable.

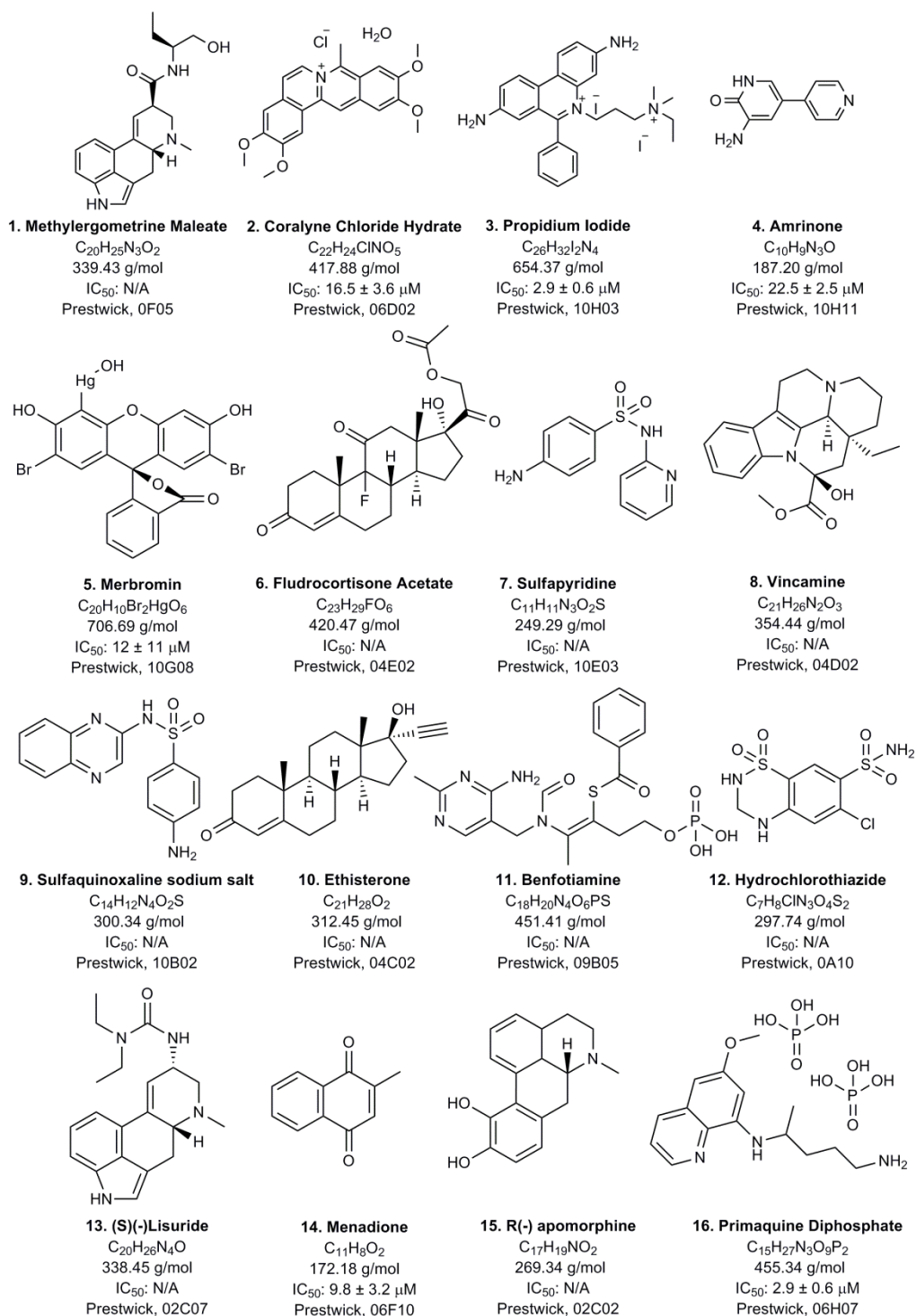


Figure 3-16b. Structure, name, molecular formula, molecular weight, half-maximal inhibitory concentration and supplier ID# for hit compounds 1-16 out of 58. Those compounds which did not display any inhibition according to the dose-response curves do not have an IC_{50} value listed and are reported as N/A or “not active”.

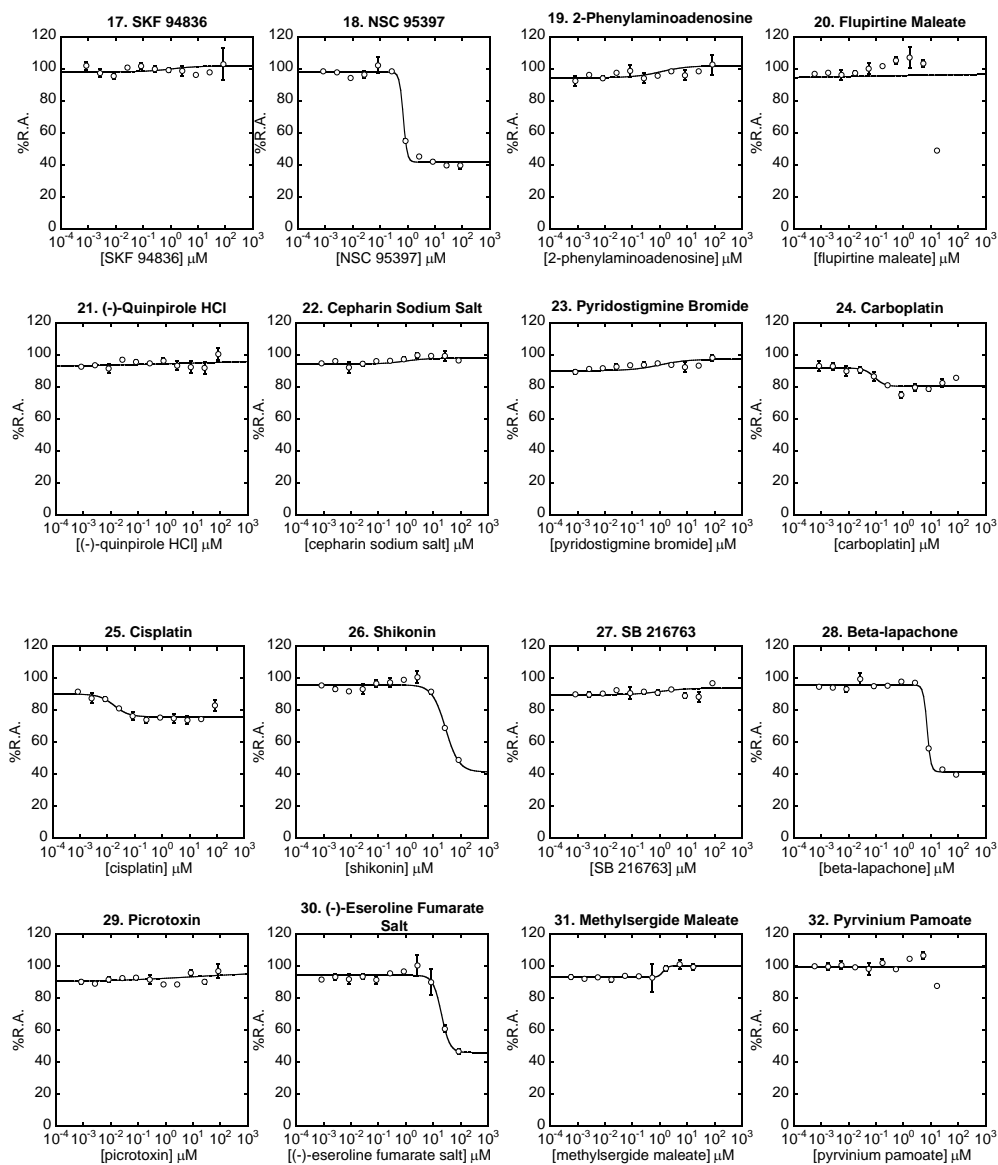


Figure 3-16c. Dose-response curves for hit compounds 17-32 out of 58. The four-point parameter Hill equation was used to fit the curves (KaleidaGraph v4.1) and determine the half-maximal inhibitory concentration if applicable.

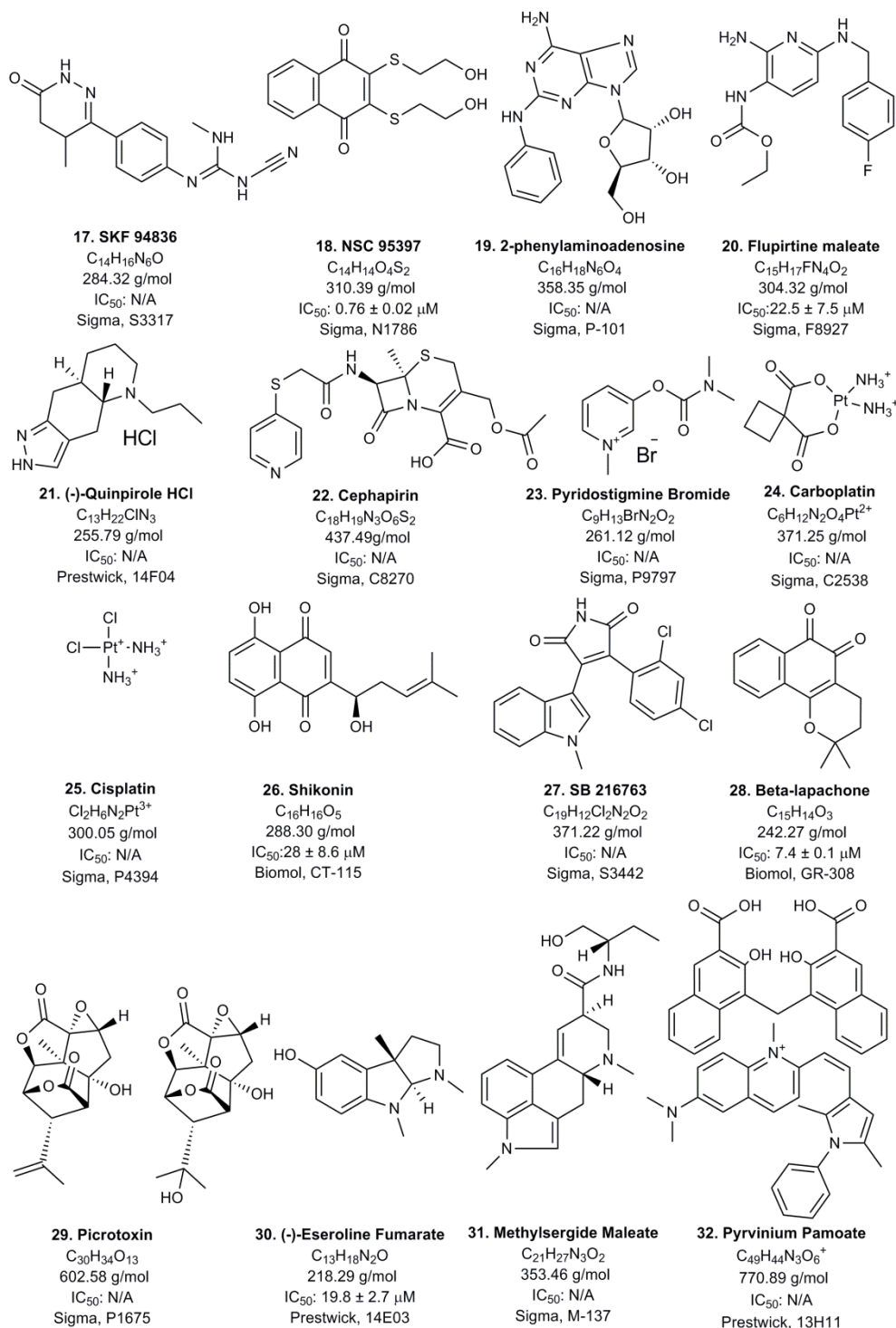


Figure 3-16d. Structure, name, molecular formula, molecular weight, half-maximal inhibitory concentration and supplier ID# for hit compounds 17-32 out of 58. Those compounds which did not display any inhibition according to the dose-response curves do not have an IC_{50} value listed are reported as N/A or “not active”.

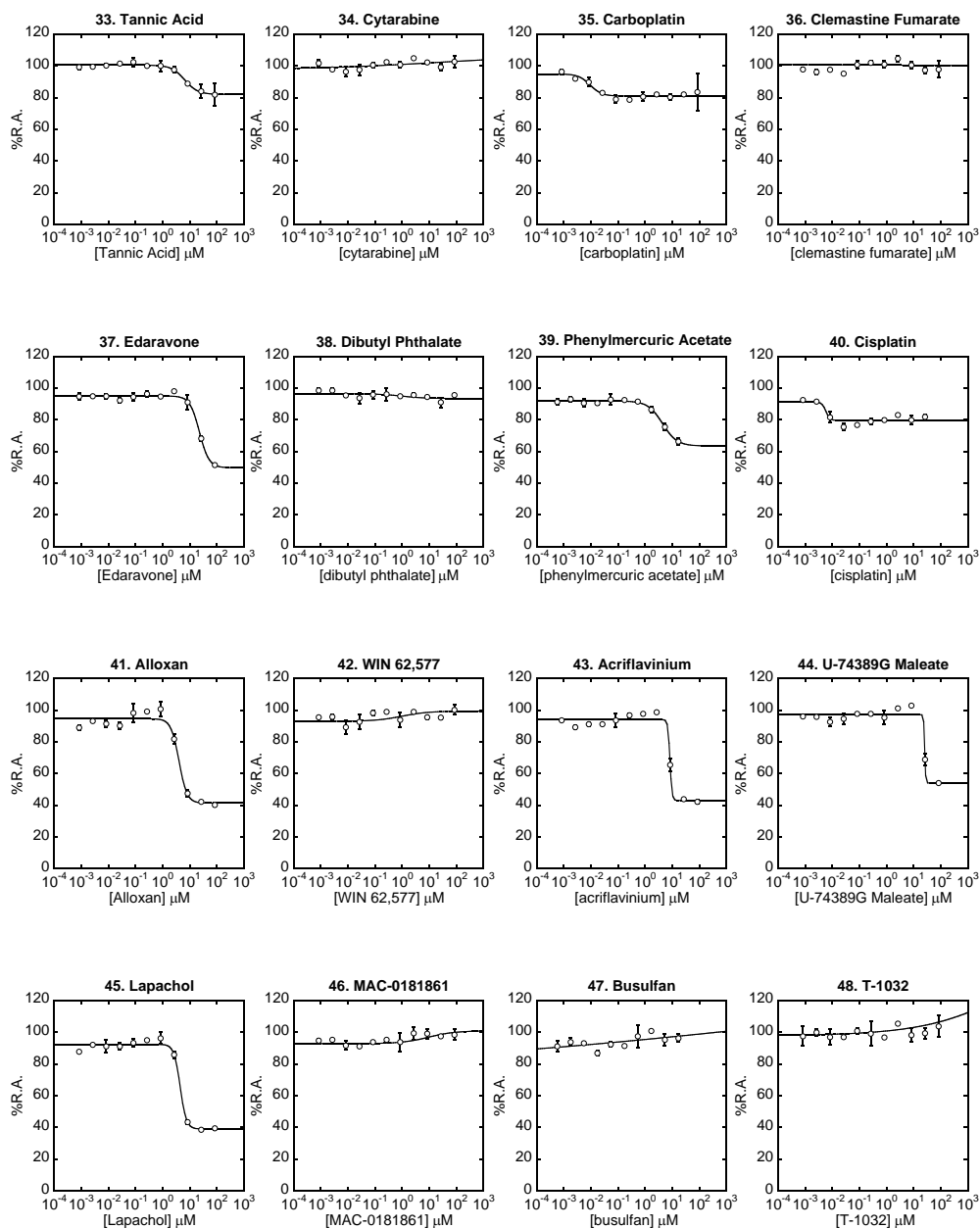


Figure 3-16e. Dose-response curves for hit compounds 33-48 out of 58. The four-point parameter Hill equation was used to fit the curves (KaleidaGraph v4.1) and determine the half-maximal inhibitory concentration if applicable. Carboplatin (24,35) and Cisplatin (25,40) appeared as hits twice because they were both present in libraries from two different suppliers. Since they were both identified as hits initially, and both verified to be false positives in the primary dose-response stage, this was a testament to the reproducibility of the assay method.

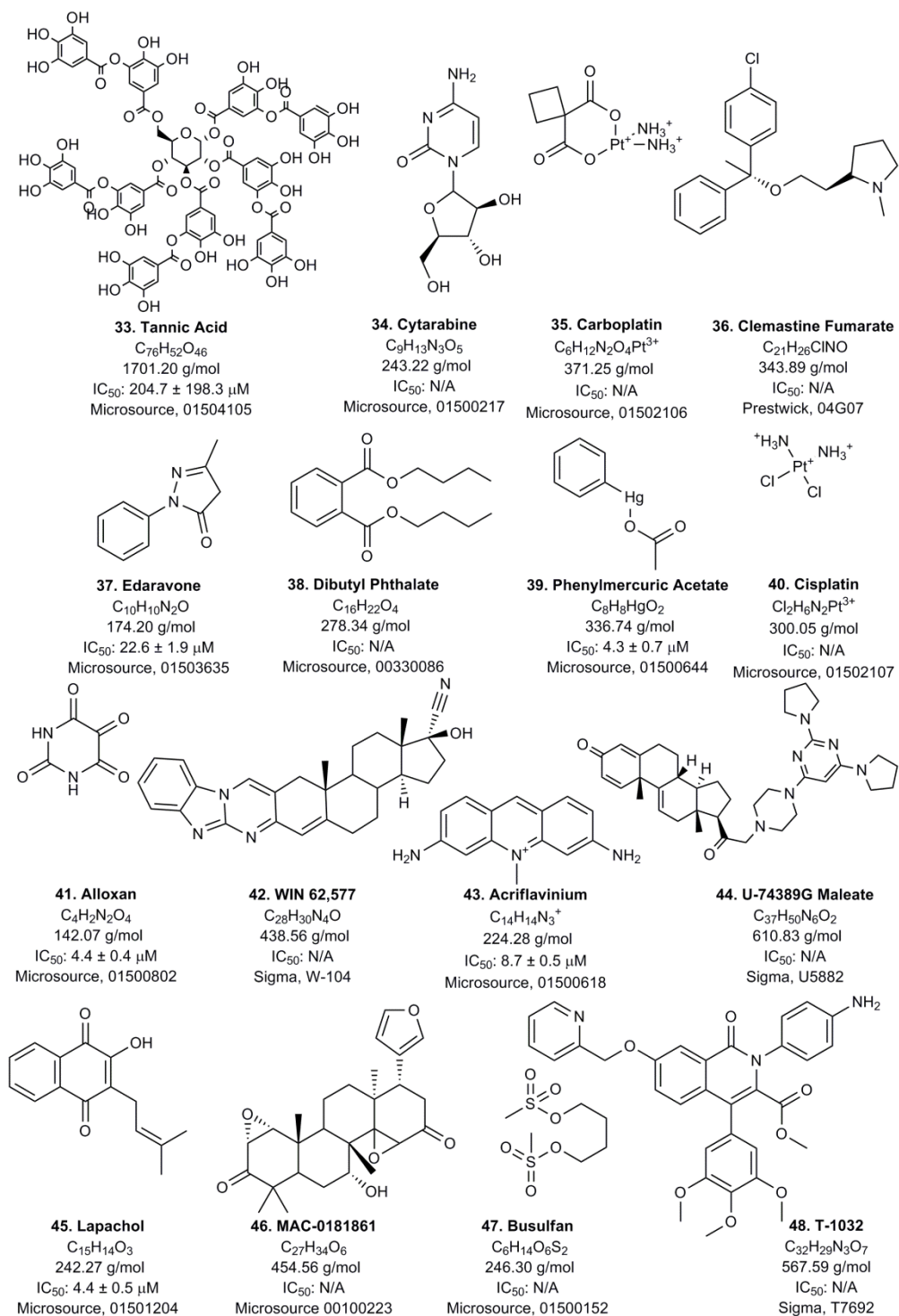


Figure 3-16f. Structure, name, molecular formula, molecular weight, half-maximal inhibitory concentration and supplier ID# for hit compounds 33-48 out of 58. Those compounds which did not display any inhibition according to the dose-response curves do not have an IC_{50} value listed are reported as N/A or “not active”.

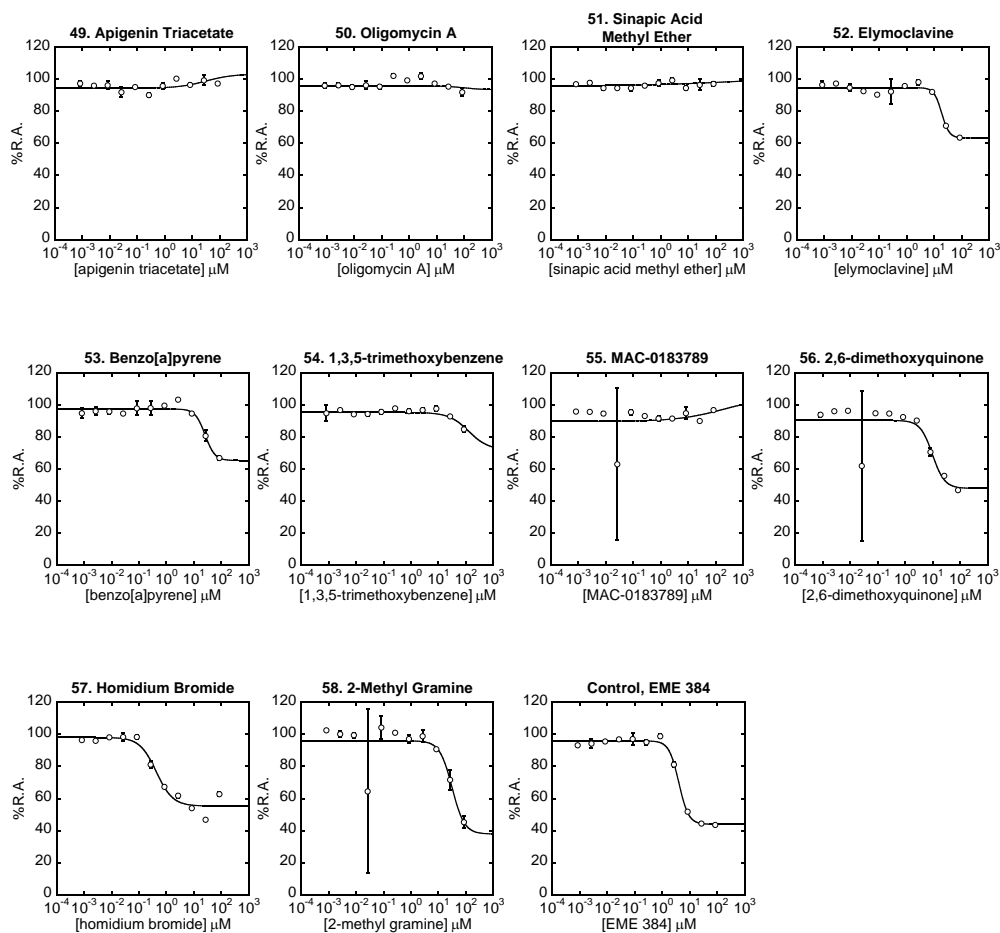


Figure 3-16g. Dose-response curves for hit compounds 49-58 out of 58. The four-point parameter Hill equation was used to fit the curves (KaleidaGraph v4.1) and determine the half-maximal inhibitory concentration if applicable.

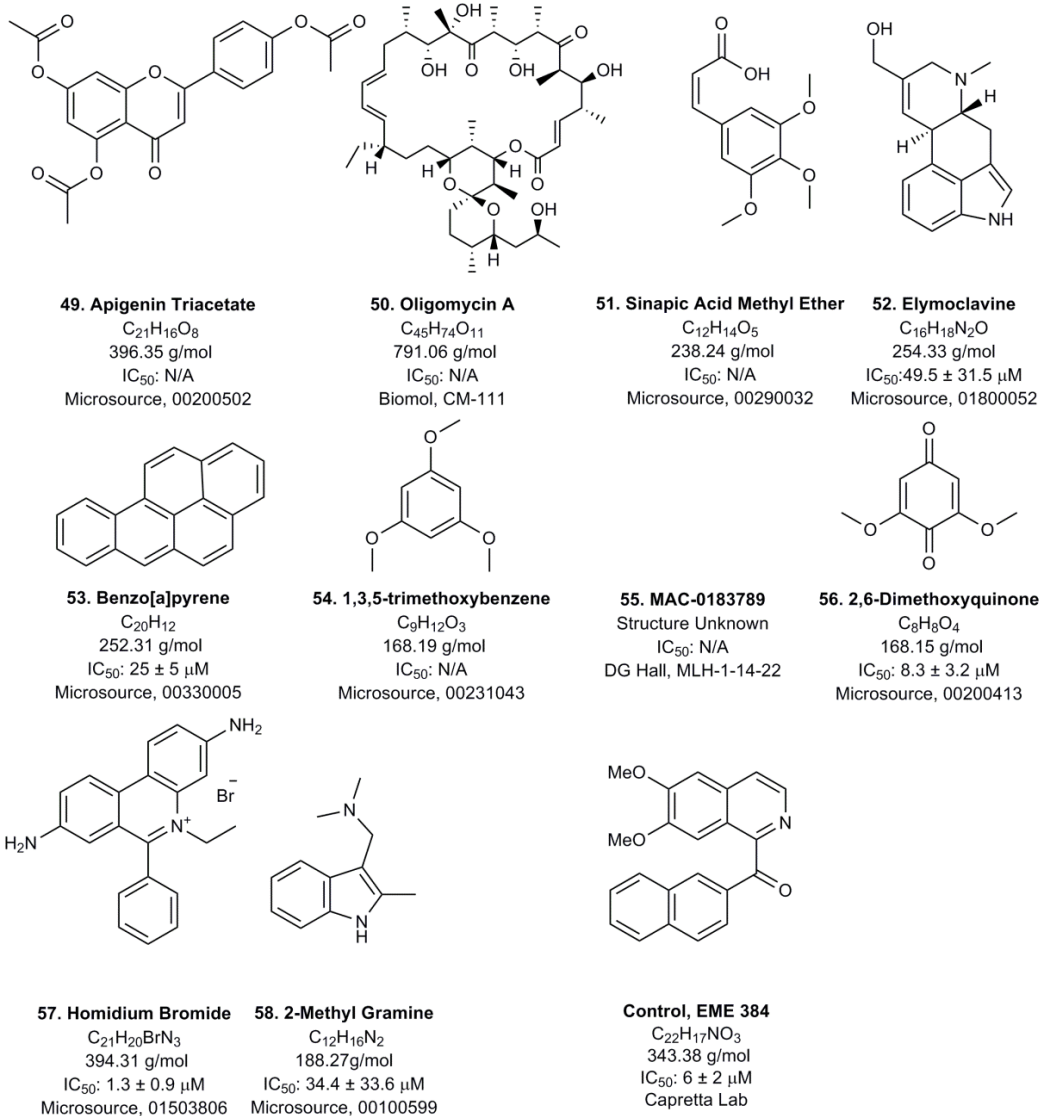


Figure 3-16h. Structure, name, molecular formula, molecular weight, half-maximal inhibitory concentration and supplier ID # for hit compounds 49-58 out of 58. Those compounds which did not display any inhibition according to the dose-response curves do not have an IC_{50} value listed are reported as N/A or “not active”. The compound MAC-0183789 is a molecule from the D.G. Hall Lab at the University of Alberta. The structure remained classified as it was not verified to be a GFAT inhibitor.

Name	Structure #	1° Dose-Response	Selected for Validation?
		IC ₅₀ (μM)	Y/N
Coralyne chloride hydrate	2	16.5±3.6	Y
Propidium iodide	3	2.9±0.6	Y
Amrinone	4	22.5±2.5	Y
Merbromin	5	12±11	N
Menadione	14	9.8±3.2	Y
Primaquine diphosphate	16	2.9±0.6	Y
NSC 95397	18	0.76±0.02	Y
Flupirtine maleate	20	22.5±7.5	Y
Shikonin	26	28±8.6	N
Beta-lapachone	28	7.4±0.1	Y
(-)-eseroline fumarate	30	19.8±2.7	N
Tannic acid	33	204.7±198.3	N
Edaravone	37	22.6±1.9	N
Phenylmercuric acetate	39	4.3±0.7	N
Alloxan	41	4.4±0.4	Y
Acridine HCl	43	8.7±0.5	Y
Lapachol	45	4.4±0.5	Y
Elymoclavine	52	49.5±31.5	N

Benzo [a] pyrene	53	25±5	N
2,6-dimethoxyquinone	56	8.3±3.2	Y
Homidium bromide	57	1.3±0.9	Y
2-methylgramine	58	34.4±33.6	N
EME 384	59	6±2	Y

Table 3-4. Hit compounds selected for validation. Out of the 58 hits identified from the primary screen, 22 displayed inhibitory activity against GFAT. Thirteen compounds were selected for purchase and secondary hit validation. Y = Yes, N = No, compounds with an N were not selected for further study.

Homidium bromide was very potent (IC_{50} : $1.3\pm 0.9 \mu M$) and had potential for use as a reference inhibitor. Acriflavinium HCl also showed good potency (IC_{50} : $8.7\pm 0.5 \mu M$), propidium iodide displayed very good potency as well (IC_{50} : $2.9\pm 0.6 \mu M$). Coralyne chloride hydrate (IC_{50} : $16.5\pm 0.6 \mu M$) had reported anti-leukemia activity¹⁷ and showed good GFAT inhibition, while primaquine diphosphate was considered very potent (IC_{50} : $2.9\pm 0.6 \mu M$) and was an anti-malarial drug.¹⁸

Another structurally similar group of hits that were purchased are the naphthoquinones, menadione (14), lapachol (45), beta-lapachone (28), NSC 95397 (18) and the benzoquinones, 2,6-dimethoxyquinone (56) and alloxan (41). Menadione displayed good potency (IC_{50} : $9.8\pm 3.2 \mu M$) and was also known as vitamin K_3 ,¹⁹ a synthetic analog and alternative to vitamin K_1 and K_2 . There was a point of controversy about menadione as a GFAT inhibitor. It had been previously reported that vitamin K_1 and vitamin K_3 were allosteric activators of GFAT isolated from rat liver.²⁰ The same authors had also reported an increase in detectable hexosamines when rats were in a state of induced hypovitaminosis K, but a decrease in glycoproteins present in the liver

and blood serum.²¹ This was in contrast to what we have observed with menadione by measurement of the Morgan-Elson assay. Whether vitamin K interacts differently with GFAT isolated from rat liver versus the recombinant human form we have used in our screen was uncertain, but the active sites of the enzyme remain highly conserved throughout different species.¹

Lapachol (IC₅₀: 4.4±0.5 µM) and beta-lapachone (IC₅₀: 7.4±0.1 µM) were natural products²² derived from the Lapacho Tree (*Tabebuia avellanedae*) in South America²³ and had been investigated for anti-cancer activity.²⁴ NSC 95397 was one of the most potent inhibitors out of the 58 hits (IC₅₀: 0.76±0.02 µM) found and was a known Cdc25 phosphatase inhibitor from the National Cancer Institute library.²⁵ 2,6-dimethoxyquinone displayed good potency (IC₅₀: 8.3±3.2 µM) and had displayed anti-cancer activity previously.²⁶

Alloxan also displayed very good potency (IC₅₀: 4.4±0.4 µM). Interestingly, alloxan, is commonly used to create diabetic-mouse models as it is toxic to pancreatic cells, but it does not have this effect on human pancreatic tissue.²⁷ Also, alloxan bears some structural similarity to UDP-*N*-acetyl-glucosamine, the end-product of the hexosamine biosynthesis pathway and allosteric negative feedback inhibitor of eukaryotic GFAT ($K_i=4$ µM for hGFAT1) (Figure 3-17).²⁸ It was uncertain whether alloxan functions in a similar manner but further characterization of this inhibitor will be necessary.

Amrinone (4) was also selected for further study. It was a known pyridine phosphodiesterase 3 inhibitor and had been used to treat patients with congestive heart failure.²⁹ While the IC_{50} for GFAT was good ($22.5 \pm 2.5 \mu\text{M}$) following the primary dose-response, it had a low toxicity profile since it was used as a drug.³⁰ This made it a promising lead as a therapeutic compound.

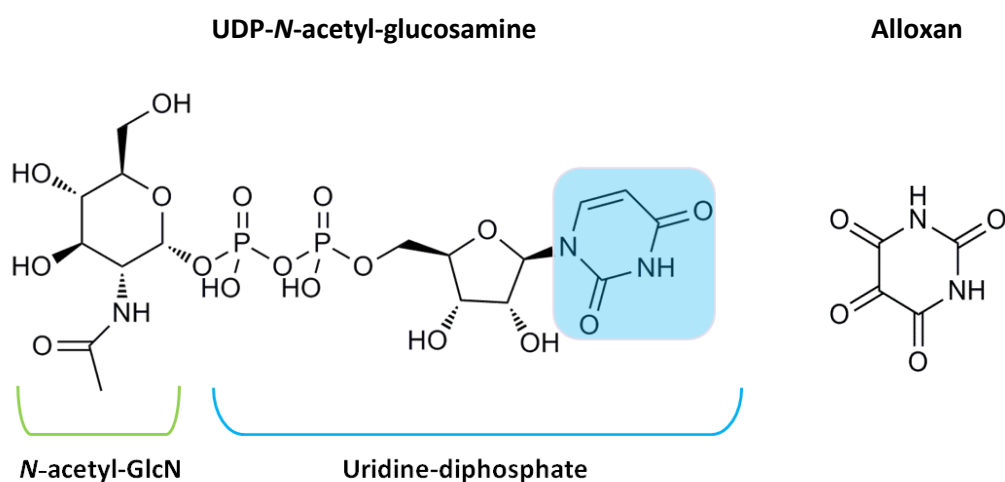


Figure 3-17. Structural comparison of UDP-N-acetyl-glucosamine and GFAT hit alloxan. The region of structural similarity of UDP-GlcNAc is high-lighted in blue.

Flupirtine maleate (20) was a fluoro-containing compound and a non-opioid analgesic.³¹ It had a good IC_{50} of $22.5 \pm 7.5 \mu\text{M}$ for GFAT and was selected for validation.

Compounds which were not selected, either due to availability (elymo-clavine, 52, was not available for shipment to Canada as it was a controlled substance), lack of potency or large amount of error in the curve fit (tannic acid, 33, 2-methylgramine, 58), mercury content (merbromin, 5, phenylmercuric acetate, 39), or high carcinogenicity (benzo[*a*]pyrene, 53).³² Shikonin (26, IC_{50} : $28 \pm 8.6 \mu\text{M}$), eseroline fumarate (30, IC_{50} : $19.8 \pm 2.7 \mu\text{M}$) and edaravone (37, IC_{50} : $22.6 \pm 1.9 \mu\text{M}$) were not studied further.

As a side note, Ehrlich's reagent or *p*-dimethylaminobenzaldehyde (DMAB) had been used in different preparations for the detection of lysergic acid diethylamide (LSD),³³ indoles,³⁴ and ergot alkaloids.³⁵ However, the limit of detection reported by Brown *et al* for LSD with 0.8 g of DMAB in 1:9 sulfuric acid (conc.)/ethanol was reported as 2 µg *via* silica-gel thin layer chromatography. At the highest concentrations in the dose-response assays, the mass of small molecules were in the sub-µg to ng range. We did not observe a linear increase in absorbance for the indoles elymoclavine, 2-methylgramine, methylsergide maleate (31), methylergometrine maleate (1), or (S)-lisuride (13) in the primary dose-response. However in future, if indole families were to be tested for GFAT inhibition, assay interference should be investigated and controls for background absorbance would be necessary.

In total, 13 of the 22 validated hits were selected for purchase and secondary dose-response testing (Figures 3-18 a,b). Table 3-3 summarizes the IC₅₀ values obtained for the 13 validated hits and compared the numbers obtained from the primary and secondary dose-response screening. Nine compounds out of the 13 purchased for secondary validation were selected as leads. Acriflavium HCl (43), flupirtine maleate (20), primaquine diphosphate (16), and propidium iodide (3) displayed too much variability to obtain an accurate IC₅₀ and were omitted from further characterization. This result highlighted the importance of performing follow-up studies after the primary screen was completed. A molecule identified as a hit from the library may have been an assay artifact or a contaminant in the original compound plate well. Coralyne chloride hydrate (2, IC₅₀: 41±26.3 µM) and homidium bromide (57, IC₅₀: 0.32±0.06 µM) were

selected for further testing due to their isoquinoline core and good levels of potency.

Amrinone (4), despite its modest potency following the secondary dose-response (IC_{50} : $91 \pm 34.1 \mu\text{M}$), was selected for further characterization due to its pharmaceutical properties and amenability to synthesize derivatives.

A trend was also beginning to emerge; 2,6-dimethoxyquinone (56, IC_{50} : $15.9 \pm 1.8 \mu\text{M}$), alloxan (41, IC_{50} : $13.9 \pm 0.8 \mu\text{M}$), beta-lapachone (28, IC_{50} : $10.4 \pm 0.5 \mu\text{M}$), lapachol (45, IC_{50} : $17.6 \pm 2.2 \mu\text{M}$), menadione (14, IC_{50} : $11.8 \pm 0.7 \mu\text{M}$), and NSC 95397 (18, IC_{50} : $41.5 \pm 1.4 \mu\text{M}$) were all in the quinone family. They have not been previously identified as a class of GFAT inhibitors. In the secondary dose-response, NSC 95397 exhibited a 50-fold increase in its IC_{50} value as compared to the primary dose-response. This emphasized the importance of purchasing or synthesizing hit-molecules directly and not relying on what was available in the library. The molecule in the storage compound plate might have been impure or the stock concentration could have been mislabeled.

The low error associated with reference inhibitor EME 384 indicated that the dose-response assay performed on the robotic platform was functioning properly. EME 384 would have continued use as a reference compound.

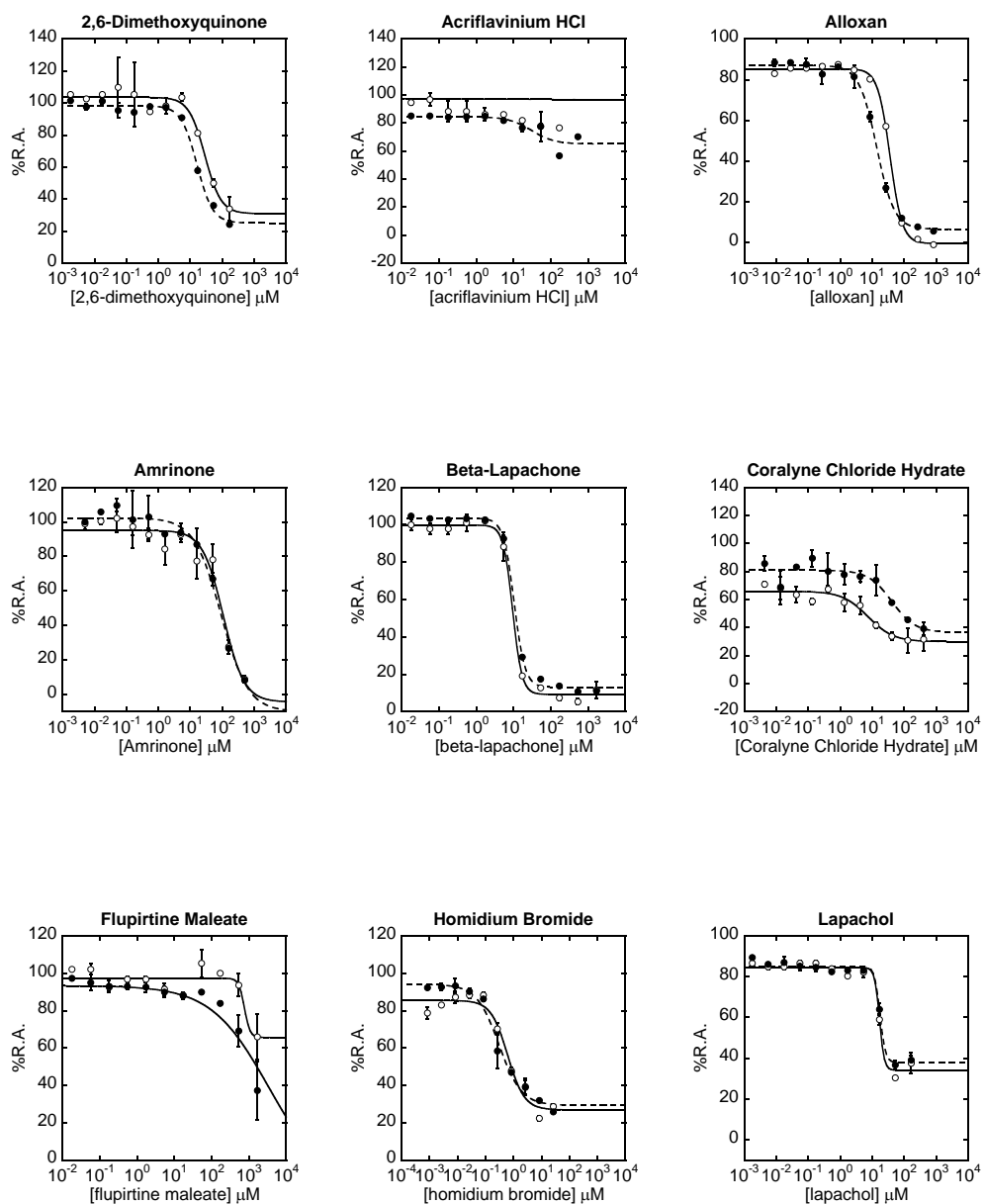


Figure 3-18a. Secondary dose-response curves 1-9 of 13 selected validated hits. Dose-response was performed with the modified Morgan-Elson assay on the HTS platform. The assay was run with both substrates at K_M (1 mM, white circles) and $10xK_M$ (10 mM, black circles). 2,6-dimethoxyquinone (56), acriflavinium HCl (43), alloxan (41), amrinone (4), beta-lapachone (28), coralyne chloride hydrate (2), flupirtine maleate (20), homidium bromide (57) and lapachol (45) are displayed. Fitted with the 4-point parameter Hill equation (KaleidaGraph v.4.1).

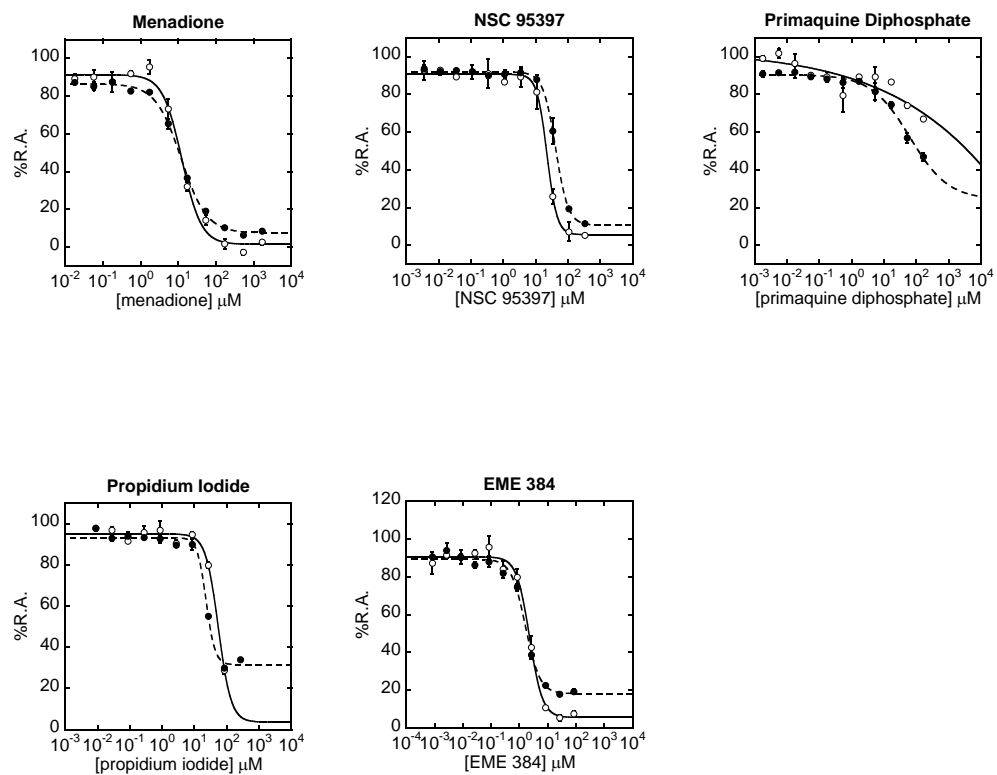


Figure 3-18b. Secondary dose-response curves 10-13 of 13 selected validated hits and control EME 384. Dose-response was performed with the modified Morgan-Elson assay on the HTS platform. The assay was run with both substrates at K_M (1 mM, white circles) and $10xK_M$ (10 mM, black circles). Menadione (14), NSC 95397 (18), primaquine diphosphate (16), and propidium iodide (3) are displayed here. Fitted with the 4-point parameter Hill equation (KaleidaGraph v.4.1).

Compound Name	Structure #	1 ° Dose-response	2 ° Dose-Response		Lead Selection Y/N
		Substrates at 10xK _M IC ₅₀ (μM)	Substrates at K _M IC ₅₀ (μM)	Substrates at 10xK _M IC ₅₀ (μM)	
2,6-dimethoxyquinone	56	8.3±3.2	28.4±6.5	15.9±1.8	Y
Acriflavinium HCl	43	8.7±0.5	N/A	30.2±26.5	N
Alloxan	41	4.4±0.4	36.2±1.5	13.9±0.8	Y
Amrinone	4	22.5±2.5	107.6±49.2	91±34.1	Y
Beta-lapachone	28	7.4±0.1	9.4±0.6	10.4±0.5	Y
Coralyne chloride hydrate	2	16.5±3.6	7.3±2.9	41±26.3	Y
Flupirtine maleate	20	22.5±7.5	N/A	N/A	N
Homidium bromide	57	1.3±0.9	0.61±0.16	0.32±0.06	Y
Lapachol	45	4.4±0.5	16.9±0.7	17.6±2.2	Y
Menadione	14	9.8±3.2	12.4±1.4	11.8±0.7	Y
NSC 95397	18	0.76±0.02	44.8±23.5	41.5±1.4	Y
Primaquine diphosphate	16	2.9±0.6	N/A	63.5±50.1	N
Propidium iodide	3	2.9±0.6	N/A	22.9±1.8	N
EME 384	59	6±2	2.2±0.2	1.6±0.2	Y

Table 3-5. Comparison of IC₅₀ values from the primary and secondary dose-response screening and lead selection. Compounds which do not have an IC₅₀ value listed exhibited too much variability to determine a value. Y = Yes, N = No, compounds with an N were not selected for further study.

Conclusion

A high-throughput screen was completed to discover novel GFAT inhibitors with a modified version of the Morgan-Elson assay. The assay was determined to be good for screening compounds as it had a Z-factor of 0.63. Overall, 3950 bioactive compounds were screened, plus 320 compounds from a small pilot screen, for a total of 4,270. A total of 58 initial leads were identified, with 22 of those compounds verified as inhibitors following primary dose-response screening. From those inhibitors, 13 were selected for purchase and secondary dose-response screening. Nine compounds, 2,6-dimethoxyquinone, alloxan, amrinone, beta-lapachone, coralyne chloride hydrate, homidium bromide, lapachol, menadione, and NSC 95397 were selected as leads. They will be characterized further to determine which compound will be best for *in vivo* GFAT inhibition. From the pilot screen, N1(8Hindeno[1,2d][1,3]thiazol2yl)decanamide was also verified as an inhibitor.

Materials & Methods

All reagents were purchased from Sigma Aldrich unless stated otherwise.

Protocol for the Modified Morgan-Elson Assay in 384-Well Plate Format for HTS

The HTS modified Morgan-Elson assay consisted of three steps, end-point detection of absorbance at 585 nm, a total assay volume per well of 87 μ L and a total assay time of 27 hours.

The master mix (Table 3-4), tested compounds and enzyme, were combined in each well, thoroughly mixed and incubated at 37 °C for one hour. Total enzyme reaction volume was 30 μ L. The enzyme reservoir was kept at 4 °C throughout the assay; all other reagents were stable at room temperature. The master mix was present for all tested compounds and high and low controls. Neat DMSO (Caledon Labs, Georgetown, ON) was used in place of test compounds for high controls, low controls used buffer in place of enzyme and DMSO in place of the test compounds, and reference controls contained enzyme and EME 384 at 83 μ M. The semi-automated assay was performed on a Biomek FX (Beckman/Coulter) platform equipped with a BioRAPTR (Beckman/Coulter), 2 reagent hotels; Cytomat 6011 incubator (set to 37 °C), Cytomat 24 microplate hotel (Thermo Scientific) and an EnVision (Perkin Elmer) plate reader at the McMaster University Center for Microbial Chemical Biology.

A 1.5% acetic anhydride solution in acetonitrile and 200 mM potassium tetraborate (Table 3-5) were added in separate addition steps to the assay plate and were incubated at room temperature for 22 hours. Total volume added to the assay

reaction was 18 μL and the total assay volume at this point was 48 μL . The acetic anhydride solution was prepared daily and added first to ensure a successful acetylation reaction.

Master Mix, 26.5 μL	Working concentration	Final Concentration in assay
L-glutamine	11.54 mM	10 mM
Fructose-6-Phosphate	11.32 mM	10 mM
PBS or Phosphate buffered Saline (pH 7.4)	1.13x	1x
EDTA	5.66 mM	5 mM
DTT	1.13 mM	1 mM
Tested Compounds, 0.5 μL	Working Concentration	Final Concentration in assay
Compound/DMSO	1 mM/100% (v/v)	16 μM /1.67% (v/v)
Enzyme, 3 μL	Working Concentration	Final Concentration in assay
Purified rhGFAT-His ₆ ²⁹⁸ (contains 1mM F6P in buffer)	0.4 mg/mL (1.3 μM)	0.04 mg/mL (0.13 μM)

Table 3-6. Reagents present in incubation step of HTS-modified Morgan-Elson Assay

Reagent	Working Concentration	Volume Added per Well (μL)	Final Concentration (in total assay volume)
1.5% acetic anhydride in acetonitrile	1.5% acetic anhydride	3	0.09375% acetic anhydride
Potassium Tetraborate in ddH ₂ O (pH 9.1)	200 mM	15	62.5 mM

Table 3-7. Reagents required for over-night acetylation reaction of HTS-modified Morgan-Elson Assay.

Ehrlich's reagent was added to the assay plate manually in a chemical fume hood with a multi-channel pipette and sealed with optically clear sealing film (Axygen, 70 μm Ultra Clear Pressure Sensitive Sealing film for Real Time PCR, Nonsterile, #UC-500). The plate was incubated at room temperature for 4 hrs, followed by measuring the

absorbance at 585 nm. Total volume added to the assay plate was 39 μ L, yielding a total assay volume of 87 μ L (Table 3-6).

Reagent	Working Concentration	Volume Added per well (μ L)	Final Concentration (in total assay volume)
Dilute Ehrlich's Reagent	224 mM	39	100.4 mM

Table 3-8. Addition of Ehrlich's reagent to the HTS-modified Morgan-Elson assay for visualization of production of *N*-acetyl-glucosamine-6-phosphate.

2 g of *p*-dimethylaminobenzaldehyde (Sigma Aldrich, Oakville, ON) was dissolved in 0.3 mL water, 2.2 mL conc. HCl, 17.4 mL glacial acetic acid, and diluted 1:2 in glacial acetic acid directly before use to create Ehrlich's reagent.

Optimization of protein concentration

The modified Morgan-Elson assay was performed under the conditions described but with manual pipetting. Protein concentration of GFAT was determined prior with the BioRAD Protein Assay Kit I (Cat. No. 500-0001, Mississauga, ON). Bovine Serum Albumin was used as the protein standard. Ten positive controls were created for each protein concentration (enzyme, substrates, DMSO) and ten negative controls (buffer in place of enzyme, substrates, DMSO). Absorbance was measured at 585 nm and the Z-factor was calculated for each.

Optimization of enzyme incubation time

The modified Morgan-Elson assay was performed under the conditions described except with manual pipetting and varying the enzyme incubation time. Samples were prepared in duplicate with enzyme, substrates and DMSO. Enzyme

activity was quenched every 30 minutes for 210 min upon addition of 1.5% acetic anhydride. The rest of the assay proceeded as described.

Solvent optimization for acetylation

The Morgan-Elson assay was performed as described except in 96-well format and with manual pipetting. GlcN standards included 0.25, 0.5, 1, 2, and 3 mM final assay concentrations. The assay was performed in singlet with the GlcN standards acetylated with either 1.5% acetic anhydride in acetone or 1.5% acetic anhydride in acetonitrile. The acetylation step took place at 40 °C overnight before Ehrlich's Reagent was added.

Ehrlich's Reagent incubation optimization

The Morgan-Elson assay was performed as described except with manual pipetting. Ten positive controls (enzyme, substrates, DMSO) and ten negative controls (enzyme, substrates, DMSO) were prepared. Absorbance at 585 nm was measured every hour for 5 hours. The Z-factor was calculated for each time point.

Measurement of GlcN standards with the standard and modified Morgan-Elson assay

A series of GlcN standards (0.25, 0.5, 1, 2, 3 mM) were tested in triplicate with either the standard or modified Morgan-Elson assay described previously, except with manual pipetting and 384-well format.

Z-factor determination for the standard Morgan-Elson assay

Ten positive controls (enzyme, substrates, DMSO) and ten negative controls (buffer in place of enzyme, substrates, DMSO) were tested with the Morgan-Elson assay

under standard conditions in 96-well format with manual pipetting. The Z-factor was calculated.

Z-factor determination for the HTS-modified Morgan-Elson assay

A 384-well format assay plate was divided into half; 192 positive controls (enzyme, substrates, DMSO) and 192 negative controls (buffer in place of enzyme, substrates, DMSO) were tested with the Morgan-Elson assay under the modified conditions on the HTS robotic platform. The Z-factor was calculated.

Five-step synthesis of N³-(4-methoxyfumaryl)-L-2,3-diaminopropanoic acid (FMDP)

i) Formation of monomethyl fumarate from dimethyl fumarate

Dimethyl fumarate (1.2 mmol, 0.17 g) was dissolved in THF (2 mL) and water (20 mL) was added. The reaction mixture was immersed in an ice bath and cooled to 0 °C. 0.25 N NaOH (8 mL) was added in small portions with stirring until the consumption of the starting diester could be detected by thin-layer chromatography with 100% EtOAc. The reaction mixture was stirred at 0 °C for 0.5 – 1 hr. 1 N HCl was added at 0 °C, NaCl was added until saturation. The monoester product was extracted with EtOAc (3 x 30 mL) and dried with sodium sulfate. The extract was evaporated *in vacuo* and purified by silica gel column chromatography (100% EtOAc) to attain the monoester, monomethyl fumarate. Yield 60%. ¹H NMR (200 MHz, CDCl₃) δ= 3.83 (3H, s), 6.87 (1H, d, J=18.0 Hz), 6.92 (1 H, d, J= 18.0 Hz); ¹³C NMR (200 MHz, acetone-*d*₆) δ= 52.4, 134.0, 134.5, 165.9, 166.1.

ii) Synthesis of *N*²- tert-butoxycarbonyl-L-2,3-diaminopropanoic acid

*N*²-*t*-butoxycarbonyl-L-asparagine (21.5 mmol, 5 g) was mixed with EtOAc (24 mL), CH₃CN (24 mL), H₂O (12 mL) and iodosobenzene diacetate (PIDA) (25.8 mmol, 8.3 g). The slurry mixture was stirred for 30 min at 16 °C. The temperature was increased to 20 °C and the reaction was stirred until completion for 4 hrs. The mixture was cooled to 0 °C and filtered. The filter cake was washed with EtOAc (10 mL) and heat dried *in vacuo* at 65 °C to yield the final product *N*²- tert-butoxycarbonyl-L-2,3-diaminopropanoic acid. Yield 55%. ¹H NMR (200 MHz, DMSO/TFA) δ= 1.39 (9H, *s*), 2.98 (1H, *m*), 3.19 (1H, *m*), 4.20 (1H, *m*), 7.22 (1H, *d*), 7.88 (3H, *bs*); ¹³C NMR (200 MHz, DMSO) δ= 27.7 (3C), 51.1, 78.5, 157.7, 170.81; TOF MS ES+ (MeOH) *m/z* calcd for C₈H₁₇N₂O₆ (MH⁺) 205.1188, found 205.1183.

iii) Synthesis of *N*-succinimidoyl ester of monomethyl fumarate

Monomethyl fumarate (0.9 mmol, 0.117 g) and *N*-hydroxysuccinimide (1 mmol, 0.112 g) were dissolved into CH₃CN, and stirred over an ice bath. *N*-(3-dimethylaminopropyl)-*N*'-ethylcarbodiimide (EDCI) (1 mmol, 0.192 g) was added at 0 °C, and stirred overnight. The solvent was removed *in vacuo*, the residue was dissolved in DCM and washed with water (3x50 mL). The DCM layer was retained and the product was purified by silica gel column chromatography with 50:50 EtOAc/hexanes. Yield 31%. ¹H NMR (200 MHz, CDCl₃) δ= 2.88 (4H, *s*), 3.85 (3H, *s*), 6.93 (1H, *d*, *J*=16.2 Hz), 7.16 (1H, *d*, *J*= 16.2 Hz); ¹³C NMR (200 MHz, CDCl₃) δ= 25.6, 52.8, 128.2, 138.0, 160.39, 164.52, 168.87; TOF MS ES+ (MeOH) *m/z* calcd for C₉H₁₀NO₆ (MH⁺) 228.0508, found 228.0513.

iv) Preparation of N^3 -tert-butoxycarbonyl-(4-methoxyfumaramoyl)-L-2,3-diaminopropanoic acid

N^2 -tert-butoxycarbonyl-L-2,3-diamino-propanoic acid (3 mmol, 0.61 g) and NaHCO_3 (3 mmol, 0.25 g) were dissolved in a water-methanol solution (10 mL, 2:1 v/v). The N -succinimidoyl ester of monomethyl fumarate was added with stirring at 0 °C, and stirred for 4 hrs. The solvent was removed *in vacuo*, and the residue was dissolved in water (5 mL). 10% citric acid was added until pH 2. The solution was extracted with ethyl acetate (3x50 mL). The organic phase was washed with brine and dried over MgSO_4 , evaporation yielded the product. The product N^3 -tert-butoxycarbonyl-(4-methoxyfumaramoyl)-L-2,3-diaminopropanoic acid was crystallized from a mixture of EtOAc-hexanes or ethyl ether-hexanes. Yield 51%. ^1H NMR (200 MHz, $\text{MeOH-}d_4$) δ = 1.45 (9H, s), 3.55 (2H, m), 3.79 (3H, s), 4.31 (1H, m), 6.67 (1H, d, J =15.8 Hz), 7.043 (1H, d, J =14 Hz); ^{13}C NMR (600 MHz, $\text{MeOH-}d_4$) δ = 28.68 (3C), 42.03, 52.65, 54.78, 80.78, 130.72, 137.51, 157.88, 166.64, 167.29, 173.61; TOF MS ES- (MeOH) m/z calcd for $\text{C}_{13}\text{H}_{19}\text{N}_2\text{O}_7(\text{MH}^-)$ 315.1192, found 315.1179.

v) Removal of the tert-butoxycarbonyl protecting group

N^3 -tert-butoxycarbonyl-(4-methoxyfumaramoyl)-L-2,3-diaminopropanoic acid (2 mmol, 0.63 g) was treated with 2N HCl in dioxane (10 mL) at r.t. for 2-3 hours. The dioxane was removed *in vacuo* and the residue was dried under vacuum. The product was crystallized from methanol-ethyl ether twice, yielding the desired compound N^3 -(4-methoxyfumaramoyl)-L-2,3-diaminopropanoic acid (FMDP) in the form of its hydrochloride. Yield 54%. ^1H NMR (200 MHz, $\text{D}_2\text{O/TFA}$) δ = 3.39 (3H, s), 3.53 (2H, m), 3.92

(1H, *m*), 6.29 (1H, *d*, *J*= 17.2 Hz), 6.63 (1H, *d*, *J*=16 Hz); TOF MS ES- (MeOH) *m/z* calcd for C₈H₁₁N₂O₅ (MH⁺) 215.0668, found 215.0675.

Pilot screen

The pilot screen was performed with the HTS-modified Morgan-Elson assay on the HTS robotic platform. Four compound plates from the P1000 library (#9-12) at the McMaster University HTS facility were chosen. 320 compounds were tested in duplicate on two 384-well format, clear, assay plates (Costar #3701). 20 positive controls (enzyme, substrates, DMSO), 20 reference controls (enzyme, substrates, 167 μM EME 384), and 20 negative controls (buffer in place of enzyme, substrates, DMSO) were included per assay plate. The Z'-factor was calculated using the positive and negative controls. The master mix, acetic anhydride solution and diluted Ehrlich's reagent were prepared directly before use.

Primary screen

The primary screen was performed with the HTS-modified Morgan-Elson assay on the HTS robotic platform. 3950 compounds were assayed. Compounds were selected from the bioactive subset of the Canadian Compound Collection and from academic libraries at McMaster University and University of Alberta (Capretta, McNulty, and Hall). 160 compounds were tested in duplicate per assay plate and 6 plates were processed per day. 24 positive controls (enzyme, substrates, DMSO), 8 reference controls (enzyme, substrates, 83 μM EME 384), and 32 negative controls (buffer in place of enzyme, substrates, DMSO) were included per assay plate. The Z'-factor was calculated using the

positive and negative controls. The master mix, acetic anhydride solution and diluted Ehrlich's reagent were prepared directly before use. The assay plate layout is shown in Figure 3-19.

Dose-Response Assays

The dose-response assays were performed with the modified Morgan-Elson assay on the HTS platform. A half-log dilution series of 11 dilutions was created in DMSO for each compound tested. All dose-response assays were performed in duplicate. Positive controls included DMSO in place of a test compound and negative controls included DMSO and buffer in place of a test compound and enzyme. For the secondary dose-response screening, two different master mixes were created. One was the same as in Table 3-4 to test inhibition at $10xK_M$, the other had a master mix with 1.15 mM L-glutamine and 1.13 mM F6P to test inhibition at $1xK_M$.

Compounds were transferred from 96 well storage plates to 384 well assay plates in four quadrants as shown in Figure 3-19.

	1	2	3	4	5	6	7	8	9	10	11	12	13	14	15	16	17	18	19	20	21	22	23	24
A	-enz	-enz	1-R1	1-R2	1-R1	1-R2	1-R1	1-R2	1-R1	1-R2	1-R1	1-R2	1-R1	1-R2	1-R1	1-R2	1-R1	1-R2	1-R1	1-R2	1-R1	1-R2	-enz	-enz
B	-enz	-enz	2-R1	2-R2	2-R1	2-R2	2-R1	2-R2	2-R1	2-R2	2-R1	2-R2	2-R1	2-R2	2-R1	2-R2	2-R1	2-R2	2-R1	2-R2	2-R1	2-R2	-enz	-enz
C	+enz	+enz	1-R1	1-R2	1-R1	1-R2	1-R1	1-R2	1-R1	1-R2	1-R1	1-R2	1-R1	1-R2	1-R1	1-R2	1-R1	1-R2	1-R1	1-R2	1-R1	1-R2	+enz	+enz
D	+enz	+enz	2-R1	2-R2	2-R1	2-R2	2-R1	2-R2	2-R1	2-R2	2-R1	2-R2	2-R1	2-R2	2-R1	2-R2	2-R1	2-R2	2-R1	2-R2	2-R1	2-R2	+enz	+enz
E	-enz	-enz	1-R1	1-R2	1-R1	1-R2	1-R1	1-R2	1-R1	1-R2	1-R1	1-R2	1-R1	1-R2	1-R1	1-R2	1-R1	1-R2	1-R1	1-R2	1-R1	1-R2	-enz	-enz
F	-enz	-enz	2-R1	2-R2	2-R1	2-R2	2-R1	2-R2	2-R1	2-R2	2-R1	2-R2	2-R1	2-R2	2-R1	2-R2	2-R1	2-R2	2-R1	2-R2	2-R1	2-R2	-enz	-enz
G	Ref.+ enz	Ref.+ enz	1-R1	1-R2	1-R1	1-R2	1-R1	1-R2	1-R1	1-R2	1-R1	1-R2	1-R1	1-R2	1-R1	1-R2	1-R1	1-R2	1-R1	1-R2	1-R1	1-R2	Ref.+ enz	Ref.+ enz
H	Ref.+ enz	Ref.+ enz	2-R1	2-R2	2-R1	2-R2	2-R1	2-R2	2-R1	2-R2	2-R1	2-R2	2-R1	2-R2	2-R1	2-R2	2-R1	2-R2	2-R1	2-R2	2-R1	2-R2	Ref.+ enz	Ref.+ enz
I	-enz	-enz	1-R1	1-R2	1-R1	1-R2	1-R1	1-R2	1-R1	1-R2	1-R1	1-R2	1-R1	1-R2	1-R1	1-R2	1-R1	1-R2	1-R1	1-R2	1-R1	1-R2	-enz	-enz
J	-enz	-enz	2-R1	2-R2	2-R1	2-R2	2-R1	2-R2	2-R1	2-R2	2-R1	2-R2	2-R1	2-R2	2-R1	2-R2	2-R1	2-R2	2-R1	2-R2	2-R1	2-R2	-enz	-enz
K	+enz	+enz	1-R1	1-R2	1-R1	1-R2	1-R1	1-R2	1-R1	1-R2	1-R1	1-R2	1-R1	1-R2	1-R1	1-R2	1-R1	1-R2	1-R1	1-R2	1-R1	1-R2	+enz	+enz
L	+enz	+enz	2-R1	2-R2	2-R1	2-R2	2-R1	2-R2	2-R1	2-R2	2-R1	2-R2	2-R1	2-R2	2-R1	2-R2	2-R1	2-R2	2-R1	2-R2	2-R1	2-R2	+enz	+enz
M	-enz	-enz	1-R1	1-R2	1-R1	1-R2	1-R1	1-R2	1-R1	1-R2	1-R1	1-R2	1-R1	1-R2	1-R1	1-R2	1-R1	1-R2	1-R1	1-R2	1-R1	1-R2	-enz	-enz
N	-enz	-enz	2-R1	2-R2	2-R1	2-R2	2-R1	2-R2	2-R1	2-R2	2-R1	2-R2	2-R1	2-R2	2-R1	2-R2	2-R1	2-R2	2-R1	2-R2	2-R1	2-R2	-enz	-enz
O	+enz	+enz	1-R1	1-R2	1-R1	1-R2	1-R1	1-R2	1-R1	1-R2	1-R1	1-R2	1-R1	1-R2	1-R1	1-R2	1-R1	1-R2	1-R1	1-R2	1-R1	1-R2	+enz	+enz
P	+enz	+enz	2-R1	2-R2	2-R1	2-R2	2-R1	2-R2	2-R1	2-R2	2-R1	2-R2	2-R1	2-R2	2-R1	2-R2	2-R1	2-R2	2-R1	2-R2	2-R1	2-R2	+enz	+enz

Figure 3-19. Assay plate layout for the primary screen. Figure courtesy of Jan Blanchard at the McMaster HTS facility. Colour scheme for two 96-well compound storage plates: 1-R1 = compound plate 1, replicate 1 (blue); 1-R2 = compound plate 1, replicate 2 (pink); 2-R1 = compound plate 2, replicate 1 (green); 2-R2 = compound plate 2, replicate 2 (purple). The primary screen transfer map illustrates the transfer of compounds from two 96 well compound plates to one 384 well assay plate, where each compound plate is tested in duplicate. The control compounds are placed in column 1 and 12 of a 96-well cone plate, and transferred to columns 1&2, 23&24 of a 384 well assay plate, which are also indicated. Ref + enz = EME 384 + GFAT (white), -enz = low control with DMSO and buffer in place of GFAT (black), +enz = high control with GFAT and DMSO (grey).

References

1. Milewski, S., Glucosamine-6-Phosphate Synthase—the Multi-Facets Enzyme. *BBA-Protein Struct. M.* **2002**, *1597* (2), 173-192.
2. Macarron, R.; Banks, M. N.; Bojanic, D.; Burns, D. J.; Cirovic, D. A.; Garyantes, T.; Green, D. V. S.; Hertzberg, R. P.; Janzen, W. P.; Paslay, J. W.; Schopfer, U.; Sittampalam, G. S., Impact of High-Throughput Screening in Biomedical Research. *Nat. Rev. Drug Discov.* **2011**, *10* (3), 188-195.
3. (a) Silber, B. M., Driving Drug Discovery: The Fundamental Role of Academic Labs. *Sci. Transl. Med.* **2010**, *2* (30),1-6; (b) Hasson, S. A.; Inglese, J., Innovation in Academic Chemical Screening: Filling the Gaps in Chemical Biology. *Curr. Opin. in Chem. Biol.* **2013**, *17* (3), 329-338.
4. Keseru, G. M.; AU - Makara, G. M., The Influence of Lead Discovery Strategies on the Properties of Drug Candidates. *Nat. Rev. Drug Discov.* **2009**, *8* (3), 203-209.
5. Inglese, J.; Johnson, R. L.; Simeonov, A.; Xia, M.; Zheng, W.; Austin, C. P.; Auld, D. S., High-Throughput Screening Assays for the Identification of Chemical Probes. *Nat. Chem. Biol.* **2007**, *3* (8), 466-479.
6. Newman, D. J.; Cragg, G. M., Natural Products As Sources of New Drugs Over the 30 Years from 1981 to 2010. *J. Nat. Prod.* **2012**, *75* (3), 311-335.
7. Shoichet, B. K., Virtual Screening of Chemical Libraries. *Nature* **2004**, *432* (7019), 862-865.
8. Bobzin, S. C.; Yang, S.; Kasten, T. P., Application of Liquid Chromatography–Nuclear Magnetic Resonance Spectroscopy to the Identification of Natural Products. *J. Chromatogr. B: Biomed. Sci. Appl.* **2000**, *748* (1), 259-267.
9. (a) Floquet, N.; Richez, C.; Durand, P.; Maigret, B.; Badet, B.; Badet-Denisot, M. A., Discovering New Inhibitors of Bacterial Glucosamine-6P synthase (GlmS) by Docking Simulations. *Bioorg. Med. Chem. Lett.* **2007**, *17* (7), 1966-1970; (b) Vyas, B.; Silakari, O.; Singh Bahia, M.; Singh, B., Glutamine: Fructose-6-Phosphate Amidotransferase (GFAT): Homology Modelling and Designing of New Inhibitors using Pharmacophore and Docking Based Hierarchical Virtual Screening protocol. *SAR QSAR Environ. Res.* **2013**, 1-20.
10. Zhang, J.-H.; Chung, T. D. Y.; Oldenburg, K. R., A Simple Statistical Parameter for Use in Evaluation and Validation of High Throughput Screening Assays *J. Biomol. Screen.* **1999**, *4*, 67-72.
11. Burghardt, C.; Kochan, J. Method for Measuring Glucosamine-6-Phosphate. EP 1 431 396 A1. 2004.
12. Awuah, E.; Capretta, A., Strategies and Synthetic Methods Directed Toward the Preparation of Libraries of Substituted Isoquinolines. *J. Org. Chem.* **2010**, *75* (16), 5627-5634.
13. Bolin, D.; Chen, S.; Mischke, S.; Qian, Y. Glutamine Fructose-6-Phosphate Amidotransferase (GFAT) Inhibitors. WO 2005/040150 A2. 6 May 2005.
14. Niwayama, S., Highly Efficient Selective Monohydrolysis of Symmetric Diesters. *J. Org. Chem.* **2000**, *65* (18), 5834-5836.
15. Zhang, L.-H.; Kauffman, G. S.; Pesti, J. A.; Yin, J., Rearrangement of N α -Protected L-Asparagines with Iodosobenzene Diacetate. A Practical Route to β -Amino-L-alanine Derivatives. *J. Org. Chem.* **1997**, *62* (20), 6918-6920.

16. Andruszkiewicz, R.; Chmara, H.; Milewski, S.; Borowski, E., Synthesis of N³-fumaramoyl-L-2,3-diaminopropanoic Acid Analogues, the Irreversible Inhibitors of Glucosamine Synthetase. *Int. J. Pept. Prot. Res.* **1986**, *27* (5), 449-453.
17. Wilson, W. D.; Gough, A. N.; Doyle, J. J.; Davidson, M. W., Coralyne. Intercalation with DNA as a possible mechanism of antileukemic action. *J. Med. Chem.* **1976**, *19* (10), 1261-1263.
18. Faucher, J.-F.; Bellanger, A.-P.; Chirouze, C.; Hustache-Mathieu, L.; Genton, S.; Hoen, B., Primaquine for Radical Cure of Plasmodium vivax and Plasmodium ovale Malaria: An Observational Survey (2008–2010). *J. Travel Med.* **2013**, *20* (2), 134-136.
19. Osada, S.; Tomita, H.; Tanaka, Y.; Tokuyama, Y.; Tanaka, H.; Sakashita, F.; Takahashi, T., The Utility of Vitamin K3 (Menadione) against Pancreatic Cancer. *Anticancer Res.* **2008**, *28* (1A), 45-50.
20. Sharaev, P.; Bogdanov, N.; Sarycheva, I.; Zhukova, E., Allosteric Regulation of Glucosamine Synthetase Activity by Naphthoquinone Derivatives and Ethyl Ester of di-(4-oxycumarinyl-3)-acetic acid. *Biochemistry - USSR* **1981**, *46* (2), 342-345.
21. Sharaev, P., Role of Vitamin K in Glycoprotein Metabolism. *Vopr. Pitan.* **1977**, *3*, 66-68.
22. Burnett, A. R.; Thomson, R. H., Naturally Occurring Quinones. Part X. The Quinonoid Constituents of *Tabebuia avellaneda*(Bignoniaceae). *J. Chem. Soc. C* **1967**, 2100-2104.
23. Müller, K.; Sellmer, A.; Wiegrebe, W., Potential Antipsoriatic Agents: Lapacho Compounds as Potent Inhibitors of HaCaT Cell Growth. *J. Nat. Prod.* **1999**, *62* (8), 1134-1136.
24. (a) Huang, L.; Pardee, A. B., Beta-lapachone Induces Cell Cycle Arrest and Apoptosis in Human Colon Cancer Cells. *Mol. Med.* **1999**, *5* (11), 711-720; (b) Rao, K. V.; McBride, T. J.; Oleson, J. J., Recognition and Evaluation of Lapachol as an Antitumor Agent. *Cancer Res.* **1968**, *28* (10), 1952-1954; (c) Shah, H. R.; Conway, R. M.; Van Quill, K. R.; Madigan, M. C.; Howard, S. A.; Qi, J.; Weinberg, V.; O'Brien, J. M., Beta-lapachone Inhibits Proliferation and Induces Apoptosis in Retinoblastoma Cell Lines. *Eye* **2007**, *22* (3), 454-460.
25. Peyregne, V. P.; Kar, S.; Ham, S. W.; Wang, M.; Wang, Z.; Carr, B. I., Novel Hydroxyl Naphthoquinones with Potent Cdc25 Antagonizing and Growth Inhibitory Properties. *Mol. Cancer Ther.* **2005**, *4* (4), 595-602.
26. Jones, E.; Ekundayo, O.; Kingston, D. G. I., Plant Anticancer Agents. XI. 2,6-Dimethoxybenzoquinone as a Cytotoxic Constituent of *Tibouchina pulchra*. *J. Nat. Prod.* **1981**, *44* (4), 493-494.
27. Szkudelski, T., The Mechanism of Alloxan and Streptozotocin Action in B Cells of the Rat Pancreas. *Physiol. Res.* **2001**, *50*, 536-545.
28. Durand, P.; Golinelli-Pimpaneau, B.; Mouilleron, S.; Badet, B.; Badet-Denisot, M. A., Highlights of Glucosamine-6P Synthase Catalysis. *Arch. Biochem. Biophys.* **2008**, *474* (2), 302-17.
29. Ko, Y.; Morita, K.; Nagahori, R.; Kinouchi, K.; Shinohara, G.; Kagawa, H.; Hashimoto, K., Myocardial Cyclic AMP Augmentation with High-Dose PDEIII Inhibitor in Terminal Warm Blood Cardioplegia. *Ann. Thorac. Cardiovas.* **2009**, *15* (5), 311-316.

30. LeJemtel, T.; Keung, E.; Sonnenblick, E.; Ribner, H.; Matsumoto, M.; Davis, R.; Schwartz, W.; Alousi, A.; Davolos, D., Amrinone: A New Non-Glycosidic, Non-Adrenergic Cardiotonic Agent Effective in the Treatment of Intractable Myocardial Failure in Man. *Circulation* **1979**, *59* (6), 1098-1104.
31. Klawe, C.; Maschke, M., Flupirtine: Pharmacology and Clinical Applications of a Nonopioid Analgesic and Potentially Neuroprotective Compound. *Expert Opin. Pharmacol.* **2009**, *10* (9), 1495-1500.
32. Dutta, K.; Ghosh, D.; Nazmi, A.; Kumawat, K. L.; Basu, A., A Common Carcinogen Benzo[a]pyrene Causes Neuronal Death in Mouse via Microglial Activation. *PLoS ONE* **2010**, *5* (4), 1-14.
33. Brown, J. K.; Shapazian, L.; Griffin, G. D., A Rapid Screening Procedure for Some "Street Drugs" by Thin-Layer Chromatography. *J. Chromatogr. A* **1972**, *64* (1), 129-133.
34. Miller, J. M.; Wright, J. W., Spot Indole Test: Evaluation of Four Reagents. *J. Clin. Microbiol.* **1982**, *15* (4), 589-592.
35. Kleinerová, E.; Kybal, J., Ergot Alkaloids. *Folia Microbiol.* **1969**, *14* (6), 602-604.

Chapter 4

Characterization of GFAT Inhibitors:
Cell Toxicity, Efficacy, Structure-Activity
Relationship Analysis and Determination
of Mode of Inhibition

Preface

This research was performed with the assistance from members of the Capretta, Werstuck and McCarry Research Groups. Dr. Peter Shi and Dan Beriault provided expertise with cell culture growth and the cell toxicity experiments. Christina Petlura and Vi Dang assisted with the UPLC-MS based assay for measurement of UDP-GlcNAc in cell culture. Prof. Brian McCarry and Dr. Ken Chalcraft provided vital analytical chemistry knowledge for the success of the UPLC-MS assay. Dr. Emelia Awuah, Dr. Nick Todorovic, Tishan Singh, Thomas Floyd, Sam Dalton, and Bilal Bagha were responsible for the synthesis of the 6,7-dimethoxyisoquinoline, aminothiazole, 1,4-naphthoquinone and amrinone derivatives.

Abstract

The most promising validated hits obtained from the high-throughput screening campaign were further characterized with respect to cell toxicity, cell permeability and efficacy. A structure-activity relationship analysis was performed on four structural families, namely isoquinolines, aminothiazoles, pyridinones, and quinones. Dehydroiso- β -lapachone was characterized as a potent, noncompetitive GFAT inhibitor with a low toxicity profile in HepG2 cells.

Introduction

The ultimate goal of the high-throughput screening campaign was to identify GFAT inhibitors that function *in vivo*. An ideal inhibitor would be able to inhibit GFAT with high-specificity while showing minimal toxicity to the model system. The nine most promising validated hits identified in the previous chapter were tested for cell toxicity, cell permeability, and efficacy in cell culture. Many authors agree that assessment of small molecules in a cell based system is necessary for the creation of high-quality chemical probes.¹ Along with characterizing the biological properties of the leads, a structure-activity relationship (SAR) analysis was performed on 6,7-dimethoxyisoquinolines, aminothiazole derivatives of the pilot screen hit, amrinone derivatives, and quinones to find a more potent derivative of the lead compounds identified. An SAR analysis is vital to improving probe quality and to gain an understanding of the mechanism of action following a screening campaign.² Compounds for SAR analysis were purchased if commercially available or created synthetically. Our intention was to treat the results of the cytotoxicity, cell efficacy and SAR as a platform to narrow down future directions of the lead structural families.

Results and Discussion

Cell toxicity of inhibitors with HepG2 cells

The primary leads identified in the screen were tested in a live/dead assay using trypan blue and HepG2 liver cells.³ Trypan blue is a dye which is unable to penetrate intact cell membranes of living cells, whereas dead cells with compromised membranes appear blue. Liver hepatocellular carcinoma cells (HepG2) were selected as the model system for biological characterization of the leads because they are a good source of hGFAT1.⁴ We had previously used HepG2 cells as a model system to measure downstream effects of GFAT over-expression as well.⁵ This property was important for measuring the efficacy of the inhibitors in cell culture. Cell toxicity was reported as a range from where cell death was first visible at the lowest concentration used to the highest concentration where all cells were no longer viable.

Our results identified a number of compounds with low cytotoxicity and had also helped to narrow our search for an ideal inhibitor (Figure 4-1). NSC 95397 (18, IC₅₀: 41.5±1.4 µM) and 2,6-dimethoxyquinone (56, IC₅₀: 15.9±1.8 µM) were shown to be very toxic, killing cells at concentrations of 10 µM or less while showing only good to modest IC₅₀ values for GFAT (Figure 4-2). As such, these compounds were eliminated from our search. Due to the role of homidium bromide⁶ (57, IC₅₀: 0.32±0.06 µM) and coralyne chloride⁷ (2, IC₅₀: 41±26.3 µM) as DNA intercalating agents we chose not to study them further biologically despite their low levels of toxicity (cell death occurring at 10-100 µM for homidium bromide, 100-500 µM for coralyne chloride) and potency in the case of homidium bromide. Homidium bromide may find use as a general reference inhibitor

due to its commercial availability. Beta-lapachone (28, IC_{50} : $10.4 \pm 0.5 \mu\text{M}$) was eliminated due to toxicity. Cell death occurred at the 1-10 μM range, which was below its IC_{50} . Menadione (14, IC_{50} : $11.8 \pm 0.7 \mu\text{M}$) displayed low levels of toxicity (cell death occurring at 10-100 μM), but it did not have as great a toxicity/efficacy profile as related 1,4-naphthoquinone lapachol (45, IC_{50} : $17.6 \pm 2.2 \mu\text{M}$), and was not pursued further. For lapachol, cell death occurred in the 100-500 μM range, which was 6-28x its IC_{50} . Alloxan (41, IC_{50} : $13.9 \pm 0.8 \mu\text{M}$) and amrinone (4, IC_{50} : $91 \pm 34.1 \mu\text{M}$) also displayed low cell toxicity, with cell death occurring in the same range as lapachol. As a result, the leads were streamlined to alloxan, amrinone and lapachol for further biological testing as they had good toxicity/efficacy profiles.

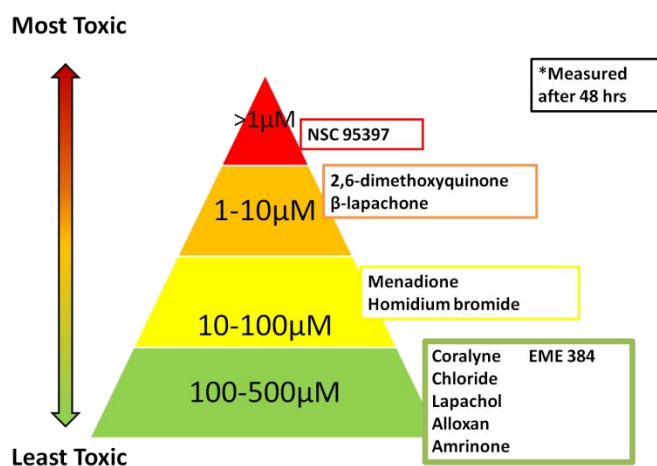


Figure 4-1. Cytotoxicity of lead compounds against HepG2 cells. Cells were treated in duplicate for 48 hours with each inhibitor over a range of concentrations (0.125, 0.25, 0.5, 1, 10, 100, 200 and 500 μM) along with an equal volume of DMSO, no DMSO and known ER-stress inducing agent tunicamycin as control. NSC 95397, 2,6-dimethoxyquinone and β -lapachone were the most toxic to HepG2 cells, menadione and homidium bromide showed moderate toxicity, and coralyne chloride, lapachol, alloxan, and amrinone were the least toxic. EME 384 displayed low toxicity against HepG2 cells.

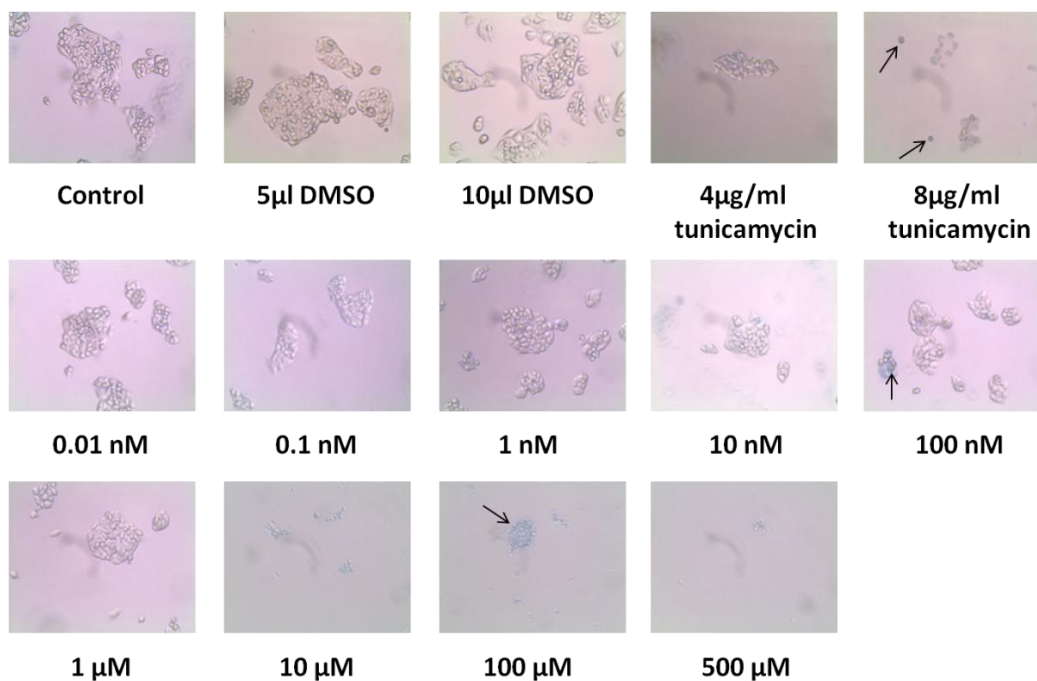


Figure 4-2. Representative images of HepG2 cells grown in the presence of varying amounts of 2,6-dimethoxyquinone and control cells with no DMSO, with DMSO, or with tunicamycin. After a 48 hr exposure, cells were stained with trypan blue and visualized under microscope. Dead cells appeared blue (arrows). A decrease in cell density may also indicate cell death. It appeared cell death began to occur at or less than 10 μM of 2,6-dimethoxyquinone.

Development of an UPLC-TOF-MS Assay for UDP-GlcNAc Detection and Assessment of Downstream HBP Activity

In order to assess the cell permeability and efficacy of potential GFAT inhibitors against native human GFAT, a method for the detection of HBP activity was developed as the Morgan-Elson assay proved to lack the sensitivity to measure GlcN6P levels in small cell-cultures. UDP-GlcNAc is the final product of the HBP and is believed to be a marker of nutrient availability since it incorporates products from sugar (glucose), amino acid (glutamine), fatty acid (acetyl CoA) and nucleotide (uridine) metabolism.^{5,8} Measurement of UDP-GlcNAc in cell culture was an excellent way to measure the downstream effects of GFAT inhibition.

An HPLC-UV method was used to detect UDP-GlcNAc levels in samples of human muscle tissue and has been described in the literature.⁹ While the method was successful at detection and separation of UDP-sugars, it suffered from long retention times. Since we were interested in testing several different compounds at different concentrations plus controls, long retention times with HPLC would be impractical. We decided to employ a UPLC method with TOF-MS detection. This allowed us to use small amounts of sample and increased the sensitivity and accuracy of detection by utilizing MS instead of UV. For separation of the polar nucleotide sugars, a ZIC®-HILIC (Zwitterionic Charge – Hydrophilic Interaction Liquid Chromatography) column (Merck SeQuant®) was employed. This column maintains a permanent zwitterionic charge (Figure 4-3) and can be considered similar to a normal phase column which uses reversed-phase type eluents. This column is useful for the separation of polar compounds such as carbohydrates or those containing ionizable groups which are not retained well on reversed-phase columns. By utilizing TOF-MS detection, samples which are not fully separated can still be detected and quantified. This detection method also allows the flexibility to measure other metabolites in the HBP for future applications.

A variety of sugar standards, metabolites involved in the HBP and other similarly related metabolites were tested first to determine which would have the highest signal to allow for ease of detection in cell culture (Figure 4-4). Relative to an internal standard dipeptide of glycine-phenylalanine, UDP-GlcNAc displayed the best signal out of the other HBP metabolites F6P and GlcN6P, and was selected as the metabolite to follow in cell culture.

UDP-GlcNAc levels were then measured in untreated HepG2 cells harvested from a 24-well plate. UDP-GlcNAc was detected in cell culture as well (Figure 4-5). This provided evidence that UDP-GlcNAc detection would allow for an indirect assay method to determine activity of native GFAT and the HBP.

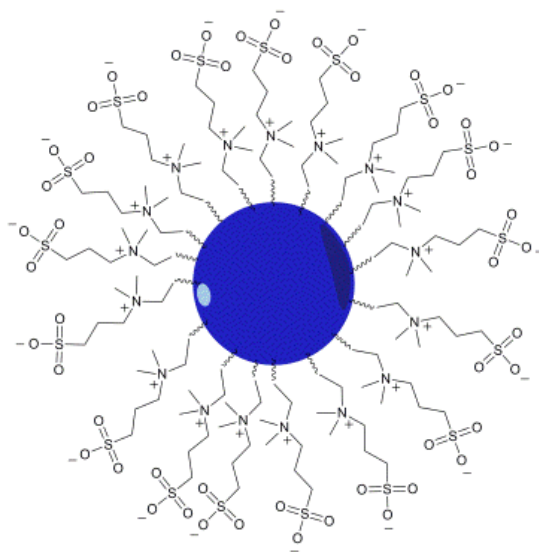


Figure 4-3. Representation of ZIC®-HILIC stationary phase. The ZIC®-HILIC column contains a permanent zwitterion bound to silica. This promotes weak electrostatic interactions and causes retention to increase with the hydrophilicity and charge of the analyte. UDP-GlcNAc is a polar compound and an ideal candidate for separation using the ZIC®-HILIC column in place of a reversed-phase system.

Using this column it was not possible to separate the epimer UDP-*N*-acetylgalactosamine (UDP-GalNAc) from UDP-GlcNAc. Separation however may not be necessary as detection of the former may not over-estimate the amount of activity in the HBP. Both molecules are used in downstream secondary modification of proteins, and UDP-GalNAc is derived from UDP-GlcNAc by the reversible enzyme UDP-galactose-4-epimerase (GALE) when in the presence of NADH.¹⁰ Measurement of both molecules provides an accurate representation of activity within the HBP.

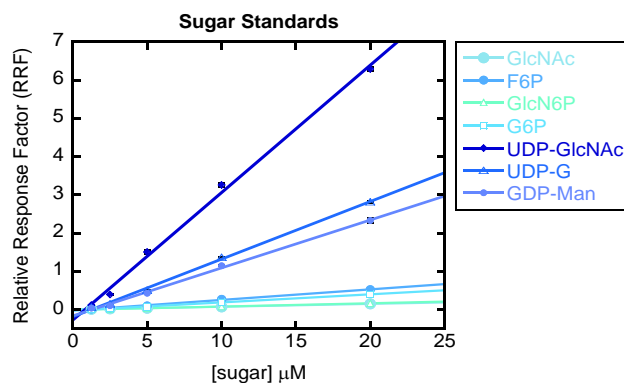


Figure 4-4. Calibration curves of sugar-standards with the ZIC®-HILIC column. *N*-acetylglucosamine (GlcNAc), glucosamine-6-phosphate (GlcN6P), fructose-6-phosphate (F6P), glucose-6-phosphate (G6P), uridine diphosphate *N*-acetylglucosamine (UDP-GlcNAc), uridine diphosphate glucose (UDP-G), guanosine diphosphate mannose (GDP-Man) were all measured in quintuplet and the signal was compared to an internal standard, a dipeptide of glycine-phenylalanine. UDP-GlcNAc displayed the most intense signal compared to the other HBP sugars F6P, and GlcN6P, and other sugar-metabolites GlcNAc, G6P, UDP-G, and GDP-Man. All calibration curves had an R^2 value of 0.996 or better.

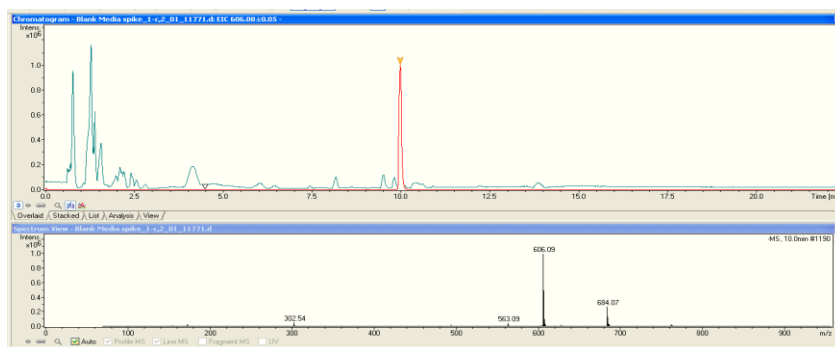


Figure 4-5. UPLC/MS chromatogram of UDP-GlcNAc detection in untreated HepG2 cells. UPLC trace of UDP-GlcNAc corresponds to the red high-lighted peak, elution time at 10 min. The MS trace corresponds to black and the peak at m/z 606.09 was predicted to be UDP-GlcNAc or UDP-GlcNAc/UDP-GalNAc. The sample was from HepG2 cells harvested from one well of a 24-well plate and resuspended in 100 μ L of 4:1 MeOH/H₂O.

To determine whether the assay method would be reproducible across samples, HepG2 cells were treated with glucosamine (GlcN) to determine if an increase in UDP-GlcNAc would result (Figure 4-6). Samples were grown in 24-well tissue culture plates and harvested by trypsinization. For MS compatibility, the media and wash buffer used for the cells was removed following collection of the cell pellet by centrifugation. The

cell lysates were prepared in a MeOH/H₂O solution containing an internal standard of dipeptide glycine-phenylalanine (gly-phe). The internal standard concentration remained the same throughout each sample and the peak area was used to compare the UDP-GlcNAc levels. This provided the relative response factor (RRF). Samples were tested in replicates of 3-5 for each treatment. A pooled sample which contained an equal volume of each sample tested and the internal standard were run after every five samples. This was to control for instrument variability. In order to normalize each replicate, the viable cells from each sample were counted in duplicate with the Countess® automated cell counter (Life Technologies). Trypan blue was used to assess cell viability in the automated system. An increase in UDP-GlcNAc levels was observed at each GlcN treatment as compared to untreated cells. A 4-fold, 5-fold and 9.5-fold increase was observed for the treatments at 0.2, 1 and 5 mM levels of GlcN respectively in comparison to the low glucose (5 mM) only treatment. Cell concentration was deemed an acceptable way to control for differences in cell growth and cell viability between samples.

HepG2 cells were treated with amrinone (Figure 4-7), alloxan (Figure 4-8) or lapachol (Figure 4-9), to determine if a decrease in UDP-GlcNAc levels could be observed as a result of native human GFAT inhibition. Cells were grown in low glucose media (5 mM) and treated with concentrations of 10, 20 or 50 µM of inhibitor for 24 hours before harvesting. All samples were counted in duplicate with the Countess®. In each case a significant decrease in UDP-GlcNAc levels was observed as compared to untreated cells.

Amrinone displayed a 27% decrease in UDP-GlcNAc concentration at 20 μM and a 42% decrease at 50 μM . Alloxan was the most potent of the three and a 40% decrease in UDP-GlcNAc was observed at 10 μM , treatments at 20 and 50 μM displayed a 70% decrease. A significant effect from lapachol was observed with a 61% decrease at 50 μM . With these results we can presume that these molecules are permeable to HepG2 cells and that they are able to modulate the downstream activity of the HBP.

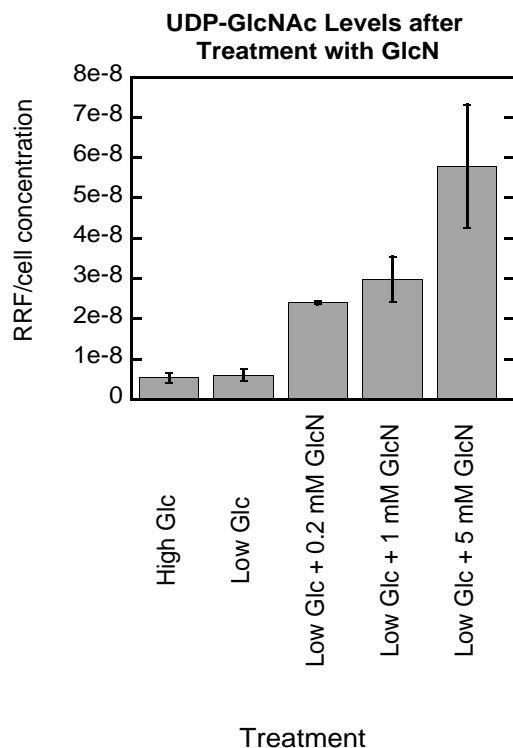


Figure 4-6. Measurement of UDP-GlcNAc levels as the relative response factor (RRF) over cell concentration in HepG2 cells treated with glucosamine (GlcN) for 24 hours. HepG2 cells grown in 5 mM glucose (Low Glc) media were treated with 24.5 mM glucose (High Glc), or 0.2, 1, or 5 mM glcN for 24 hours before harvesting. Treatment of 5 mM GlcN (N=5) vs untreated cells (low or high glucose) was found to be significant ($p < 0.0001$) after performing a one-way ANOVA and a Tukey's All Pairs Comparison. The 0.2 mM (N=4) and 1 mM (N=5) GlcN treatments also showed a significant increase in UDP-GlcNAc levels compared to the untreated cells ($p = 0.02$, $p = 0.001$ respectively). There was no significant difference found between cells grown in high glucose (N=4) media and low glucose (N=5) media.

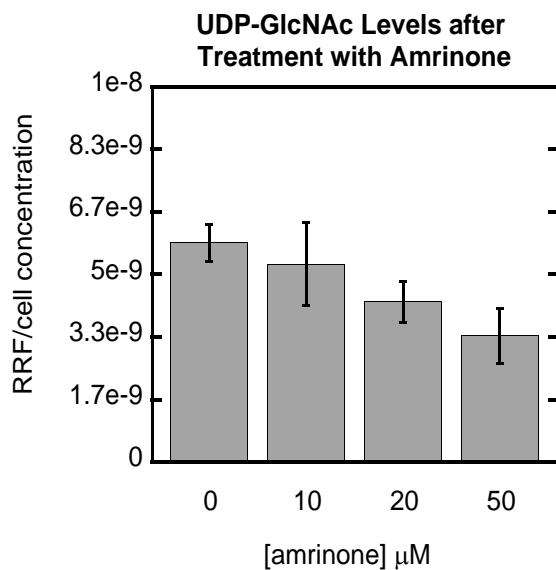


Figure 4-7. UDP-GlcNAc levels in HepG2 cells following 24-hr treatment with amrinone. Compared to the untreated cells (N=4), there was a significant difference in UDP-GlcNAc levels following treatment with 20 μM (N=4, $p=0.0584$) and 50 μM (N=3, $p=0.0065$) amrinone after a one-way ANOVA with Tukey's All Pairs Comparison was performed. There was no significant difference observed between the untreated cells and treatment at 10 μM (N=4) or between treatments at 20 and 50 μM.

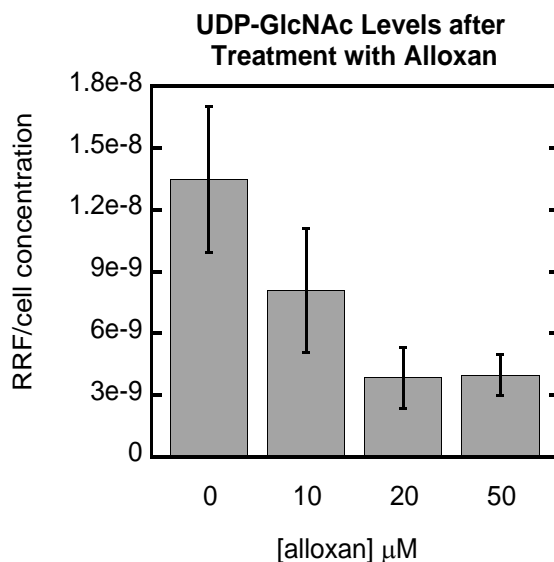


Figure 4-8. UDP-GlcNAc levels in HepG2 cells following 24-hr treatment with alloxan. Following assessment with a one-way ANOVA and a Tukey's All Pairs Comparison, at 10 μM alloxan (N=4, $p=0.03$), 20 μM (N=5, $p=0.0002$), and 50 μM (N=6, $p<0.0001$), each treatment was deemed to be significant in comparison to the untreated cells (N=5). There was no significant difference observed between treatments.

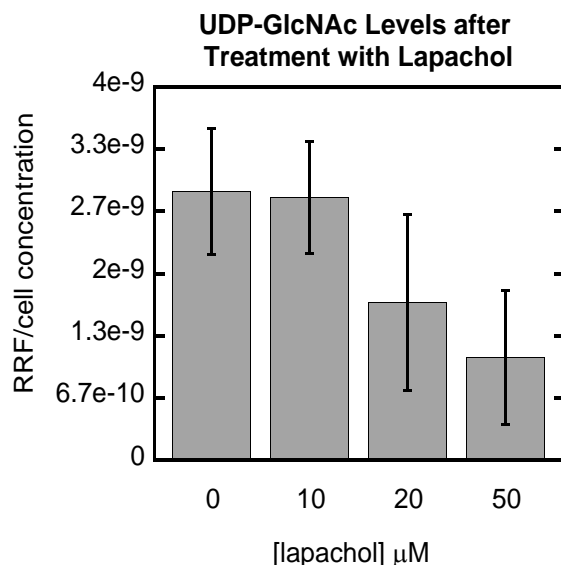


Figure 4-9. UDP-GlcNAc levels in HepG2 cells following 24-hr treatment with lapachol. Following assessment with a one-way ANOVA and a Tukey's All Pairs Comparison, only treatment at 50 μM lapachol (N=5, $p=0.0082$) displayed a significant difference in UDP-GlcNAc levels as compared to the untreated cells (N=5). Treatment at 10 μM (N=5), and 20 μM (N=5) were not significant compared to the untreated cells using a 95% confidence interval.

Structure-Activity Relationship Analysis of GFAT Inhibitors

From the screen we had identified 3 new structural classes of inhibitors for GFAT and had verified 1 class previously described. We decided to characterize 6,7-dimethoxyisoquinoline, aminothiazole, pyridinone and quinone derivatives further. A structure-activity relationship (SAR) analysis was performed *in vitro* with both commercially available and synthetic compounds using the Morgan-Elson assay. Inactive compounds from the initial screen which were closely related were also included in the SAR data. Since a complete crystal structure of hGFAT1 was not available, inhibitors could not be designed to coordinate with particular amino acids. Thus, the SAR analysis was limited to a trial and error approach. As the first round of analysis is described here, emphasis was on including variety onto the core structures versus highly controlled variability between compounds.

i) *6,7-dimethoxyisoquinolines*

As touched on in Chapter 1, isoquinolines were first identified as GFAT inhibitors in 2000, with the discovery of aaptamine by Monsanto scientists.¹¹ Aaptamine (see Table 1-3) was isolated from the dichloromethane extract of the marine sponge *Aaptos* species harvested offshore from Manado, Indonesia. Aaptamine was the first non-substrate like derivative discovered to inhibit GFAT, with an IC_{50} of 120 μ M (the IC_{50} was performed with an ion-exchange assay and a radiometric readout of GFAT activity. The enzyme source and assay mechanism were not mentioned). Later in 2005, Hoffmann-La Roche scientists patented 1-arylcarbonyl-6,7-dimethoxyisoquinolines and their derivatives as GFAT inhibitors.¹² More recently in 2011, the same scientists published their findings after creating a library of these compounds.¹³ They mention one molecule in particular, “Compound 28” (see Table 1-3) which displayed an IC_{50} of 1 μ M for GFAT expressed in COS cells. They also successfully used Compound 28 in an *in vivo* assay with an ob/ob (obese) mouse model. The oral glucose tolerance test (OGTT), is a test where an animal is given a dose of 1 g glucose/kg bodyweight after a period of fasting and blood sugar levels are measured to determine clearance. This test was administered along with treatment of Compound 28 and it was found that glucose excursion levels were lowered as compared to controls. These studies not only validate isoquinolines as GFAT inhibitors, but emphasize the potential of GFAT as a therapeutic target.

Since we had a successful synthetic scheme in hand for creating isoquinolines, we decided to proceed with a generation of our own library. We also chose to explore removing the carbonyl from position 1 to assess the affect of aryl-substituents.

Nineteen 6,7-dimethoxyisoquinoline derivatives were synthesized. Syntheses were performed as described in Chapter 3 by Dr. Emelia Awuah¹⁴ (Figure 3-6) and by Dr. Nick Todorovic¹⁵ (Figure 4-10). From the SAR data available, only those compounds with an aryl-carbonyl substituent at position 1 displayed inhibitory activity against GFAT. Tetrahydroisoquinolines (EME 109) also lacked any inhibitory activity (Figure 4-11). EME 384 (IC₅₀: 1.6±0.2 μM) was the most potent and EME 443 followed a close second (IC₅₀: 1.7±0.2 μM).

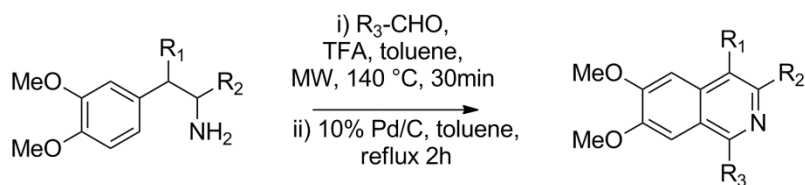
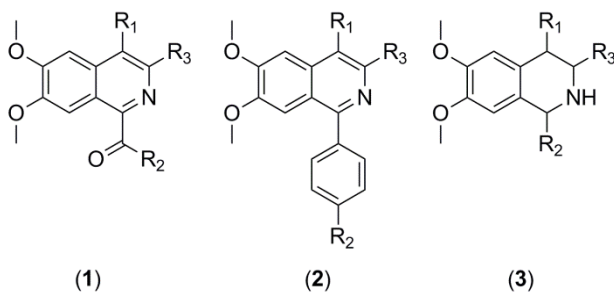


Figure 4-10. Microwave assisted Pictet-Spengler/oxidation reaction for the synthesis of substituted isoquinolines. Adapted from Todorovic *et al.* Substituted β-arylethylamines and *para*-substituted benzaldehydes (R₃-CHO) provided variety for the 6,7-dimethoxyisoquinoline SAR analysis.



Name	Core #	R ₁	R ₂	R ₃	MW g/mol	IC ₅₀ μM
EME 384	1	H		H	343.4	1.6±0.2
EME 443	1	COOH		H	417.41	1.7±0.2

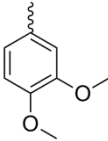
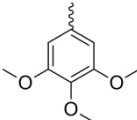
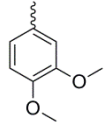
EME 458	1	CN		H	378.38	2.3±0.3
EME 467R2	1	H		H	383.39	12.7±2.4
EME 109	3	H		H	329.36	N/A
NT-5-77	2	CH ₃	Cl	Ph	389.87	N/A
NT-5-80	2	CH ₃	H	Ph	355.43	N/A
NT-5-81	2	CH ₃	CH ₃	Ph	369.46	N/A
NT-5-82	2	CH ₃	CH ₃ O	Ph	399.48	N/A
NT-5-83	2	CH ₃	CN	Ph	380.44	N/A
NT-5-85	2	CH ₃	F	Ph	373.42	N/A
NT-5-86	2	CH ₃	Cl	<i>p</i> -Ph-Cl	424.32	N/A
NT-5-87	2	CH ₃	Ph	<i>p</i> -Ph-Cl	389.87	N/A
NT-5-88	2	CH ₃	CH ₃	<i>p</i> -Ph-Cl	403.90	N/A
NT-5-89	2	CH ₃	CH ₃ O	<i>p</i> -Ph-Cl	419.90	N/A
NT-5-90	2	CH ₃	CN	<i>p</i> -Ph-Cl	414.88	N/A
NT-5-91	2	CH ₃	F	<i>p</i> -Ph-Cl	407.86	N/A
NT-5-93	2	CH ₃	Cl	CH ₂ CH ₃	341.83	N/A
NT-6-3	2	Ph	H	Ph	417.50	N/A

Figure 4-11. SAR data of synthetic 6,7-dimethoxyisoquinoline derivatives. These synthetic isoquinolines were all tested for GFAT inhibitory activity with the Morgan-Elson assay. EME compounds 384, 443, 458, 467R2 displayed inhibitory activity. All IC₅₀ values reported were performed with the Morgan-Elson assay with substrates at 10xK_M unless otherwise specified. N/A indicates an inactive compound. # refers to the corresponding core structure.

ii) *Aminothiazoles*

After the hit N1(8Hindeno[1,2d][1,3]thiazol2yl) decanamide, (Maybridge collection, ID #: RH01165) was identified during the pilot screen (see Fig. 3-12), six aminothiazole derivatives were synthesized by the one-step Hantzsch reaction.¹⁶ Aminothiazole syntheses were performed by Dr. Nick Todorovic (NT) and Tishaan Singh (TS).¹⁷ This reaction utilized substituted indanones and thiourea as the precursors (Figure 4-12).

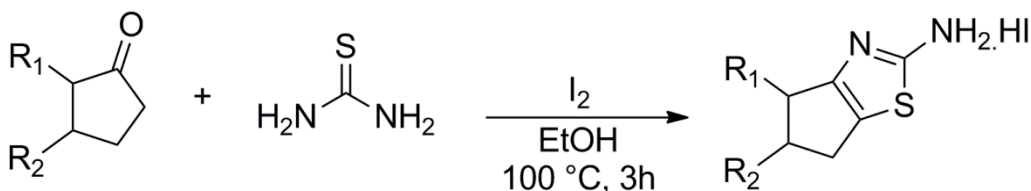
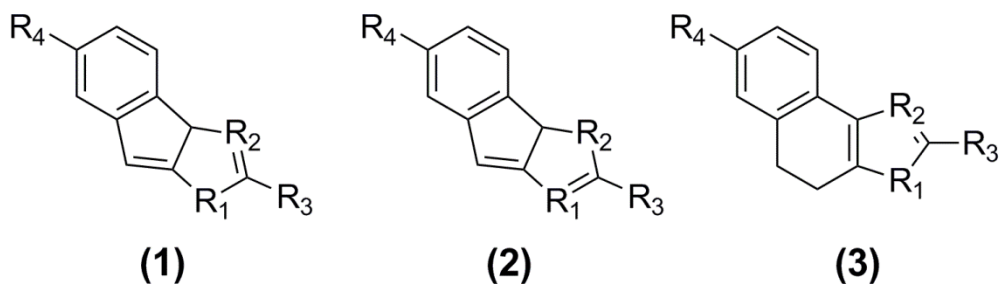


Figure 4-12. Hantzsch reaction for aminothiazole synthesis. Adapted from Tishaan Singh's Senior Thesis. The one-step Hantzsch reaction was performed with substituted indanones and thiourea in the presence of iodine to yield an aminothiazole. Commercially available indanones such as 1-indanone, 2-indanone, α -tetralone, and 5-methyl-1-indanone were used. Yields ranged from 52-78%.

While the hit compound was not purchased for validation, the Hantzsch reaction provided a facile method to create a small library of aminothiazoles. Our initial hypothesis was that the aliphatic chain of RH01165 was not necessary for inhibition. Following the SAR analysis, it appeared that the aliphatic chain from the original lead did play a role in enzyme inhibition, further study focused on this area of the molecule will be necessary (Figure 4-13). TS-1-24 was the only derivative to display any inhibition against GFAT (Figure 4-14). As noted by Singh, one drawback of the Hantzsch reaction was the lack of commercially available indanones. This reflects the small sample of aminothiazole compounds available.



Name	Core #	R ₁	R ₂	R ₃	R ₄	MW g/mol	IC ₅₀ μM
RH01165	1	S	N	NHCO(CH ₂) ₈ CH ₃	H	342.50	38.1±6
NT-5-49	1	S	N	NHCOCH ₃	H	230.29	N/A
NT-5-47	1	S	N	NH ₂	H	188.25	N/A
TS-1-21	1	S	N	NH ₂ .HI	CH ₃	330.19	N/A
TS-1-24	1	S	N	NH ₂ .HI	CH ₃ O	346.19	@K _M : 42±7 @10xK _M : 279±532
TS-1-15	2	N	S	NH ₂ .HI	H	316.16	N/A
TS-1-18	3	S	N	NH ₂ .HI	H	330.19	N/A

Figure 4-13. SAR data of aminothiazole derivatives. NT and TS compounds were synthesized after lead compound RH01165 (Maybridge Collection) was identified as an inhibitor. Only compound TS-1-24 displayed any inhibitory activity against GFAT. All IC₅₀ values reported were performed with the Morgan-Elson assay with substrates at 10xK_M unless otherwise specified. N/A indicates an inactive compound. # refers to the corresponding core structure.

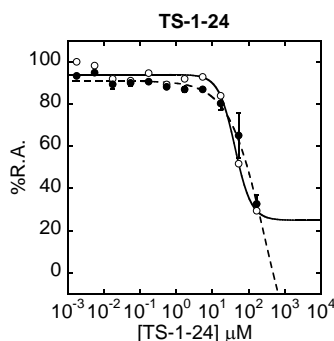


Figure 4-14. Dose-response for aminothiazole TS-1-24. TS-1-24 was the only synthesized aminothiazole which displayed any inhibitory activity against GFAT. A dose-response was performed with the modified Morgan-Elson assay on the HTS platform. The assay was run with both substrates at or near K_M (1 mM, white circles) and $10xK_M$ (10 mM, black circles). Fitted with the 4-point parameter Hill equation (KaleidaGraph v.4.1).

iii) *Pyridinones*

While amrinone only displayed modest GFAT inhibition (IC_{50} : $91 \pm 34.1 \mu M$), we wanted to pursue an SAR analysis due to its current use as a drug, low apparent-toxicity, cell permeability and amenability to create a focused synthetic library.

Seventeen pyridinone derivatives were synthesized by Bilal Bagha (BB-labeled compounds).¹⁸ These compounds were synthesized by a Suzuki cross-coupling reaction with a variety of phenyl boronic acids to introduce diversity in the pyridine ring (Figure 4-15). Six of these synthesized derivatives were identified as more potent or equal to amrinone (BB-4, 8, 10, 11, 14, 28). The nitrogen in the pyridine ring was not necessary for inhibition and substitution at the *para* position with a weakly electron-donating group worked best. Substitutions in the *ortho* position decrease the potency of the inhibitor. The best inhibitor, BB-10, has a methoxy substituent in the *para*-position (IC_{50} : $38.1 \pm 5.7 \mu M$). Since few compounds have been tested with modifications on the amide-

ring it was difficult to make any conclusions about what role this portion of the molecule played in GFAT inhibition (Figure 4-16).

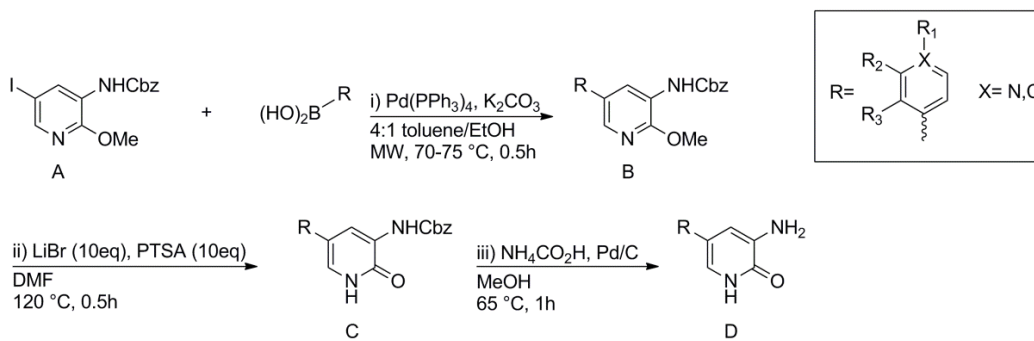
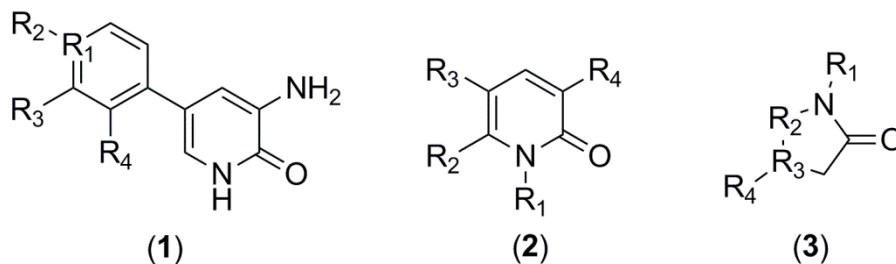


Figure 4-15. Schematic of pyridinone focused library synthesis with microwave-assisted Suzuki cross-coupling reactions. Adapted from Bilal Bagha's Senior Thesis. Starting material (A) (5-iodo-2-methoxy-3-(NHCbz)pyridin-2-one) was synthesized in 5 steps from commercially available 3-nitropyridin-2-one with an overall yield of 16-48% (not shown). (A) was combined with various phenyl boronic acids with a tetrakis(triphenylphosphine)palladium-catalyzed Suzuki reaction.¹⁹ The large variety of phenyl boronic acids commercially available provided plenty of diversity with the Suzuki reaction. Two deprotecting steps ii)²⁰ and iii) provided the final compounds (D). Overall yields varied from 33-70%.



Name	Core #	R ₁	R ₂	R ₃	R ₄	MW g/mol	IC ₅₀ μM
Amrinone	1	N	-	H	H	187.2	91±34.1
BB-4	1	C	O-CH ₂ -R ₃	O-CH ₂ -R ₂	H	230.22	52.9±7.9
BB-8	1	C	CH ₃	H	H	200.24	79.5±29.9
BB-9	1	C	H	H	OCH ₃	216.24	N/A
BB-10	1	C	OCH ₃	H	H	216.24	38.1±5.7

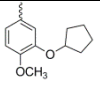
BB-11	1	C	OCH ₃	H	OCH ₃	246.27	40.3±11.2
BB-12	1	C	OCF ₃	H	H	270.21	N/A
BB-13	1	C	CF ₃	H	H	254.21	N/A
BB-14	1	C	H	H	H	186.21	67.8±21.9
BB-19	1	C	H	F	H	204.20	N/A
BB-21	1	C	Br	H	H	265.11	N/A
BB-23	1	C	H	H	NH ₂	201.23	N/A
BB-27	1	C	H	COCH ₃	H	228.25	N/A
BB-28	1	C	NHCOCH ₃	H	H	243.27	69±36.1
BB-28a	1	C	NH ₂	H	H	201.23	N/A
BB-29	1	C	CN	H	H	211.22	N/A
BB-30	1	C	H	H	CH ₂ OH	216.24	N/A
Milrinone	2	H	CH ₃	Ph	CN	210.23	N/A
Pirfenidone	2	Ph	H	CH ₃	H	185.22	N/A
*Edaravone	3	Ph	N	C	CH ₃	174.20	22.6±1.9
**Rolipram	3	H	CH ₂	CH		275.34	N/A

Figure 4-16. SAR data of pyridinone derivatives. All compounds labeled BB were created synthetically, the rest are commercially available and were tested during the primary screen. *Edaravone is a pyrazolone, ** Rolipram is a pyrrolidinone, both bare similarity to pyridinones and were included in the SAR. All IC₅₀ values reported were performed with the Morgan-Elson assay with substrates at 10xK_M unless otherwise specified. N/A indicates an inactive compound. # refers to the corresponding core structure.

iv) *Quinones*

Quinones are a common structure amongst natural products and can be thought of as soft electrophiles or Michael acceptors.²¹ Naphthoquinones and *para*-

quinones were identified as a common structure of the lead compounds beta-lapachone, lapachol, menadione, alloxan and 2,6-dimethoxyquinone. From the primary screen alone, 15 quinones were tested for GFAT inhibition, which provided enough information to draw some conclusions (Figure 4-17). Compounds which displayed 73% or less enzyme activity were considered to be “active”. Those which displayed greater enzyme activity were considered to be “inactive”. Substitution at positions 2 and 3 of the 1,4-naphthoquinones had a dramatic effect of GFAT inhibition. For instance, lawsone had a hydroxyl substituent at position 3 and was inactive, whereas menadione had a methyl group and was a moderate inhibitor (IC_{50} : $11.8 \pm 0.7 \mu\text{M}$). Lapachol also had a hydroxyl substituent at position 3, a butenyl group at position 2, and it was a moderate inhibitor as well (IC_{50} : $17.6 \pm 2.2 \mu\text{M}$). With the exception of shikonin (1° dose-response IC_{50} : $28 \pm 8.6 \mu\text{M}$), any substitution of the benzene ring resulted in no inhibition. For SAR analysis of quinones, compounds with varied substituents in the 2 or 3 positioned were desired.

The *para*-quinones alloxan and 2,6-dimethoxybenzoquinone both displayed moderate enzyme inhibition. Fewer of these compounds had been assayed for GFAT which made any conclusion difficult. Perhaps the unsaturated benzene ring of the 1,4-naphthoquinones was not necessary for inhibition, only the modifications at positions 2 and 3 made the most difference. Further study comparing naphthoquinones and the *para*-quinones will be necessary.

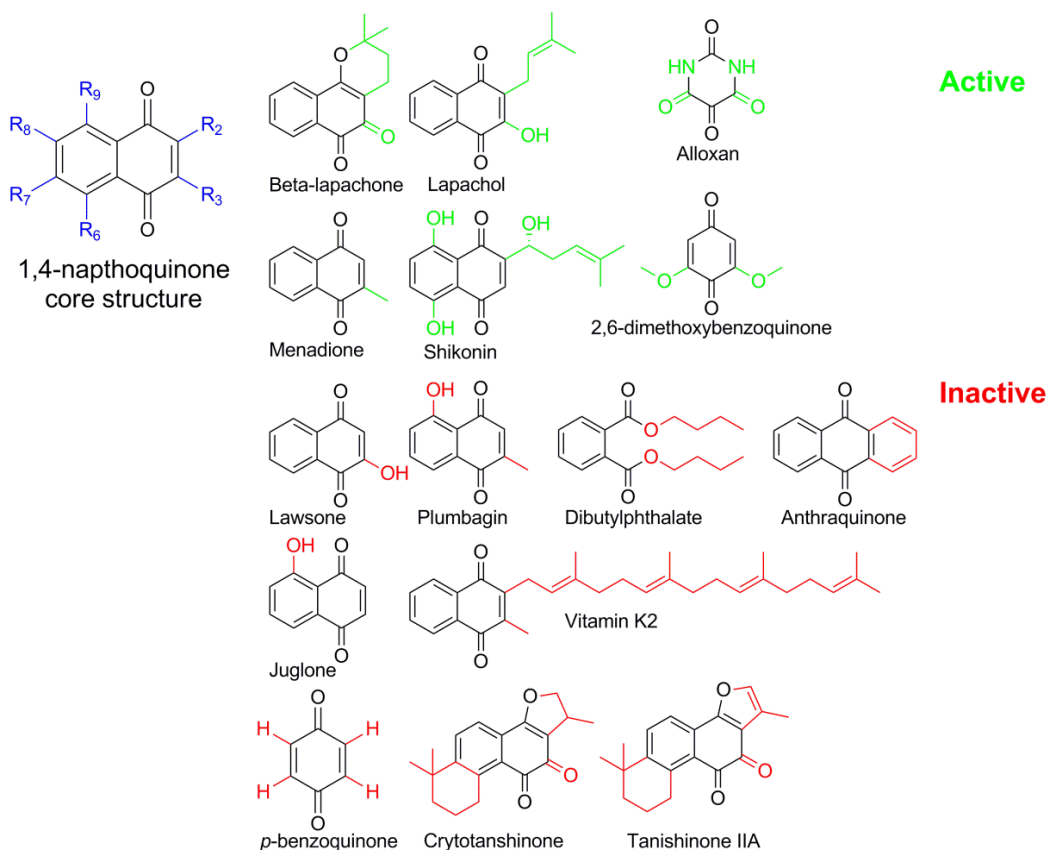


Figure 4-17. Active and inactive quinones identified from the primary screen. A number of compounds containing the core structure of a 1,4-naphthoquinone were assayed in the primary screen, those which displayed 73% or less enzyme activity were considered to be “active”. Compounds with substituents highlighted in green were validated as hits (with the exception of shikonin which was not validated). Those highlighted in red were not identified as hits and are inactive towards GFAT. One common trend observed was that any substitution on the naphtho-ring resulted in an inactive compound (with the exception of shikonin). Also substitution at the R₂ or R₃ position varied wildly.

A handful of 1,4-naphthoquinones were synthesized *via* Suzuki-type coupling²² or by a ligand-free Heck reaction²³ using lawsone as the starting material (Figure 4-18). Aryl and alkyl substitutions at position 3 coupled with a hydroxyl group at position 2 had not been explored with the compounds from the primary screen. Thomas Floyd²⁴ (TF) and Sam Dalton²⁵ (SD) were responsible for the syntheses. Aryl and alkyl substitutions were tolerated as shown in the TF and SD labeled compounds. Of these, TF-4 with a primary amide displayed good inhibitory activity against GFAT (IC₅₀: 3.1±0.2 μM). While

the aryl substituted compounds displayed moderate inhibition (IC_{50} 's from 44-315 μ M), they indicated some substitution on the aryl-ring was necessary for inhibition.

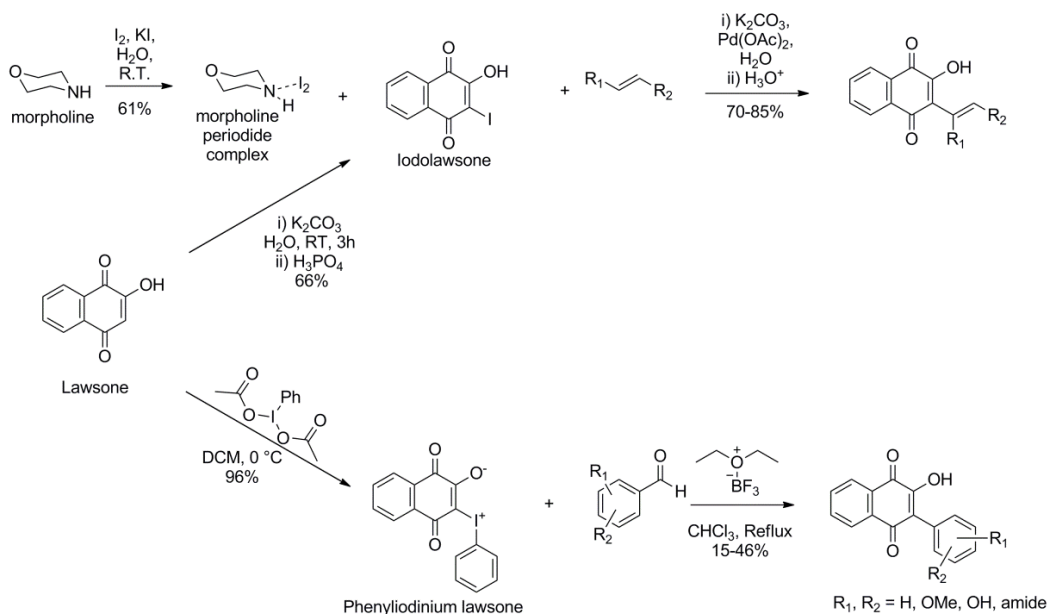
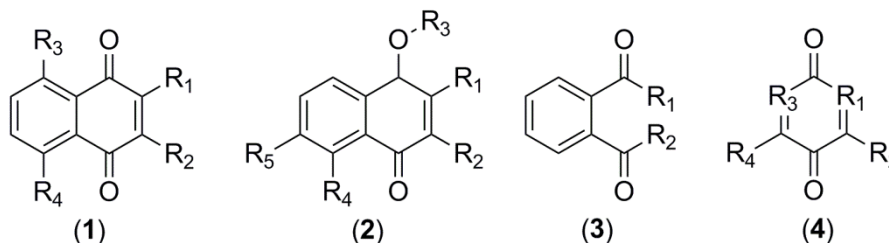


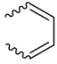
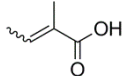
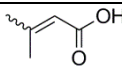
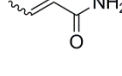
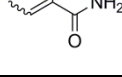
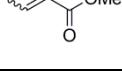
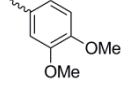
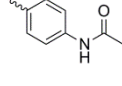
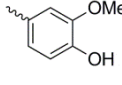
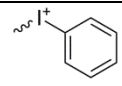

Figure 4-18. Schematic of substituted 1,4-naphthoquinones with lawsone precursor. Adapted from Thomas Floyd's and Sam Dalton's Senior Theses. An iodinated lawsone intermediate was desired to create chemical diversity by utilizing the Heck reaction (Top) or Suzuki-type boron trifluoride diethyl etherate mediated coupling (Bottom).²⁶ Iodolawsone, was synthesized by iodination of lawsone with a morpholine periodide complex in good yield.²⁷ The ligand-free Heck reaction with palladium diacetate catalyst and trans-substituted alkenes produced a variety of 1,4-naphthoquinones with 70-85% yield.²³ To expand the 1,4-naphthoquinones to include aryl derivatives, (diacetoxyiodo)benzene was used to give intermediate phenylidinium lawsone.²⁸ This was $BF_3 \cdot Et_2O$ - coupled with mono- or di- substituted benzaldehydes with a modest 15-46% yield of aryl-substituted 1,4-naphthoquinones.

We also sought out a variety of commercially available 2- or 3- substituted 1,4-naphthoquinones, namely 2-methoxy-3-methyl-1,4-naphthoquinone, 2-methoxy-1,4-naphthoquinone, 2-acetoxy-3-isobutyl-1,4-naphthoquinone, 2,3-dimethoxy-1,4-naphthoquinone, 4-butoxy-1,2-naphthoquinone and dehydroiso- β -lapachone. Out of all of the quinones tested during the SAR analysis, dehydroiso- β -lapachone was the most potent inhibitor (IC_{50} : $1.5 \pm 0.5 \mu$ M), 10 fold more than related inhibitor β -lapachone (IC_{50} :

10.4±0.5 μM) (Figure 4-20). For this reason, we were interested in characterizing this compound further. The SAR data for quinones was tabulated in Figure 4-19.



Name	Core #	R ₁	R ₂	R ₃	R ₄	R ₅	MW g/mol	IC ₅₀ μM
Menadione	1	H	CH ₃	H	H	-	172.18	11.8 ±0.7
Vitamin K ₂	1		CH ₃	H	H	-	444.65	N/A
Lawsone	1	H	OH	H	H	-	174.15	N/A
Lapachol	1		OH	H	H	-	242.27	17.6 ±2.2
Shikonin	1		H	OH	OH	-	288.30	28± 8.6
2-methoxy-1,4-naphthoquinone	1	OCH ₃	H	H	H	-	188.18	*50
2,3-dimethoxy-1,4-naphthoquinone	1	OCH ₃	OCH ₃	H	H	-	218.21	N/A
2-acetoxy-3-isobutyl-1,4-naphthoquinone	1	OCOCH ₃		H	H	-	272.30	*50- 500
2-methoxy-3-methyl-1,4-naphthoquinone	1	OCH ₃	CH ₃	H	H	-	202.21	N/A
Juglone	1	H	H	OH	H	-	174.15	N/A
Plumbagin	1	H	CH ₃	OH	H	-	188.18	N/A

Antraquinone	1		See R ₂	H	H	-	208.21	N/A
TF-1	1	OH		H	H	-	258.23	N/A
TF-2	1	OH		H	H	-	258.23	N/A
TF-3	1	OH		H	H	-	243.21	17.2 ±2.5
TF-4	1	OH		H	H	-	257.24	3.1± 0.2
TF-5	1	OH		H	H	-	272.25	34.2 ±2.3
TF-6	1	OH	I	H	H	-	300.05	N/A
SD-1	1	OH	<i>p</i> -Ph-OMe	H	H	-	280.27	N/A
SD-2	1	OH		H	H	-	310.30	44.7 ±2.7
SD-3	1	OH		H	H	-	307.30	N/A
SD-4	1	OH		H	H	-	296.27	315 ±26 9
SD-5	1	O ⁻		H	H	-	376.15	92± 30.2
SD-6	1	OH	Ph	H	H	-	250.25	N/A
β-lapachone	2	See R ₃	O		H	H	242.27	10.4 ±0.5

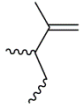

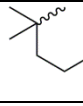
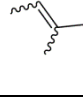
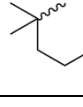
Dehydroiso- β -lapachone	2	See R ₃	O		H	H	240.25	1.5±0.5
4-butoxy-1,2-naphthoquinone	2	H	O	C ₄ H ₉	H	H	230.26	N/A
Cryptotanshinone	2	See R ₃	O			See R ₄	296.36	N/A
Tanshinone IIA	2	See R ₃	O			See R ₄	294.34	N/A
Dibutylphthalate	3	O-(CH ₂) ₃ CH ₃	O-(CH ₂) ₃ CH ₃	-	-	-	278.34	N/A
<i>p</i> -benzoquinone	4	CH ₂	H	CH ₂	H	-	108.09	N/A
2,6-dimethoxyquinone	4	CH ₂	OCH ₃	CH ₂	OCH ₃	-	168.15	15.9±1.8
Alloxan	4	NH	O	NH	O	-	142.07	13.9±0.8

Figure 4-19. SAR data of quinone derivatives. Compounds labeled TF or SD were created synthetically, all others were commercially available. An asterisk (*) indicates compounds which displayed inhibitory activity at one or more concentrations tested, but a full dose-response was not performed. All IC₅₀ values reported were performed with the Morgan-Elson assay with substrates at 10xK_M unless otherwise specified. N/A indicates an inactive compound. # refers to the corresponding core structure.

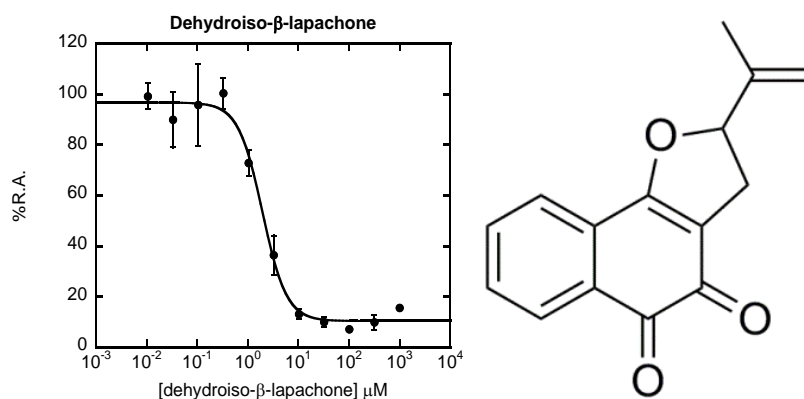


Figure 4-20. Dose-Response curve and structure of dehydroiso- β -lapachone, identified as a potent GFAT inhibitor. When performed with the Morgan-Elson assay with substrates at 10 mM, dehydroiso- β -lapachone had an IC₅₀ of 1.5±0.5 μ M against rhGFAT1-His₆²⁹⁸. Dehydroiso- β -lapachone is similar in structure to lead compound β -lapachone.

The findings from co-workers at the Pittsburgh Molecular Library Screening Center at the University of Pittsburgh Drug Discovery Institute (Pittsburgh, PA) involving

quinones in screening campaigns are important to highlight here. Johnston *et al* mentioned the promiscuous activity of compounds containing a quinone scaffold in assays which contained strong reducing agents such as DTT or TCEP.²⁹ They suggested these molecules were able to non-specifically inhibit proteins sensitive to oxidation due to production of hydrogen peroxide in the presence of DTT. They screened the Library of Pharmacologically Active Compounds (LOPAC) and the National Institutes of Health Small Molecule Repository (NIH-SMR) libraries to identify redox cycling compounds in the presence of reducing agents.³⁰ The authors mentioned quinones, beta-lapachone and NSC 95397, and some 1,2-naphthoquinones were able to produce H₂O₂ when in the presence of TCEP or DTT, but not in the presence of weaker reducing agents glutathione, β-mercaptoethanol, or L-cysteine.

However, Lal *et al* emphasized that DTT was only able to produce H₂O₂ under acidic conditions. Under basic or near-neutral conditions, like in our Morgan-Elson assay, DTT mainly exists in equilibrium with a deprotonated thiolate.³¹ As shown by Han & Han, DTT had a decrease in its reducing potential under acidic conditions, and would not be as effective at maintaining proteins sensitive to oxidation.³² Kumagai *et al* reviewed naphthoquinones extensively and identified that their biological mechanism of action was often due to the production of reactive oxygen species (ROS) under the reducing conditions present in the cytoplasm.³³ While the studies by Johnston *et al* drew attention to the issues of inhibitor promiscuity due to individual compound reactivity with assay conditions, under our parameters this specific issue was not deemed to

interfere with our assay. Further testing with weaker reducing agents would provide more information about this issue.

Mode of inhibition of dehydroiso- β -lapachone at the isomerase and glutaminase binding domains

Dehydroiso- β -lapachone (a.k.a. 2,3-dihydro-2-(1-methylethenyl)naphtho(1,2-B)furan-4,5-dione, CAS # 74693-31-5) is a natural product isolated from the roots of the rainforest plant *Lantana involucrata*.³⁴ The same authors had reported the cytotoxic effects of this compound against a number of tumor cell lines with IC₅₀ values ranging from 1-10 μ M. The mechanism of action was not reported. The natural product extract was a racemic mixture and only recently had a synthesis been reported to obtain an enantiomerically pure form of (-)-dehydroiso- β -lapachone.³⁵ Our source of dehydroiso- β -lapachone was obtained commercially and it was unknown how the activity would differ from an enantiomerically pure form of the compound. The cytotoxic effects were not previously reported for HepG2 cells and we found this compound to be mildly toxic against this cell line. When cell viability was measured with the Countess[®] cell counter and trypan blue, cell death began to occur at 50 μ M, with 20% viability remaining at 100 μ M (Figure 4-21). In relation to its sister compounds, dehydroiso- β -lapachone was less toxic than β -lapachone but more toxic than lapachol in HepG2 cells.

As one of the most potent inhibitors we had identified as a result of our screening efforts, we decided to elucidate the mode of inhibition (MOI) of dehydroiso- β -lapachone. GFAT has two catalytic sites, the isomerase binding domain and the glutaminase binding domain. To determine the MOI at each site, a dose-response was performed varying one substrate concentration while leaving the other in excess. The

MOI at both the isomerase (Figure 4-22) and glutaminase (Figure 4-23) binding domains were determined to be noncompetitive because the change observed in IC_{50} did not linearly correlate with a change in substrate.³⁶

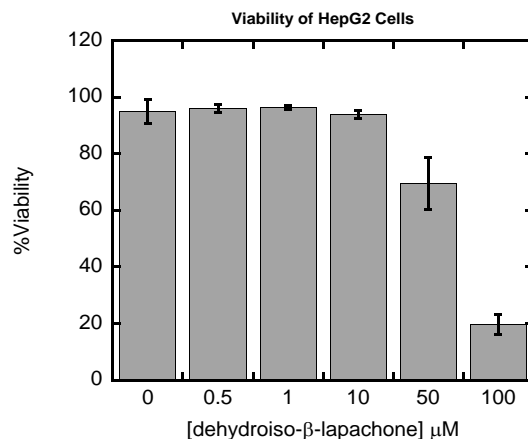


Figure 4-21. Viability of HepG2 cells treated with dehydroiso-β-lapachone. Cell death began to occur in HepG2 cells treated with dehydroiso-β-lapachone around 50 μM . Cells were grown in 24-well plates and treated (or untreated) in duplicate ($N=2$). Cell viability was measured with the Countess® cell counter after cells were harvested and treated with trypan blue. Between the 50 μM treatment and the untreated cells, the difference was determined to be significant ($p=0.0093$). The difference between the 50 and 100 μM treatments was determined to be significant as well ($p=0.0002$).

A noncompetitive inhibitor is one which can bind to a target with or without the presence of its substrate (Figure 4-24). A change in substrate concentration would have little to no effect on the ability of the inhibitor to bind, depending on the relative affinity of the inhibitor for the free enzyme versus the enzyme-substrate complex. It may bind to an allosteric site on the enzyme which could change the conformation of the active site as well. In the case of a bisubstrate enzyme such as GFAT, the noncompetitive inhibitor may bind to one active site which could affect the conformation and catalytic ability of the other active site. From the data available we are unable to identify where on the enzyme this inhibitor binds. One possibility is covalent binding of dehydroiso-β-lapachone to the thiol functional group on Cys1. Li *et al* have previously shown the

covalent addition of menadione to cytochrome C at an internal cysteine residue.³⁷

Further study will also be necessary to determine whether or not the inhibitor is reversible or irreversible. Strategies to determine reversibility are discussed further in Chapter 5.

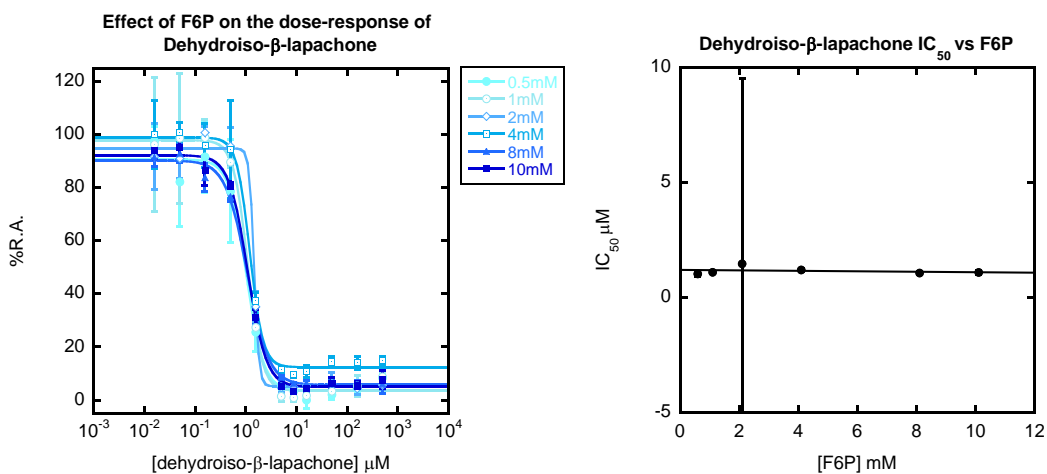


Figure 4-22. Effect of F6P on the dose-response and IC₅₀ of dehydroiso-β-lapachone. Dose-response was performed in triplicate with the Morgan-Elson assay with L-gln in excess at 20 mM and varying concentrations of F6P, 0.5, 1, 2, 4, 8, and 10 mM. The IC₅₀ concentration was plotted against the varied substrate concentration, no linear correlation was observed.

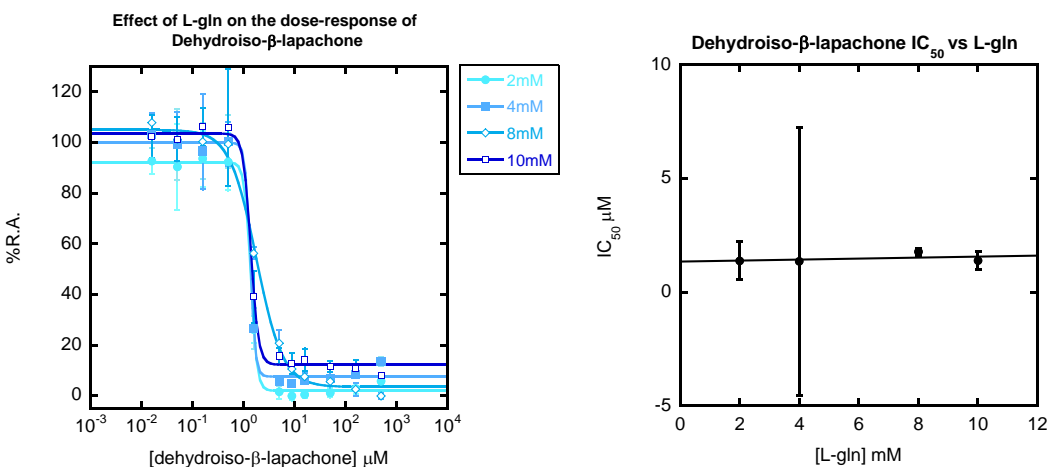


Figure 4-23. Effect of L-gln on the dose-response and IC₅₀ of dehydroiso-β-lapachone. Dose-response was performed in triplicate with the Morgan-Elson assay with F6P in excess at 20 mM and varying concentrations of L-gln, 2, 4, 8, and 10 mM. The IC₅₀ concentration was plotted against the varied substrate concentration, no linear correlation was observed.

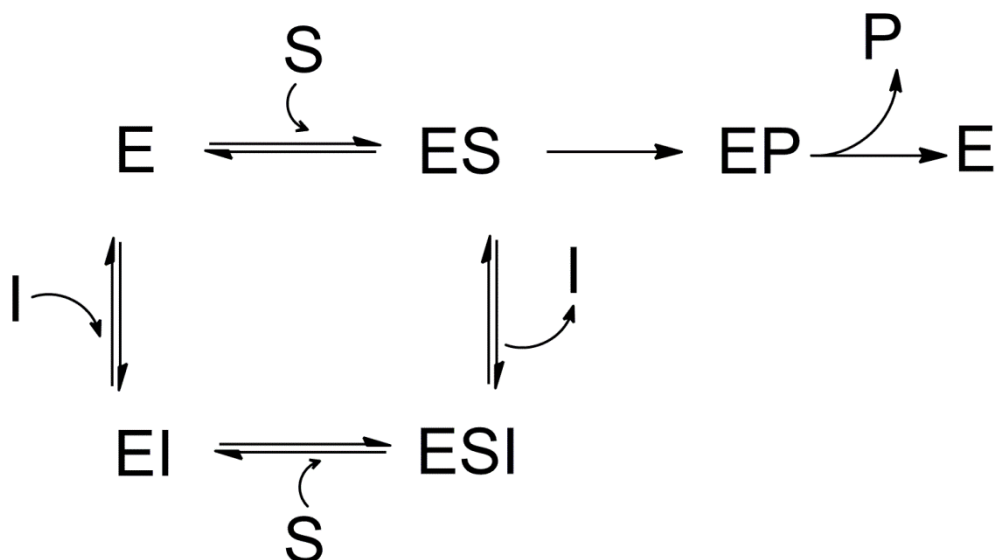


Figure 4-24. A representation of a reversible noncompetitive inhibitor. Where: (E) free unbound enzyme, (S) substrate, (I) inhibitor, (P) product. A noncompetitive inhibitor can bind to either the free unbound enzyme (E) or the enzyme-substrate complex (ES) to form an enzyme-substrate-inhibitor complex (ESI). The affinity of the inhibitor for the free enzyme can be equal to the affinity for ES, or the inhibitor may favour binding to one over the other. Non-competitive inhibitors will all decrease the V_{max} of an enzyme with an increase in inhibitor, and can increase, decrease or have no effect on K_M depending on the affinity for E vs ES.

Conclusion

Follow-up studies have identified inhibitors amrinone, alloxan and lapachol as cell permeable and able to modulate the HBP in cell culture. We have developed an UPLC-TOF-MS assay for the detection of UDP-GlcNAc in cell culture. From our SAR analysis we found 6,7-dimethoxyisoquinoline inhibitors needed an aryl-carbonyl substituent to function as a GFAT inhibitor. Amrinone derivatives did not require a pyridine ring to maintain inhibitory activity, and inhibition could be increased when modifications in the para position of the pyridine ring take place. 1,4-naphthoquinone derivatives had inhibitory activity increased or removed based on substitutions at positions 2 and 3. Dehydroiso- β -lapachone was identified as a novel and potent, noncompetitive 1,4-naphthoquinone inhibitor of GFAT. Future work will be required to assess the cell permeability and efficacy of this inhibitor in cell culture.

Materials & Methods

Measurement of inhibitor cell toxicity in HepG2 cells

Human hepatocarcinoma cells (HepG2) (American Type Culture collection, Manassas, Virginia) were cultured into sterile 24-well tissue culture plates (Becton Dickinson Labware) in Dulbecco's modified Eagle's medium (Life Technologies, Burlington, Ontario) containing 10% fetal bovine serum, 1% penicillin, streptomycin and 24.5 mM glucose. The cells were maintained at 37 °C with 5% CO₂. Cells were treated in duplicate with growth media and either 5 µL DMSO, 10 µL DMSO, 4 µg/mL tunicamycin, 8 µg/mL tunicamycin, or a range of inhibitor concentrations (0.01 nM, 0.1 nM, 1 nM, 10 nM, 100 nM, 1 µM, 10 µM, 100 µM, 500 µM) prepared in DMSO and growth media. After a 48 hr incubation period, growth media was removed and cells were stained with trypan blue. Cells were counted visually under microscope.

UPLC-TOF-MS assay for detection of UDP-GlcNAc, Sample Preparation and Analysis

The sugar standard stock solutions were prepared in HPLC grade methanol (Caledon Laboratories) containing 20 µM of the internal standard glycine-phenylalanine (Cat. G2752, Sigma-Aldrich).

HepG2 cells were cultured in Dulbecco's modified Eagle's medium containing 10% fetal bovine serum, 1% penicillin, streptomycin and either 5 or 24.5 mM (low or high) glucose. The cells were maintained at 37 °C with 5% CO₂. Cells grown in sterile, 24-well tissue-culture plates were treated with glucose (EM Science), glucosamine, amrinone, alloxan or lapachol (Sigma-Aldrich). Glucose and glucosamine were prepared

directly in the growth media while the inhibitors were dissolved in DMSO prior to dilution in the growth media.

For UDP-GlcNAc measurement in cells treated with glucosamine, cells were cultured in low glucose growth media for 48 hours followed by the addition of glucosamine (0.2, 1 or 5 mM) or high glucose (24.5 mM) for 24 hours before harvesting.

For UDP-GlcNAc measurement in cells treated with amrinone, alloxan or lapachol, cells were cultured in high glucose growth media and allowed to incubate with an inhibitor for 2 hrs before harvesting (10, 20 or 50 μ M). Inhibitors were added to five wells at each concentration and an additional five wells were left untreated.

To prepare cells for analysis, the growth media was removed and the cells were washed with 1xPBS buffer, pH 7.4 (Life Technologies, Burlington, ON). Trypsin was added and the plate was allowed to incubate at 37 °C for 3 min. The cells were transferred to a 2 mL microcentrifuge tube and were centrifuged for 3 min at 13000 rpm, 4 °C (Eppendorf Microcentrifuge, 5418). The supernatant was removed and the pellets were resuspended in 100 μ L of 1xPBS. The cell quantity and viability was assessed by taking a 15 μ L sample of the resuspended cells and mixing thoroughly with 15 μ L of 0.4% trypan blue stain (Life Technologies, Burlington, ON). From this solution, 10 μ L was injected into one well of a chamber slide for cell counting on the Countess® Automated Cell Counter (Life Technologies, Burlington, ON). Samples were counted in duplicate. The remainder of the cells (85 μ L) was centrifuged for 10 min at 13000 rpm at 4 °C and the buffer was removed. For resuspension of the cell pellet, 100 μ L of 4:1 MeOH/H₂O containing 20 μ M of the internal standard glycine-phenylalanine (gly-phe)

dipeptide was used. A small stainless-steel ball-bearing was added to each sample and the microcentrifuge tubes were vortexed at maximum speed for 5 min. A magnetic plate was used to remove the beads and the tubes were centrifuged for 15 min at 13000 rpm at 4 °C. The supernatant was removed and stored in a 1.5 mL microcentrifuge tube at -20 °C until future use.

For analysis of UDP-GlcNAc in the cell extracts, a 2 μ L sample was injected using the autosampler on an Agilent 1290 HPLC and the sugar was separated by UPLC using the ZIC®-HILIC column (50 mm x 2.1 mm, 3 μ m, 100 Å, Merck® SeQuant) and detected by mass spectrometry in negative ion mode with the Bruker microTOF II. The mobile phase consisted of HPLC grade acetonitrile (eluent A) and 10 mM ammonium acetate in HPLC grade water (eluent B) (Caledon Laboratories Ltd). The flow rate was set to 0.2 mL/min and a binary solvent gradient was employed (95 to 30% eluent A) for 20 min, followed by an equilibration period of 10 min. To control for instrument variability, a pooled sample composed of an equal volume of all samples in the analysis, and the 20 μ M gly-phe internal standard, was run after every five samples. Data analysis was performed with Bruker Daltonics DataAnalysis software. To determine the relative response factor (RRF), the peak area of UDP-GlcNAc (m/z 606.09) was divided by the peak area of gly-phe (m/z 221.1). The values were normalized to the cell concentration of viable cells obtained from the cell counter.

Dose-response of dehydroiso- β -lapachone

The dose response of dehydroiso- β -lapachone was assessed with the Morgan-Elson assay with F6P and L-gln both at 10 mM. Final concentrations of 500, 158, 50, 15.8, 5, 1.58, 0.5, 0.158, 0.05, 0.0158, 0.005 μ M dehydroiso- β -lapachone were used. The assay was performed in triplicate, positive controls included enzyme and 10% DMSO in place of inhibitor, negative controls included buffer in place of enzyme and 10% DMSO in place of inhibitor. Other dose-response assays were performed similarly.

HepG2 cell viability with dehydroiso- β -lapachone measured with the Countess[®] cell counter

HepG2 cells were cultured in Dulbecco's modified Eagle's medium containing 10% fetal bovine serum, 1% penicillin, and streptomycin and 5 mM glucose. The cells were maintained at 37 °C with 5% CO₂. Cells grown in sterile, 24-well tissue-culture plates were treated with dehydroiso- β -lapachone (Cat. S970123, Sigma-Aldrich). The inhibitor was dissolved in DMSO prior to dilution in the growth media. Cells were treated for 24 hrs before harvesting. To prepare cells for counting, the growth media was removed and the cells were washed with 1xPBS buffer, pH 7.4 (Life Technologies, Burlington, ON). Trypsin was added and the plate was allowed to incubate at 37 °C for 3 min. The cells were transferred to a 2 mL microcentrifuge tube and were centrifuged for 3 min at 13000 rpm, 4 °C. The supernatant was removed and the pellets were resuspended in 100 μ L of 1xPBS. To quantify the cells, a 15 μ L sample of the resuspended cells was combined with 15 μ L of 0.4% trypan blue stain (Life Technologies, Burlington, ON) and mixed thoroughly. From this solution, 10 μ L was injected into one

well of a chamber slide for cell counting on the Countess[®] Automated Cell Counter (Life Technologies, Burlington, ON). Samples were counted in duplicate.

Dose-response of dehydroiso- β -lapachone with varied F6P

The dose response of dehydroiso- β -lapachone was assessed with the Morgan-Elson assay with varied concentrations of F6P (0.5, 1, 2, 4, 8, and 10 mM) with a constant concentration of L-gln (20 mM). Final concentrations of 500, 158, 50, 15.8, 8.9, 5, 1.58, 0.5, 0.158, 0.05, 0.0158 μ M dehydroiso- β -lapachone were used. The assay was performed in triplicate, positive controls included enzyme and 10% DMSO, negative controls included buffer in place of enzyme and 10% DMSO.

Dose-response of dehydroiso- β -lapachone with varied L-gln

The dose response of dehydroiso- β -lapachone was assessed with the Morgan-Elson assay with varied concentrations of L-gln (2, 4, 8, and 10 mM) with a constant concentration of F6P (20 mM). Final concentrations of 500, 158, 50, 15.8, 8.9, 5, 1.58, 0.5, 0.158, 0.05, 0.0158 μ M dehydroiso- β -lapachone were used. The assay was performed in triplicate, positive controls included enzyme and 10% DMSO, negative controls included buffer in place of enzyme and 10% DMSO.

References

1. (a) Simon, G. M.; Niphakis, M. J.; Cravatt, B. F., Determining Target Engagement in Living Systems. *Nat. Chem. Biol.* **2013**, *9* (4), 200-205; (b) Frye, S. V., The Art of the Chemical Probe. *Nat. Chem. Biol.* **2010**, *6* (3), 159-161.
2. Kritzer, J. A., Grand Challenge Commentary: Beyond discovery: Probes that See, Grab and Poke. *Nat. Chem. Biol.* **2010**, *6* (12), 868-870.
3. Strober, W., Trypan Blue Exclusion Test of Cell Viability. In *Current Protocols in Immunology*, John Wiley & Sons, Inc.: 2001.
4. Nerlich, A. G.; Sauer, U.; Kolm-Litty, V.; Wagner, E.; Koch, M.; Schleicher, E. D., Expression of Glutamine:Fructose-6-Phosphate Amidotransferase in Human Tissues: Evidence for High Variability and Distinct Regulation in Diabetes. *Diabetes* **1998**, *47* (2), 170-178.
5. Sage, A. T.; Walter, L. A.; Shi, Y.; Khan, M. I.; Kaneto, H.; Capretta, A.; Werstuck, G. H., Hexosamine biosynthesis pathway flux promotes endoplasmic reticulum stress, lipid accumulation, and inflammatory gene expression in hepatic cells *Am. J. Physiol.-Endoc. M.* **2010**, *298* (3), E499-E510.
6. Vergani, L.; Gavazzo, P.; Mascetti, G.; Nicolini, C., Ethidium Bromide Intercalation and Chromatin Structure: A Spectropolarimetric Analysis. *Biochemistry* **1994**, *33* (21), 6578-6585.
7. Lee, J. S.; Latimer, L. J. P.; Hampel, K. J., Coralyne binds tightly to both T.cntdot.A.cntdot.T- and C.cntdot.G.cntdot.C+-containing DNA triplexes. *Biochemistry* **1993**, *32* (21), 5591-5597.
8. Wells, L.; Vosseller, K.; Hart, G. W., A Role for N-acetylglucosamine as a Nutrient Sensor and Mediator of Insulin Resistance. *Cell. Mol. Life Sci.* **2003**, *60* (2), 222-228.
9. Span, P. N.; Pouwels, M.-J. J. M.; Olthaar, A. J.; Bosch, R. R.; Hermus, A. R. M. M.; Sweep, C. G. J., Assay for Hexosamine Pathway Intermediates (Uridine Diphosphate-N-Acetyl Amino Sugars) in Small Samples of Human Muscle Tissue. *Clin. Chem.* **2001**, *47* (5), 944-946.
10. Thoden, J. B.; Wohlers, T. M.; Fridovich-Keil, J. L.; Holden, H. M., Human UDP-Galactose 4-Epimerase: Accomodation of UDP-N-acetylglucosamine within the Active Site. *J. Biol. Chem.* **2001**, *276* (18), 15131-15136.
11. Bobzin, S. C.; Yang, S.; Kasten, T. P., Application of Liquid Chromatography–Nuclear Magnetic Resonance Spectroscopy to the Identification of Natural Products. *J. Chromatogr. B: Biomed. Sci. Appl.* **2000**, *748* (1), 259-267.
12. Bolin, D.; Chen, S.; Mischke, S.; Qian, Y. Glutamine Fructose-6-Phosphate Amidotransferase (GFAT) Inhibitors. WO 2005/040150 A2. 6 May 2005.
13. Qian, Y.; Ahmad, M.; Chen, S.; Gillespie, P.; Le, N.; Mennona, F.; Mischke, S.; So, S.-S.; Wang, H.; Burghardt, C.; Tannu, S.; Conde-Knape, K.; Kochan, J.; Bolin, D., Discovery of 1-arylcarbonyl-6,7-dimethoxyisoquinoline Derivatives as Glutamine Fructose-6-phosphate Amidotransferase (GFAT) Inhibitors. *Bioorg. Med. Chem. Lett.* **2011**, *21* (21), 6264-6269.
14. Awuah, E.; Capretta, A., Strategies and Synthetic Methods Directed Toward the Preparation of Libraries of Substituted Isoquinolines. *J. Org. Chem.* **2010**, *75* (16), 5627-5634.

15. Todorovic, N.; Awuah, E.; Albu, S.; Ozimok, C.; Capretta, A., Synthesis of Substituted Isoquinolines via Pd-Catalyzed Cross-Coupling Approaches. *Org. Lett.* **2011**, *13* (23), 6180-6183.
16. Hantzsch, A.; Weber, J. H., Ueber Verbindungen des Thiazols (Pyridins der Thiophenreihe). *Ber. Dtsch. Chem. Ges.* **1887**, *20* (2), 3118-3132.
17. Singh, T. Exploring Carbonylation Reactions: Synthesis of Indanones – Towards Inhibitors of GFAT. Research, McMaster University, Hamilton, ON, 2012.
18. Bagha, B. Parallel Synthesis of a Diverse Library of Pyridinone Compounds to Probe the Chemical Space of Binding to L-glutamine:D-fructose-6-phosphate amidotransferase (GFAT). Research, McMaster University, Hamilton, ON, 2013.
19. Durrant, S. J.; Pinder, J. L.; Charrier, J.; Jiminez, J.; Brenchley, G.; Collier, P. N.; Kay, D.; Miller, A.; Pierard, F.; Ramaya, S.; Sadiq, S.; Twin, H. C., Synthesis of a Stable Pyridyl Boronate and its Reaction with Aryl and Heteroaryl Halides. *Heterocycles* **2006**, *70* (1), 509-517.
20. Soni, A.; Dutt, A.; Sattigeri, V.; Cliffe, I. A., Efficient and Selective Demethylation of Heteroaryl Methyl Ethers in the Presence of Aryl Methyl Ethers. *Synthetic Commun.* **2011**, *41* (12), 1852-1857.
21. Njuguna, N. M.; Masimirembwa, C.; Chibale, K., Identification and Characterization of Reactive Metabolites in Natural Products-Driven Drug Discovery. *J. Nat. Prod.* **2012**, *75* (3), 507-513.
22. Kazantzi, G.; Malamidou-Xenikaki, E.; Spyroudis, S., Functionalized Hydroxyquinones through Suzuki-Type Coupling of Phenyliodonium Ylides of Hydroxyquinones with Arylboronic Acids. *Synlett* **2006**, *2006* (16), 2597-2600.
23. Perez, A. L.; Lamoureux, G.; Zhen-Wu, B. Y., Synthesis of 2-hydroxy-3-substituted Naphthoquinones Using the Heck reaction. *Tetrahedron Lett.* **2007**, *48* (23), 3995-3998.
24. Floyd, T. Synthesis of 2-hydroxy-3-substituted-1,4-naphthoquinones to be Screened for Their Inhibiting Properties of Enzyme L-glutamine: D-fructose-6-phosphate amidotransferase (GFAT). Research, McMaster University, Hamilton, ON, 2013.
25. Dalton, S. Synthesis and Structure-Activity Relationships of 3-aryl substituted 2-hydroxy-1, 4-naphthoquinones for Potential Inhibition of Glutamine Fructose-6-Phosphate Amidotransferase. Research, McMaster University, Hamilton, ON, 2013.
26. Glinis, E.; Malamidou-Xenikaki, E.; Skouros, H.; Spyroudis, S.; Tsanakopoulou, M., Arylation of Lawsone Through BF₃-mediated Coupling of its Phenyliodonium Ylide with Activated Arenes and Aromatic Aldehydes. *Tetrahedron* **2010**, *66* (31), 5786-5792.
27. Perez, A. L.; Lamoureux, G.; Herrera, A., Synthesis of Iodinated Naphthoquinones Using Morpholine Iodine Complex. *Synthetic Commun.* **2004**, *34* (18), 3389-3397.
28. Malamidou-Xenikaki, E.; Spyroudis, S., Zwitterionic Iodonium Compounds: Useful Tools in Organic Synthesis. *Synlett* **2008**, *2008* (EFirst), 2725-2740.
29. Johnston, P. A.; Soares, K. M.; Shinde, S. N.; Foster, C. A.; Shun, T. Y.; Takyi, H. K.; Wipf, P.; Lazo, J. S., Development of a 384-Well Colorimetric Assay to Quantify Hydrogen Peroxide Generated by the Redox Cycling of Compounds in the Presence of Reducing Agents. *Assay Drug Dev. Techn.* **2008**, *6* (4), 505-518.
30. Blackmon, N.; Johnston, P. A.; Lazo, J. S.; Shinde, S. N.; Shun, T. Y.; Soares, K. M.; Takyi, H. K.; Wipf, P., Profiling the NIH Small Molecule Repository for Compounds that

Generate H₂O₂ by Redox Cycling in Reducing Environments. *Assay Drug Dev. Techn.* **2010**, *8* (2), 152-174.

31. Lal, M.; Rao, R.; Fang, X.; Schuchmann, H.-P.; von Sonntag, C., Radical-Induced Oxidation of Dithiothreitol in Acidic Oxygenated Aqueous Solution: A Chain Reaction. *J. Am. Chem. Soc.* **1997**, *119* (24), 5735-5739.

32. Han, J. C.; Han, G. Y., A Procedure for Quantitative Determination of Tris(2-Carboxyethyl)phosphine, an Odorless Reducing Agent More Stable and Effective Than Dithiothreitol. *Anal. Biochem.* **1994**, *220* (1), 5-10.

33. Kumagai, Y.; Shinkai, Y.; Miura, T.; Cho, A. K., The Chemical Biology of Naphthoquinones and Its Environmental Implications. *Annu. Rev. Pharmacol* **2012**, *52* (1), 221-247.

34. Hayashi, K.-i.; Chang, F.-R.; Nakanishi, Y.; Bastow, K. F.; Cragg, G.; McPhail, A. T.; Nozaki, H.; Lee, K.-H., Antitumor Agents. 233.1 Lantalucratins A–F, New Cytotoxic Naphthoquinones from *Lantana involucrata*. *J. Nat. Prod.* **2004**, *67* (6), 990-993.

35. Kimachi, T.; Torii, E.; Kobayashi, Y.; Doe, M.; Ju-ichi, M., Synthesis of Biologically Active (-)-dehydroiso-beta-lapachone and the Determination of its Absolute Configuration. *Chem. Pharm. Bull.* **2011**, *59* (6), 753-756.

36. Copeland, R. A., *Evaluation of Enzyme Inhibitors in Drug Discovery: A Guide for Medicinal Chemists and Pharmacologists*. John Wiley & Sons, Inc.: Hoboken, NJ, 2005.

37. Li, W.-W.; Heinze, J.; Haehnel, W., Site-Specific Binding of Quinones to Proteins through Thiol Addition and Addition–Elimination Reactions. *J. Am. Chem. Soc.* **2005**, *127* (17), 6140-6141.

Chapter 5

Development of Alternate Screening Strategies for GFAT Inhibitors and Future Research Directions

Preface

Preliminary experiments described were performed with assistance from the Brennan Research Group. Erica Forsberg provided valuable technical knowledge for the development of a mass spectrometry based assay. Meghan J. McFadden provided her expertise with the magnetic-bead pull-down assay and Meaghan O'Brien helped performed the experiments.

Introduction

Key to the identification of GFAT inhibitors is the access to a robust screening strategy and assay. As outlined in the previous chapters, the Morgan-Elson assay utilized allowed for a useful screening of compounds “one at a time”. A more useful strategy would allow for mixture screening where multiple molecules could be examined for their inhibitory properties simultaneously. This approach allows for increased throughput and, in the best case, the screening of natural product extracts.

Initial development of a mass spectrometry based assay for measuring GFAT activity

While the Morgan-Elson assay proved useful for “one-well, one-molecule” inhibitor screening and dose-response assessments, assays for GFAT can be improved upon. For example, a GFAT assay based on a mass spectrometry (MS) platform would offer several advantages over other methods: they require minute quantities of sample; are precise and sensitive; can simultaneously detect multiple substrates and/or products or other small molecules; can be coupled with a separation device or autosampler; can be performed in a kinetic or end-point only manner; and can be used for mixture screening (one-well, many-molecules). Disadvantages for utilizing MS for a biological assay include identifying an MS-compatible low ionic strength buffer, detection limitations by metabolites which are not easily ionizable or separated, reproducibility issues, ion-suppression due to metal cofactors and extra sample preparation or derivitization.

Brennan, Capretta and Werstuck have previously employed an MS-based assay to screen inhibitors as discrete compounds or as mixtures for glycogen synthase kinase

3β (GSK- 3β).¹ GSK- 3β was incubated with its substrates and a single small molecule or a mixture of 10 compounds each in an MS compatible buffer. The reaction was quenched and diluted with MeOH before direct injection into an ESI-MS system. Enzyme activity was compared to controls with no added inhibitors. Samples with decreased enzyme activity were deconvoluted to identify specific inhibitors from the mixtures. Inhibitors were identifiable from both discrete samples and from mixtures using this assay. A similar MS assay for GFAT would be highly desirable. There are some specific advantages over the spectrophotometric Morgan-Elson assay: MS can be used to monitor all four metabolites of GFAT; has increased sensitivity; does not require acetylation of GlcN6P; and, in terms of testing inhibitors, it is unaffected by UV-Vis properties of the compounds screened.

The metabolite pairs L-gln and L-glu and F6P and GlcN6P only differ by one mass unit each. Fortunately, mass spectrometry is sensitive enough to make such a distinction. Both product and substrate ions from individual solutions were measured with MS/MS on an ion-trap mass spectrometer (LCQ) to yield unique parent and daughter ions (Table 5-1).

Mass spectrometry experiments were performed with a mixture of 2.5 μ M F6P and L-gln in 50:50 methanol/20 M ammonium acetate by direct injection on a linear ion trap/triple quadrupole mass spectrometer (QTrap). The parent and daughter ions of both L-gln and F6P were identifiable by MS and MS₂ scans with positive polarity. Specific ionization parameters were identified (Table 5-2). This could be used to establish a multiple reaction monitoring (MRM) experiment. Mass spectrometer

parameters on the QTrap involving GFAT products GlcN6P and L-Glu also need to be performed and an MRM experiment with all 4 molecules can be assessed.

Compound	Molecular Weight	Parent Ion	Daughter Ion	Optimal Collision Energy
L-glutamine	146.14	147	130	22%
fructose-6-phosphate disodium salt hydrate	304.10/260	305/261	243	40%
glucosamine-6-phosphate	259.15	260	242	20%
L-glutamic acid	147.13	148	130	30%

Table 5-1. Mass spectrometry data for substrates and products of GFAT from the Finnigan LCQ Deca Mass Spectrometer. Stock solutions of 10 μ M were created for each of the four compounds in 50:50 methanol/20 M ammonium acetate. Samples of 250 μ L were run individually and the collision energy was manipulated in order to obtain a distinct spectrum for each. Fructose-6-phosphate was commercially available as a disodium salt hydrate, which had a mass of 304.10.

Mass Spectrometer Parameters	L-glutamine, 2.5 μ M	fructose-6-phosphate dipotassium salt, 2.5 μ M
Declustering Potential	100 V	40.0 V
Entrance Potential	6.0 V	7.0 V
Collision Energy	15.0 V	20.0 V
Collision Cell Exit Potential	2.4 V	5.0 V
Molecular Weight	146.14	336.3
Parent Ion	147	337
Daughter Ion(s)	130, 84	175

Table 5-2: Mass Spectrometer Parameters for the AB Applied Biosystems MDS Sciex QTrap LC/MS/MS System with GFAT substrates F6P and L-gln. These parameters can be used for future MRM experiments. Note the dipotassium salt of F6P was utilized in this experiment. The daughter ions for L-gln and F6P from MS/MS with the Q-Trap differ from those found with the LCQ Deca previously.

However, with day-to-day analysis of the sugars F6P and GlcN6P we noticed that the electrospray source would often become clogged and require maintenance. This was because sugars are poorly ionizable due to their high polarity.² One potential solution to this problem is through the use of sugar-binding boronic acids. Boronic acids have been known to form tight complexes with diols³, and thus have been used as a method to detect carbohydrates.⁴ They also help to increase the ionization of sugars, making them

a useful additive to quantify sugars with mass spectrometry based experiments.^{4a,5} The Hall Research Group has identified benzoboroxole (Figure 5-1) as a boronic acid which has an affinity for monosaccharides, including glucose, in neutral water.⁶ Unlike most other boronic acids it was functional under biological conditions.⁷ More recently, Cheng *et al* reported the use of fluorescent isoquinolinylboronic acids that have high affinities for glucose and fructose at physiological pH.⁸

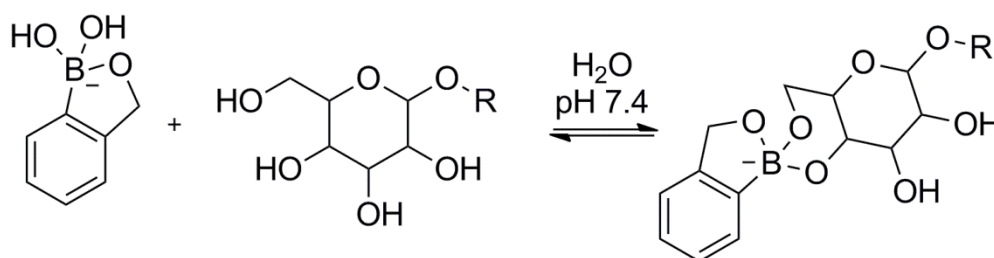


Figure 5-1. Benzoboroxole binding to a glycopyranoside under biological pH. Adapted from Dowlut *et al*. Benzoboroxole had a pK_a of 7.2 and was able to bind both pyranose and furanose sugars, such as glucose and fructose, in aqueous conditions.

To the best of our knowledge, there have not been any studies performed with GFAT metabolites fructose-6-phosphate and glucosamine-6-phosphate to the aforementioned boronic acid in terms of binding or adaptability for MS. It is logical that benzoboroxole should have a fair affinity for these sugars as well, despite the phosphate groups or the amine. This is evidenced by work from the Anslyn research group. They have published a report on the use of a boronic acid as a sensor for phosphor sugars⁹. They utilized a cadmium-centered tris-boronic acid receptor and measured its binding properties towards various sugars at neutral pH, including glucose-6-phosphate and ribose-5-phosphate. The boronic acid had the greatest affinity for the furanose sugars over the pyranose form, but the phosphate groups did not hinder the binding of the boronic acid.

Before any studies begin for a MS-based assay, it would be necessary to elucidate the binding affinity of benzoboroxole to F6P and GlcN6P. There is a colorimetric assay which is able to quantitatively determine the binding constants of boronic acids to sugars under aqueous conditions based on the competitive release of alizarin red S (ARS).¹⁰ Unbound ARS is red and absorbance can be measured at 525 nm while the bound form is a yellow colour and has maximum absorbance at 450 nm. A decrease in absorbance at 450 nm after a boronic acid is bound would indicate an increase in the boronate ester with the competing cis-diol. (Figure 5-2). Derivatization of polar analytes often increases the ionization efficiency, increases the molecular weight of the analyte, improves fragmentation pattern and decreases matrix effects.¹¹ If benzoboroxole is able to bind to F6P and GlcN6P, this would only be the start of assay development on an MS platform. Optimization of the boronic acid to sugar ratio, an MS compatible buffer which maintains GFAT functionality, and identifying the limit of detection, will all be necessary before a functional assay can be employed.

Development of a magnetic-bead pull-down assay for mixture screening of GFAT inhibitors

In addition to an MS-based assay to measure GFAT activity in the presence of inhibitors, we have also begun studies to utilize magnetic beads (MBs) as a separation method with MS detection. Magnetic beads are a commercially available product which combines small polymer (agarose or silica) coated particles 20-70 μm in size with a magnetic core and an affinity tag on the exterior (usually Ni-NTA, streptavidin, or a custom tag). They are reusable and provide a wide-range of applications from small-scale protein purification to immobilized enzyme assays for screening.

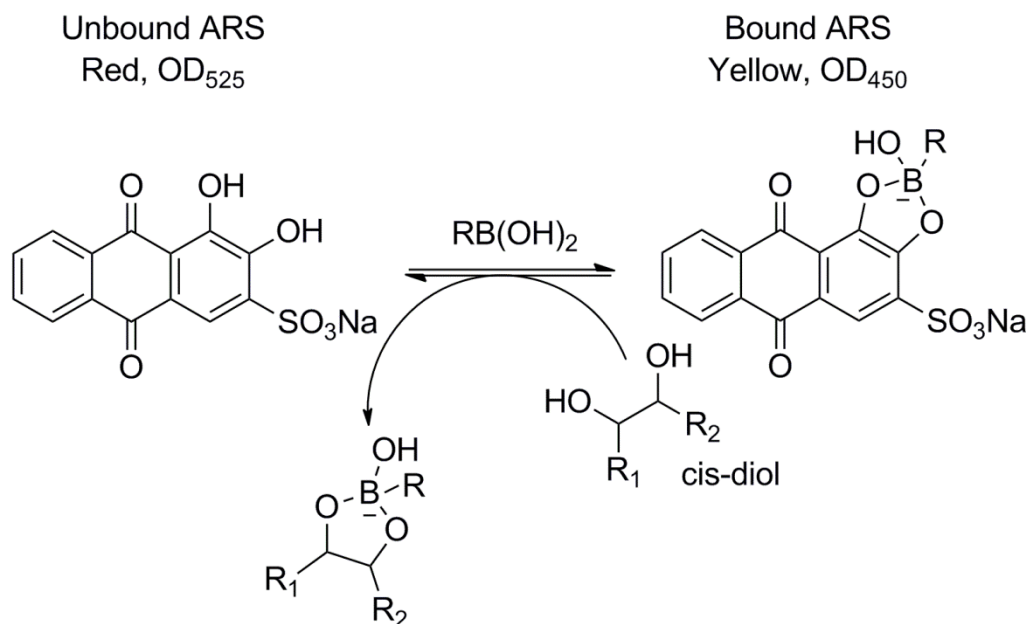


Figure 5-2. Schematic for the Alizarin Red S Assay. Adapted from Springsteen and Wang. The unbound form of ARS is red, and turns yellow in the presence of a boronic acid. If a cis-diol, like fructose, is included, the ARS will compete to bind the boronic acid. Sugars which bind strongly will result in unbound ARS and an increase in absorbance at 525 nm.

We developed an alternate assay that employed nickel-coated magnetic beads and used them to bind our His-tagged enzyme. First, rhGFAT1-His₆²⁹⁸ was incubated with a mixture of small molecules and those molecules with affinity for the enzyme would bind. The magnetic beads were then added to the mixture screening solution and adhered to the enzyme-ligand complex. Those molecules with no affinity for the enzyme (i.e. unbound small molecules) stayed in solution. The magnetic bead-enzyme-ligand complex is “pulled down” from the mixture-screening solution using a magnet. The retrieved magnetic beads were resuspended into a solvent (MeOH) able to denature the enzyme and release the ligands. The ligands were then identified by their molecular weight following detection by mass spectrometry (Figure 5-3).

We have pursued the development of a MB assay applicable to mixture screening as a way to increase throughput and screen natural product extracts. Our HTS

campaign assayed compounds at a rate of 1 molecule/well, if we were able to increase the rate to 10, 20 or even 100 molecules per well this would dramatically limit the costs and time required for probe discovery. The concept of mixture screening could also be applied to natural product extracts, which would allow for the discovery of new molecular entities. This method has been applied successfully in the Brennan research group to identify ligands which can disrupt protein-protein interactions.¹²

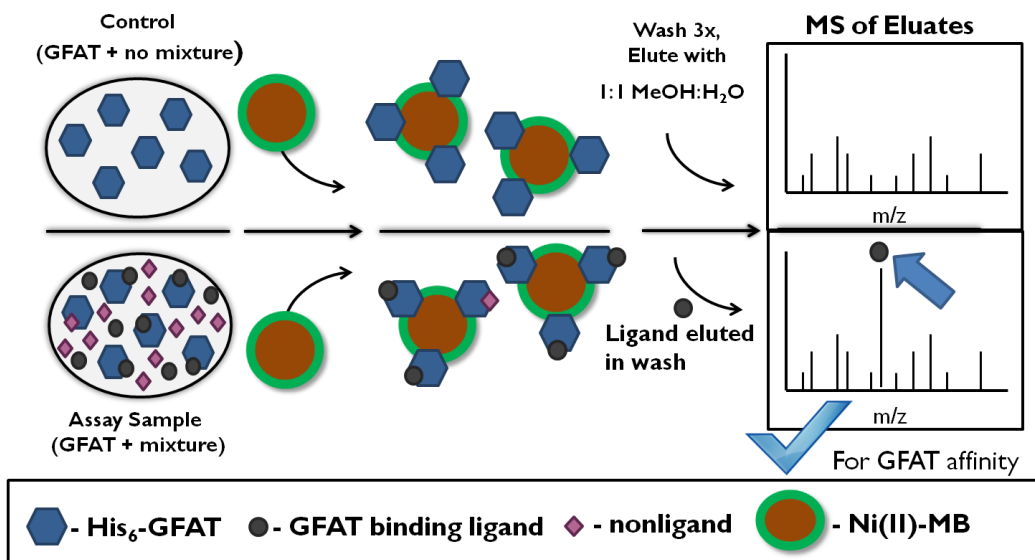


Figure 5-3. Schematic of a Magnetic-Bead (MB) pull-down assay with MS detection. Adapted from Meaghan O'Brien's Senior Thesis.¹³ A mixture of GFAT and small molecules were incubated together, and molecules with an affinity for the enzyme would bind. A control was included with enzyme only. The nickel-coated magnetic beads (Ni(II) – MB), were added to the enzyme/small molecule mixture. The His₆-tagged GFAT-ligand complex bound to the Ni (II)-MBs and a magnetic separator was used to collect the Ni (II)-MBs and remove the supernatant. Molecules with no enzyme affinity stayed in the supernatant. To remove any ligands with non-specific binding, the Ni(II)-MB-enzyme-ligand complex was washed in triplicate in a low ionic strength buffer. The ligands were eluted after resuspending the beads in 1:1 MeOH/H₂O. The supernatant was submitted to MS for identification of the ligands based on molecular weight.

The main advantages to this assay are increased throughput and, if each member of a library to be screened has a unique mass, then no mixture deconvolution is necessary. However, it is important to note that this is a binding assay only. Any identified molecules would require further testing to determine if they decrease enzyme

activity. Disadvantages include non-specific binding to the magnetic beads instead of the enzyme, or failure to bind potential inhibitors due to the orientation of the enzyme bound to the magnetic bead.

Studies performed in conjunction with Meaghan O'Brien have shown that rhGFAT1-His₆²⁹⁸ did bind to the MBs specifically and were amenable to ligand fishing of discrete compounds or from small molecule mixtures.¹³ As a proof of concept, EME 384 was incubated in solution with GFAT. Dry nickel-coated magnetic beads (Millipore, Billerica, MA) were added to the solution and the magnetic bead-enzyme-ligand complex was pulled down using a magnet. The supernatant, containing unbound sample, was removed and the beads were washed in a low-salt mass spectrometry compatible buffer. To elute any bound ligand, MBs were incubated in 1:1 water/methanol mixture and this supernatant was submitted to ESI-MS for detection of any small molecules bound to the enzyme. EME 384 was detected by this method as compared to controls (Figure 5-4).

Mixture screening was then performed with five different small molecule mixtures consisting of 10 compounds each. The molecules were selected from the bioactive subset of the McMaster University Canadian Compound Collection and did not contain any small molecules previously identified as hits. In addition, one of the mixtures was spiked with inhibitor EME 384. The mixtures tested had a final working concentration of 10 μ M each per assay. Each sample was analyzed with protocol described above. Mixture One, which contained EME 384 and nine other bioactives, returned a spectra with a molecular ion peak [M+H] corresponding to EME 384 (Figure 5-5). This was a promising result for mixture screening as it showed that introduction of

other small molecules did not inhibit binding of a known ligand to the enzyme. In Mixture Two, another ligand was eluted from the sample. Its mass spectrum identified the bound ligand as solasodine (Figure 5-6), a naturally occurring glycoalkaloid.¹⁴ While this molecule showed affinity for GFAT, upon further validation with the Morgan-Elson assay it did not inhibit the enzyme. The other three mixtures did not show any ligands in the eluent.

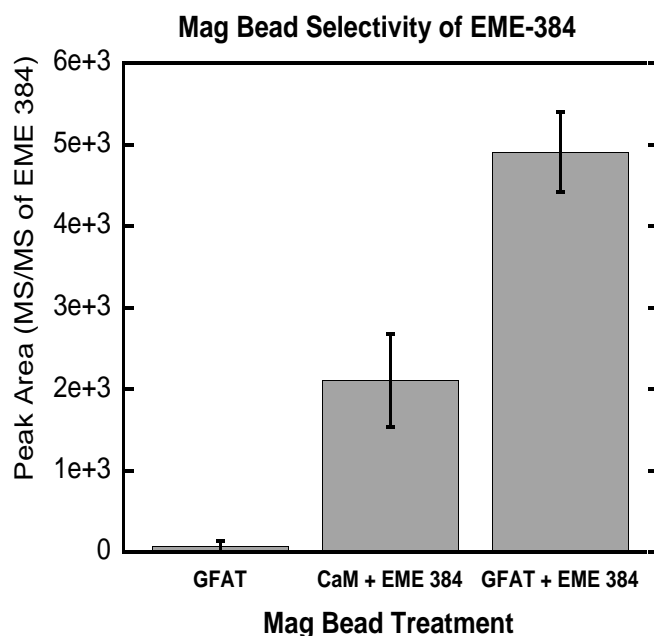


Figure 5-4. Comparison of ligand fishing for GFAT inhibitor EME 384. Adapted from Meaghan O'Brien's Senior Thesis.¹³ rhGFAT1-His₆²⁹⁸ (GFAT) as the control (N=3), His-tagged calmodulin (CaM) + EME 384 as the reference control (N=2) and rhGFAT1-His₆²⁹⁸ (GFAT) + EME 384 as the positive control (N=2). ESI-MS/MS was used to detect the presence of any eluted EME 384. Following a One-Way ANOVA with Tukey's All Pairs Comparison (KaleidaGraph, v.4.1), selection of EME 384 with MB-bound GFAT was deemed to be significant as compared to the control ($p=0.0003$) and reference treatment CaM + EME 384 ($p=0.0039$). These results showed a 2.5 fold increase in EME 384 recovery with GFAT as compared to CaM.



Figure 5-5. ESI-MS/MS spectra of 5 bioactive mixtures with the MB pull-down assay. Figure adapted from Meaghan O'Brien's Senior Thesis. Each set of spectra displays what was eluted from Mixtures 1-5 (in ascending order). Each mixture consisted of ten compounds each and were tested at equal concentrations of 10 μ M. Mixture 1 was spiked with EME 384 (MW 343) and was present in the first MS trace (m/z 344). The second MS trace corresponding to Mixture 2, displayed a peak for m/z 415. This was identified as solasodine based on its molecular weight (MW 414). Mixtures 3-5 did not show any significant peaks in the spectra.

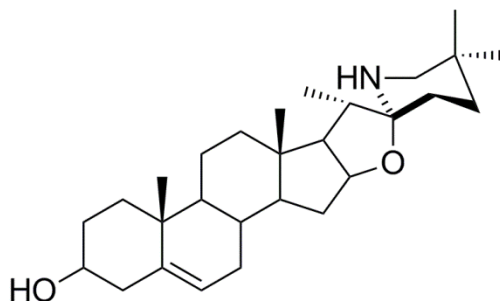


Figure 5-6. Structure of solasodine. This toxic glycol-alkaloid was pulled out of Mixture 2 from the MB pull-down assay. This compound showed an affinity for GFAT but it did not show any inhibitory activity upon testing with the Morgan-Elson assay.

These results are promising for mixture screening by use of the magnetic beads.

We were able to show that GFAT can be immobilized on the beads and discrete compounds can be extracted from solution with the MB-GFAT complex. The question now lies as to the limitations of this mixture screening technique. Determination of the maximum number of compounds in a mixture needs to be determined. In addition, a comparison of the effect of weak and strong binding ligands as well as multiple ligand concentration will need to be ascertained before this technique can be applied to much more complex natural product extracts.

Enhanced characterization of dehydroiso- β -lapachone

Dehydroiso- β -lapachone was identified as an inhibitor during a secondary screen to elucidate the SAR of the 1,4-naphthoquinone class of inhibitors. We have shown that it acts as a noncompetitive inhibitor at both the glutaminase and isomerase binding domains of GFAT. Further characterization of this inhibitor is necessary if we wish to use it in an *in vivo* assay. With a UPLC-MS assay developed for detection of UDP-GlcNAc, we can subject HepG2 cells to treatment with dehydroiso- β -lapachone and

determine its cell permeability and efficacy as an inhibitor in cell culture. This experiment was attempted but the effect of treatment with inhibitor was not significant (Figure 5-7). Repetition of this experiment is in progress.

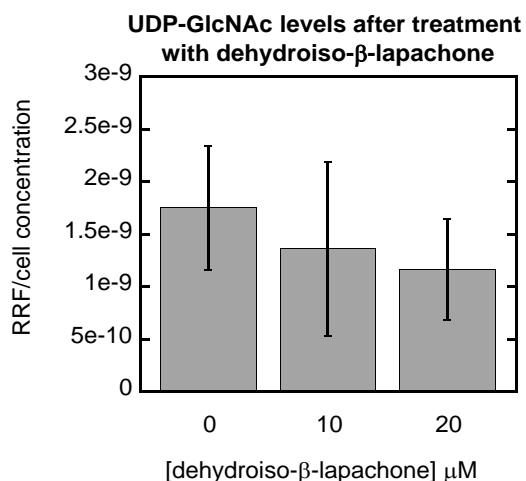


Figure 5-7. Treatment of HepG2 cells with dehydroiso-β-lapachone and detection of UDP-GlcNAc via UPLC-TOF-MS. HepG2 cells grown in 5 mM glucose were left untreated (N=5) or treated for 2 hrs with 10 (N=5) or 20 (N=5) μM inhibitor before harvesting. Following a one-way ANOVA with Tukey's All Pairs Comparison, neither of the treatments was deemed significant in the reduction of UDP-GlcNAc.

While we were able to determine the mode of inhibition for dehydroiso-β-lapachone, we do not know whether it binds to the enzyme as a reversible or irreversible inhibitor. Since some GFAT activity is required to maintain basic metabolic processes, an irreversible inhibitor may prove too toxic to use in a living organism. Knowledge of reversibility may also help guide the dosage used when beginning *in vivo* studies. To determine the reversibility of the inhibitor for GFAT, the Morgan-Elson assay can once again be employed. A technique described by R.A. Copeland¹⁵ involves incubating the target enzyme at a concentration over 100 times necessary for assay activity and the inhibitor at a concentration 10 times its IC₅₀. After incubation, the mixture is diluted 100-fold into reaction buffer which contains substrates. The enzyme

activity of the diluted sample can be compared to a control sample diluted without the presence of inhibitor. In this situation, the enzyme is diluted to a level normally used in the assay, but the inhibitor is now at a fraction of its IC_{50} concentration. If the inhibitor is rapidly reversible, then activity will be similar to the control sample. If the inhibitor is slowly reversible or irreversible, enzyme activity will not fully recover. To confirm an irreversible inhibitor, an experiment should be executed as described previously. Instead of measuring activity, the protein is denatured and isolated from any small molecules. Covalent bonding of an inhibitor to a protein is detectable by mass spectrometry when compared to a sample without added inhibitor. If the mass (or retention times if coupled with LC) are different, an irreversible inhibitor is present.

Alternatively, the magnetic-bead pull-down assay could also be employed to determine reversibility. The last step of the assay calls for elution of ligands from the MB-enzyme complex by resuspension in MeOH/H₂O. Any ligand which is reversible for the enzyme will be found in the supernatant and detected by MS. An irreversible ligand will remain covalently bound to the denatured enzyme and will evade detection.

Secondary SAR analysis with dehydroiso- β -lapachone derivatives

While dehydroiso- β -lapachone has been identified as a potent inhibitor, only five 1,2-furan and 1,2-pyran varieties of 1,4-naphthoquinones have been tested. A secondary SAR study focusing on this structure will give insight about how these compounds function as GFAT inhibitors. Schaffner-Sabba *et al* have previously described a synthesis for a series of β -lapachone derivatives.¹⁶ They utilized lawsone as the starting material and a series of allyl bromide derivatives introduced variety on the pyran ring of

β -lapachone (Figure 5-8). An alternate synthetic method for *para* and *ortho* furan substituted naphthoquinones was described by Müller *et al* (Figure 5-9).¹⁷ Aldehydes with varying alkyl chain lengths could be incorporated to bring further variety onto the furan ring. A secondary SAR of dehydroiso- β -lapachone derivatives would allow us to pinpoint which structural features are important for inhibition, increase potency and specificity to GFAT, and provide some hint about the binding site.

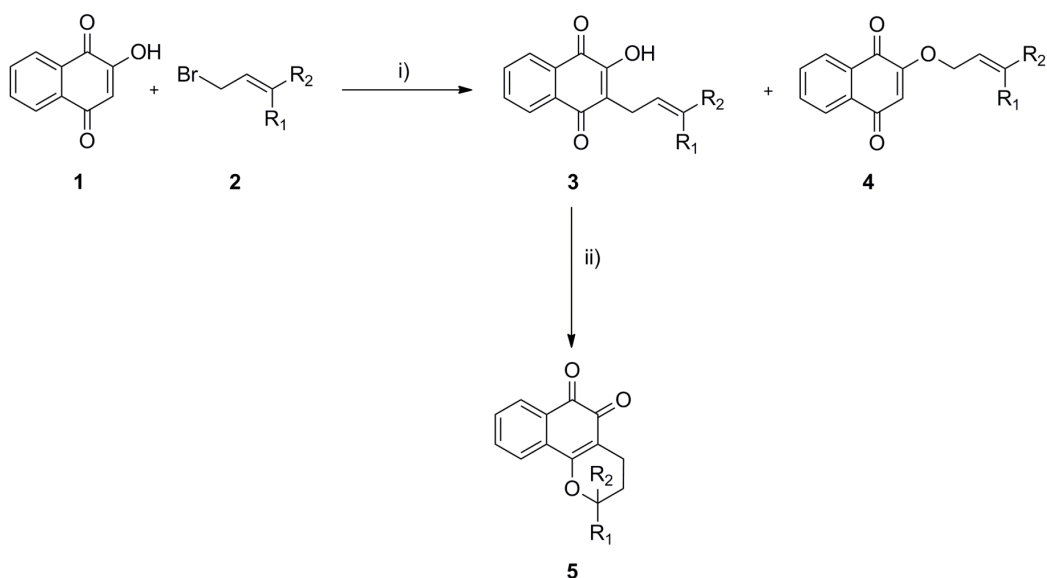


Figure 5-8. β -lapachone derivative reaction scheme. Adapted from Schaffner-Sabba *et al*. The potassium salt of lawsone (1) was used as the starting material. The allyl bromide (2) was synthesized from the corresponding allyl alcohols in a mixture of pyridine and phosphorous bromide. i) The potassium salt of (1), was dissolved in hexamethylphosphorous triamide (HMPT), KI was added followed by the allyl bromide. The reaction yielded both products (3) and (4). These were separated through extraction with toluene and aqueous base. ii) The ring closure was performed with (3) under strongly acidic conditions. Recrystallization yields pure product (5). Yields for (5) ranged from 29-93%.

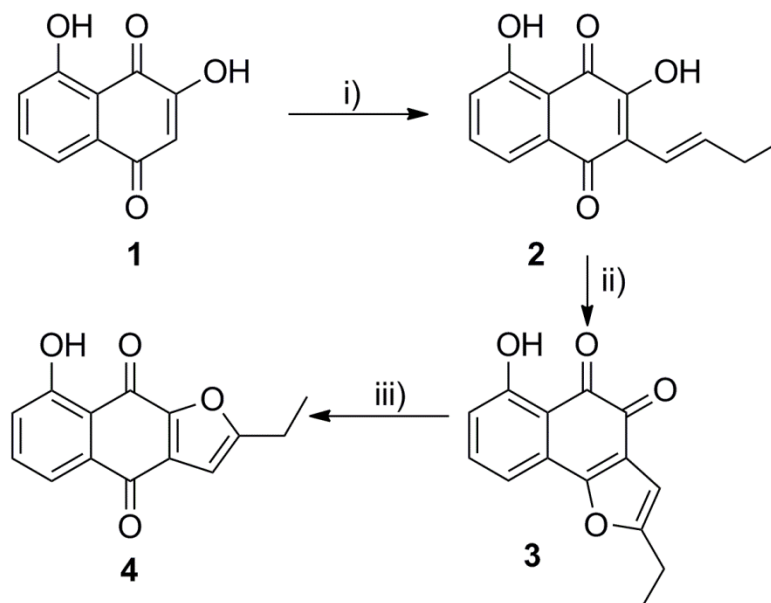


Figure 5-9. Synthetic scheme for *ortho* and *para* substituted 1,4-naphthoquinones. Adapted from Müller *et al.* 2,8-dihydroxy-1,4-naphthoquinone (1) was subjected to i) condensation with *n*-butyraldehyde to yield lapacho derivative (2). ii) Oxidative cyclization of (2) with mercuric acetate yielded *ortho*-quinone (3). If the *para*-quinone was desired, iii) strong acidic conditions resulted in (4). Yields ranged from 11-31%.

In vivo inhibition of GFAT to probe for modulation of downstream effects

Over-expression of GFAT in mice results in insulin resistance,¹⁸ impaired glucose tolerance, hyperlipidemia and obesity.¹⁹ With our inhibitors we have been able to modulate the activity of the HBP in cell culture. In order to observe how this will perturb the downstream effects *in vivo* (including ER stress), a mouse model is necessary. To date, modulation of GFAT activity by a chemical probe in a diabetic and atherosclerosis prone mouse model has not been employed. However, previous work by the Werstuck research group demonstrated that glucosamine fed apolipoprotein E deficient (-ApoE) mice with streptozotocin induced diabetes developed atherosclerosis and displayed markers of ER stress.²⁰ ApoE deficient mice provide an excellent model to study the development of atherosclerosis,²¹ while streptozotocin destroys pancreatic β -cells resulting in hyperglycemia.²² With a potent molecular probe at our disposal, a similar

study could be repeated. This would directly show whether GFAT inhibition will have an immediate effect on prevention of atherosclerosis. At the molecular level, UDP-GlcNAc levels could be detected in various tissues harvested from the mouse model with our UPLC-MS assay. This would provide confirmation that the probe is functioning *in vivo* and information about the bio-distribution of the probe. The tissue preparation will require some modification in comparison to the procedure used for the cell cultures. We could employ the facile technique described by Bligh and Dyer, where they extracted the lipids from fish muscle tissue using a chloroform and water/methanol mixture.²³

Alternative therapeutic uses for GFAT inhibitors

The importance of researching GFAT is not limited to its role in the prevention of secondary side-effects related to diabetes. The enzyme is present in every living thing and is essential for life. This makes GFAT or GlmS in prokaryotic species, a potential target for anti-bacterial, anti-fungal, or anti-parasitic therapeutics. For bacterial and fungal species, the role of UDP-GlcNAc is compulsory for construction of cell walls. Floquet *et al* have performed a docking study in search of inhibitors for *E.coli* GlmS²⁴ whereas Wojciechowski *et al* reviewed molecular modeling studies for anti-fungal capabilities of GFAT inhibition.²⁵ Wojciechowski states that it is possible to achieve specificity between fungal GFAT and the human variety because fungi are more sensitive to short-term periods of inhibition. More recently, Japanese researchers studying the metabolic profile of the model species *Entamoeba invadens*, have found an increase in the transcript level of GFAT during the encystation process of the parasite.²⁶ They also observed glucose-6-phosphate and fructose-6-phosphate levels were depleted and

suggested that the chitin biosynthesis pathway (similar to the HBP) was taking precedent over glycolysis. Thus inhibition of GFAT may be a potential target for anti-biotic therapies.

Conclusion

Through our research efforts, we now have a renewable form of GFAT at our disposal, an HTS-compatible assay, a novel noncompetitive inhibitor, a variety of SAR data and an assay method amenable to cell culture. As presented here, there are multiple research avenues remaining to be explored with GFAT. Utilizing our newfound probes in a diabetic mouse-model will provide us with more clues about the role of GFAT in this endemic disease. The development of new assays will enhance the ways we can study the enzyme and its interaction with inhibitors. With so much therapeutic potential for enzymatic probes in other microbiological species, the discovery of new molecular probes cannot be overemphasized. We have gained new tools to study the enzyme further, but only time will tell what secrets they will unlock.

Materials & Methods

Sample preparation of L-gln, L-glu, F6P and GlcN6P for MS-detection

10 μ M stock solutions of L-glutamine, L-glutamate, D-fructose-6-phosphate disodium salt and D-glucosamine-6-phosphate (Sigma Aldrich) were created for each of the four compounds in 50:50 HPLC Grade MeOH/20 M NH_4OAc (Caledon Laboratories). Samples of 250 μ L each were run through a Finnigan LCQ Deca mass spectrometer individually from a syringe pump with a flow rate of 10 μ L/min. The collision energy was manipulated in order to obtain a distinct spectrum for each.

Sample preparation of L-gln and F6P for MS-detection

A 2.5 μ M stock solution of fructose-6-phosphate dipotassium salt and L-glutamine (Sigma Aldrich) was prepared in 50:50 HPLC Grade MeOH/20 M NH_4OAc . From a syringe pump with a flow rate of 10 μ L/min, the mixture was run on an AB Applied Biosystems, MDS Sciex QTrap LC/MS system.

Protocol for Magnetic Bead (MB) Pull-Down Assay with rhGFAT1-His₆²⁹⁸

The magnetic beads (PureProteome nickel magnetic beads, 10 μ m diameter, 0.2 g of MBs/mL in water, Millipore, Billerica, MA) were received as a 25% w/v slurry in 1% benzyl alcohol. The MBs were vortexed to create a uniform suspension, and 200 μ L were transferred to a clean 1.5 mL microcentrifuge tube. The supernatant was removed after magnetically collecting the MBs by a magnetic separator (BioClone Inc., San Diego, CA). The MBs were resuspended in 500 μ L of MB wash buffer (50 mM sodium phosphate, 300 mM NaCl, 10 mM imidazole, pH 8) and vortexed at high speed before

collecting the MBs and removing the supernatant. This process was repeated twice with the MB wash buffer and thrice with the GFAT wash buffer (50 mM Tris-HCl, 200 mM NaCl, 10 mM imidazole, 1 mM F6P, 2 mM, TCEP, 1 mM PMSF, pH 7.8) to a total volume of 200 μ L. The stocks were stored at 4 °C until further use.

The general pull-down assay with discrete compounds was performed at room temperature in a 48-well polystyrene microwell plate (BD Biosciences, Mississauga, ON) with a final assay volume of 100 μ L (Table 5-3). Tested compounds were present in a 10-fold molar excess to enzyme ratio to ensure any available binding sites were completely saturated. Enzyme, buffer and test compounds were first aspirated into the wells and incubated on a microplate shaker for 10 minutes. Alternate fresh wells had 40 μ L of MBs added to them, the supernatant was removed when magnetic separation was applied. To those wells containing 'dry' MBs, the 100 μ L test samples (enzyme, buffer, test compound) were added and resuspended with the MBs. The microplate was incubated for a further 40 minutes on a microplate shaker to allow affinity binding of the enzyme to the MBs. The assay was terminated by magnetic collection of the supernatant and thus removal of any unbound sample. The MBs were washed twice with 200 μ L of a low salt MB buffer (20 mM Tris-HCl, pH 7.8) and transferred to a fresh well before an additional third and final wash. To elute any bound sample and submit for detection by ESI-MS/MS analysis, the supernatant of the final low salt wash was removed after magnetic separation and the MBs were incubated in 100 μ L of 1:1 (v/v) methanol/water for 30 minutes on a microplate shaker. The MBs were magnetically

separated and the supernatant was retained for analysis of any samples bound to the MB-GFAT complex.

Mixture screening was performed under similar assay conditions. Mixtures of 10 molecules each were prepared in DMSO with a final 100 μM stock concentration of each molecule. This yielded a working concentration of 10 μM each under the pull-down assay conditions. The remainder of the assay was repeated as previously stated and any bound sample was detected by ESI-MS/MS analysis on a Thermo Scientific LCQ Fleet mass spectrometer.

Assay Reagent	GFAT Enzyme	GFAT Wash Buffer	Test Compounds*	'dry' MBs**
Volume	50 μL in GFAT storage buffer	40 μL	10 μL in DMSO	40 μL or 0.8 mg after supernatant is removed
Stock Concentration	2 μM	-	100 μM	25% w/v
Final Concentration in Assay	1 μM or 100 μmol	-	10 μM or 1000 μmol	0.8 mg/100 μL

Table 5-3. Reagents for Magnetic Bead Affinity Pull-Down assay with rhGFAT-His₆²⁹⁸ *Test compounds were dissolved in DMSO and neat DMSO was used for low and high controls. ** Dry MBs refers to the MB stock which had been prepared previously and had the supernatant it was stored in removed before use in the pull-down assay.

References

1. Partserniak, I.; Werstuck, G.; Capretta, A.; Brennan, J. D., An ESI-MS/MS Method for Screening of Small-Molecule Mixtures Against Glycogen Synthase Kinase-3beta (GSK-3beta). *Chembiochem* **2008**, *9* (7), 1065-73.
2. Williams, D.; Lee, T. D.; Dinh, N.; Young, M. K., Oligosaccharide Profiling: The Facile Detection of Mono-, Di- and Oligosaccharides by Electrospray Orthogonal Time-of-Flight Mass Spectrometry Using 3-Aminophenylboronic acid Derivatization. *Rapid Commun. Mass Sp.* **2000**, *14* (16), 1530-1537.
3. Lorand, J. P.; Edwards, J. O., Polyol Complexes and Structure of the Benzeneboronate Ion. *J. Org. Chem.* **1959**, *24* (6), 769-774.
4. (a) Li, Q.; Ricardo, A.; Benner, S. A.; Winefordner, J. D.; Powell, D. H., Desorption/Ionization on Porous Silicon Mass Spectrometry Studies on Pentose-Borate Complexes. *Anal. Chem.* **2005**, *77* (14), 4503-4508; (b) Lipták, M.; Dinya, Z.; Herczegh, P.; Jekő, J., Studies on the Complexation of Polyols and Carbohydrates with Excess Borate Using Thermospray Mass Spectrometry. *Org. Mass Spectrom.* **1993**, *28* (7), 780-784.
5. Harvey, D. J., Matrix-Assisted Laser Desorption/Ionization Mass Spectrometry of Carbohydrates. *Mass Spectrom. Rev.* **1999**, *18* (6), 349-450.
6. (a) Bérubé, M.; Dowlut, M.; Hall, D. G., Benzoboroxoles as Efficient Glycopyranoside-Binding Agents in Physiological Conditions: Structure and Selectivity of Complex Formation. *J. Org. Chem.* **2008**, *73* (17), 6471-6479; (b) Dowlut, M.; Hall, D. G., An Improved Class of Sugar-Binding Boronic Acids, Soluble and Capable of Complexing Glycosides in Neutral Water. *J. Am. Chem. Soc.* **2006**, *128* (13), 4226-4227.
7. Hoeg-Jensen, T., Preparation and Screening of Diboronate Arrays for Identification of Carbohydrate Binders. *QSAR Comb. Sci.* **2004**, *23* (5), 344-351.
8. Cheng, Y.; Ni, N.; Yang, W.; Wang, B., A New Class of Fluorescent Boronic Acids that have Extraordinarily High Affinities for Diols in Aqueous Solution at Physiological pH. *Chem. – Eur. J.* **2010**, *16* (45), 13528-13538.
9. Zhang, T.; Anslyn, E. V., A Colorimetric Boronic Acid Based Sensing Ensemble for Carboxy and Phospho Sugars. *Org. Lett.* **2006**, *8* (8), 1649-1652.
10. Springsteen, G.; Wang, B., Alizarin Red S as a General Optical Reporter for Studying the Binding of Boronic Acids with Carbohydrates. *Chem. Commun.* **2001**, (17), 1608-1609.
11. Iwasaki, Y.; Nakano, Y.; Mochizuki, K.; Nomoto, M.; Takahashi, Y.; Ito, R.; Saito, K.; Nakazawa, H., A New Strategy for Ionization Enhancement by Derivatization for Mass Spectrometry. *J. Chromatogr. B* **2011**, *879* (17-18), 1159-1165.
12. McFadden, M. J.; Junop, M. S.; Brennan, J. D., Magnetic “Fishing” Assay to Screen Small-Molecule Mixtures for Modulators of Protein-Protein Interactions. *Anal. Chem.* **2010**, *82* (23), 9850-9857.
13. O'Brien, M. The Development of a Magnetic Bead Pull-Down Assay to Screen Mixtures for L-glutamine-D-fructose-6-phosphate amidotransferase (GFAT) Inhibitors. Research, McMaster University, Hamilton, ON, 2011.
14. Keeler, R.; Brown, D.; Douglas, D.; Stallknecht, G.; Young, S., Teratogenicity of the Solatium Alkaloid Solasodine and of ‘Kennebec’ Potato Sprouts in Hamsters. *B. Environ. Contam. Tox.* **1976**, *15* (5), 522-524.

15. Copeland, R. A., *Evaluation of Enzyme Inhibitors in Drug Discovery: A Guide for Medicinal Chemists and Pharmacologists*. John Wiley & Sons, Inc.: Hoboken, NJ, 2005.
16. Schaffner-Sabba, K.; Schmidt-Ruppin, K. H.; Wehrli, W.; Schuerch, A. R.; Wasley, J. W. F., Beta-lapachone: Synthesis of Derivatives and Activities in Tumor Models. *J. Med. Chem.* **1984**, *27* (8), 990-994.
17. Müller, K.; Sellmer, A.; Wiegrebe, W., Potential Antipsoriatic Agents: Lapacho Compounds as Potent Inhibitors of HaCaT Cell Growth. *J. Nat. Prod.* **1999**, *62* (8), 1134-1136.
18. Hebert, L. F.; Daniels, M. C.; Zhou, J.; Crook, E. D.; Turner, R. L.; Simmons, S. T.; Neidigh, J. L.; Zhu, J. S.; Baron, A. D.; McClain, D. A., Overexpression of Glutamine:fructose-6-phosphate amidotransferase in Transgenic Mice Leads to Insulin Resistance. *J. Clin. Invest.* **1996**, *98* (4), 930-936.
19. Veerababu, G.; Tang, J.; Hoffman, R. T.; Daniels, M. C.; Hebert, L. F.; Crook, E. D.; Cooksey, R. C.; McClain, D. A., Overexpression of Glutamine: fructose-6-phosphate amidotransferase in the Liver of Transgenic Mice Results in Enhanced Glycogen Storage, Hyperlipidemia, Obesity, and Impaired Glucose Tolerance. *Diabetes* **2000**, *49* (12), 2070-2078.
20. Werstuck, G. H.; Khan, M. I.; Femia, G.; Kim, A. J.; Tedesco, V.; Trigatti, B.; Shi, Y., Glucosamine-Induced Endoplasmic Reticulum Dysfunction Is Associated With Accelerated Atherosclerosis in a Hyperglycemic Mouse Model. *Diabetes* **2006**, *55* (1), 93-101.
21. (a) Osada, J.; Joven, J.; Maeda, N., The Value of Apolipoprotein E Knockout Mice for Studying the Effects of Dietary Fat and Cholesterol on Atherogenesis. *Curr. Opin. Lipidol.* **2000**, *11* (1), 25-29; (b) Zadelaar, S.; Kleemann, R.; Verschuren, L.; de Vries-Van der Weij, J.; van der Hoorn, J.; Princen, H. M.; Kooistra, T., Mouse Models for Atherosclerosis and Pharmaceutical Modifiers. *Arterioscler. Thromb., Vasc. Biol.* **2007**, *27* (8), 1706-21.
22. Rees, D. A.; Alcolado, J. C., Animal Models of Diabetes Mellitus. *Diabetic Med.* **2005**, *22* (4), 359-370.
23. Bligh, E. G.; Dyer, W. J., A Rapid Method of Total Lipid Extraction and Purification. *Can. J. Biochem. Phys.* **1959**, *37* (8), 911-917.
24. Floquet, N.; Richez, C.; Durand, P.; Maigret, B.; Badet, B.; Badet-Denisot, M. A., Discovering New Inhibitors of Bacterial Glucosamine-6P synthase (GlmS) by Docking Simulations. *Bioorg. Med. Chem. Lett.* **2007**, *17* (7), 1966-70.
25. Wojciechowski, M.; Milewski, S.; Mazerski, J.; Borowski, E., , Glucosamine-6-phosphate Synthase, a Novel Target for Antifungal Agents. Molecular Modelling Studies in Drug Design. *Acta Biochim. Pol.* **2005**, *52* (3), 647-653.
26. Jeelani, G.; Sato, D.; Husain, A.; Escueta-de Cadiz, A.; Sugimoto, M.; Soga, T.; Suematsu, M.; Nozaki, T., Metabolic Profiling of the Protozoan Parasite *Entamoeba invadens* Revealed Activation of Unpredicted Pathway during Encystation. *PLoS ONE* **2012**, *7* (5),1-11.